

N.E.A. Data Bank
Banque de Données
de l'A.E.N.

N.E.A. Data Bank

de l'A.E.N.

N.E.A. Data Bank
Banque de Données
de l'A.E.N.

N.E.A. Data Bank
Banque de Données
de l'A.E.N.

N.E.A. Data Bank
Banque de Données

PRE-EQUILIBRIUM EFFECTS

An International Nuclear Model and Code Comparison

NEWSLETTER

No. 32

SEPTEMBER 1985

NEWSLETTER

OF THE NEA DATA BANK

BULLETIN

DE LA BANQUE DE DONNEES DE L'AEN

SEPTEMBRE 1985

No. 32

SEPTEMBER 1985

NUCLEAR ENERGY AGENCY
AGENCE POUR L'ENERGIE NUCLEAIRE

ORGANISATION FOR ECONOMIC CO-OPERATION AND DEVELOPMENT
ORGANISATION DE COOPERATION ET DE DEVELOPPEMENT ECONOMIQUES

LEGAL NOTICE

Neither the Organisation for Economic Co-operation and Development or any of its Member Countries, nor any person acting either on behalf of any of them or other-wise in furtherance of the activities of the NEA Data Bank:

1. Makes any warranty or representation, expressed or implied, with respect to the accuracy, completeness, or usefulness of the information contained herein, or that the use of any information, apparatus, method, or process disclosed herein may not infringe privately owned rights;

2. Assumes any liabilities with respect to the use of, or for damage resulting from the use of, any information, apparatus, method or process disclosed herein.

At present, the Member countries participating in the NEA Data Bank are the following: Austria, Belgium, Denmark, Finland, France, Federal Republic of Germany, Italy, Japan, the Netherlands, Norway, Portugal, Spain, Sweden, Switzerland, Turkey and the United Kingdom.

AVERTISSEMENT

L'Organisation de Coopération et de Développement Économiques, ses pays Membres, les personnes agissant en leurs noms ou pour le compte de la Banque de Données de l'AEN:

1. Ne garantissent, expressément, ou implicitement ni que les informations ci-jointes sont exactes et complètes, ni que l'utilisation de ces informations, ainsi que les appareils, méthodes ou procédés décrits ne portent pas atteinte à des droits acquis.

2. N'assument aucune responsabilité en ce qui concerne l'utilisation desdites informations, appareils, méthodes ou procédés ainsi que les conséquences pouvant en résulter.

A l'heure actuelle, les pays Membres qui participent à la Banque de Données de l'AEN sont les suivants : République fédérale d'Allemagne, Autriche, Belgique, Danemark, Espagne, Finlande, France, Italie, Japon, Norvège, Pays-Bas, Portugal, Royaume-Uni, Suède, Suisse et Turquie.

For information please write to:

NEA Data Bank

Pour toute information s'adresser à :

Banque de Données de l'AEN

**F91191 Gif sur Yvette CEDEX
France**

Tél. (6) 908 49 12 - (6) 908 46 53 - Télex NEADATA 690920 F - Télégr. NUCLAGENCE GIF - 91191 Gif sur Yvette

**INTERNATIONAL NUCLEAR MODEL AND CODE COMPARISON ON
PRE-EQUILIBRIUM EFFECTS**

H. Gruppelaar
Netherlands Energy Research Foundation ECN, Petten

P. Nagel
NEA Data Bank, Gif-sur-Yvette, France

Abstract

The results of an International nuclear model and code comparison on pre-equilibrium effects are presented and discussed. Participants from fourteen laboratories calculated reaction cross-sections, emission spectra and angular distributions on the nucleus ^{93}Nb with incident neutron energies ranging from 10 to 25.7 MeV. The results of twenty computer codes are analysed and compared to experimental data. The different classes of physical models underlying the codes (exciton, hybrid and modified Hauser-Feshbach) are compared. Recommendations for future development of the models and codes are presented.

Other nuclear model comparisons available from the NEA Data Bank

- **Determination of Average Resonance Parameters**
NEA Data Bank Newsletter No. 27, July 1982
- **Spherical Optical and Statistical Model**
NEANDC-152"A"; INDC(NEA)4 October 1983
- **Coupled-Channel Model**
NEANDC-182"A"; INDC(NEA)3 January 1984
- **Spherical Optical Model for Charged Particles**
NEANDC-198"U"; INDC(NEA)5 May 1985

ERRATUM

Table of Contents

1 Introduction	7
2 Received contributions	8
3 Angle- and energy-integrated cross sections	9
4 Angle-integrated total emission spectra	11
5 Angular distributions	14
6 Photon-production spectra	18
7 Model description and intercomparison	19
8 Conclusions	22
9 References	24
Tables 1-4	29
Notes to Tables 1-4	45
Tables 5-6	49
Participants' notes to Table 6	54
Figure captions	69
Figures	72
Codes available from the NEA Data Bank	105
Appendix A: Specifications of the comparison	117
Appendix B: Participant Questionnaire	131

N.E.A. DATA BANK

PRE-EQUILIBRIUM EFFECTS
An International Nuclear Model and Code Comparison

Newsletter No. 32
September 1985

Table of Contents

1 Introduction	1
2 Received contributions	2
3 Angle- and energy-integrated cross sections	3
4 Angle-integrated total emission spectra	5
5 Angular distributions	8
6 Photon-production spectra	12
7 Model description and intercomparison	13
8 Conclusions	16
9 References	18
10 Tables 1-4	23
11 Notes to Tables 1-4	39
12 Tables 5-6	43
13 Participants' notes to Table 6	48
14 Figure captions	63
15 Figures	66
16 Codes available from the NEA Data Bank	99
17 Appendix A: Specifications of the comparison	111
18 Appendix B: Participant Questionnaire	125

1 Introduction

This report contains the final results of an international effort to compare statistical nuclear models and codes that calculate reaction cross sections, emission spectra and angular distributions, taking into account pre-compound or pre-equilibrium effects. These models are widely used in nuclear data evaluations and in predictions of neutron-induced reaction cross sections at energies of 5 to 50 MeV, i.e. in an energy range that is of interest for technological applications. The specification of the exercise is given in the appendix (NEANDC-177U). The participants were asked to calculate cross sections of neutron-induced reactions on Nb-93 at incident energies of 10, 14.6, 20 and 25.7 MeV. This nucleus was chosen because it is well-studied, both experimentally and theoretically, and because pronounced precompound effects were observed in neutron emission spectra at 14.6 and 25.7 MeV. At lower incident energies (below 5 to 10 MeV) precompound effects become of minor importance and the usual Hauser-Feshbach models with a correction for width fluctuation effects could be used.

This report is organised in the following way. Section 2 gives a survey of the received contributions that are grouped into three classes: A, B and C. First, the angle- and energy-integrated cross sections are discussed, using tables for the four incident energies and the three classes (Section 3). Then, in Section 4, the total neutron-emission cross sections are given in a series of figures for two incident energies (14.6 and 25.7 MeV) and for each class. The discussion includes a comparison with experimental data (class D) as well. Next, the corresponding angular distributions are reviewed. Figures are shown of Legendre coefficients, of spectra at various angles and of angular distribution functions at two fixed outgoing energies. These results - based upon quite recent models - are discussed in Section 5. The last results reviewed in this report concern the total photon-production spectra, see Section 6. After these calculated results the physics of the nuclear-model codes is discussed, following the participants' responses to the questions formulated in the appendix. Finally, some conclusions are presented, including a few recommendations for future development of the models and codes.

2 Received contributions

The contributions received are as follows:

Class A, Modified HF codes, unified models

STAPRE (IRK), S. Wiboolsak, B. Strohmaier, M. Uhl [1]
STAPRE (LLL-1), D.G. Gardner, M.A. Gardner [2]
GNASH (LAS), P.G. Young [3]
GNASH (JAE), K. Shibata [3]
EMPIRE (IBJ), M. Herman [4]
PERINNI (ECN-1), H. Gruppelaar, H.A.J. van der Kamp [5]
HAUSER-V (TRM-1), S.B. Garg, A. Sinha [6]
TNG (ORL), C.Y. Fu [7]

Class B, Exciton-model codes (spin-independent)

PRANG (ECN-2), H. Gruppelaar, H.A.J. van der Kamp [8]
PEQGM (SLO), E. Béták [9]
PREM (TOH), G. Keeni, S. Yoshida [10]
PREANG1 (TRM), S.B. Garg, A. Sinha [11]
PRECO-D2 (TNL-1), C. Kalbach [12]
PRECO-D2 (TNL-2), with updated Q-factor, C. Kalbach [12]
AMAPRE (TUD), H. Kalka, D. Hermsdorf, D. Seeliger [40]

Class C, Hybrid and geometry-dependent hybrid models

ALICE hybrid + evaporation model (LLL-2), M. Blann [13]
ALICE GDH + evaporation model (LLL-3), M. Blann [13]
ALICE, GDH + evaporation model - refraction (LLL-4), M. Blann [13]
SECDIST + HF model (KFK), I. Broeders, U. Fischer, H. Jahn,
E. Wiegner [14,46,47] (belongs also to Class A)
EMPIRE (IBJ), M. Herman (belongs also to class A) [4]

Angular distributions are calculated by the codes:

GNASH (LAS), TNG (ORL), PRANG (ECN-2), PREANG1 (TRM-2),
PRECO-D (TNL-1), PRECO-DG (TNL-2), AMAPRE (TUD),
ALICE (LLL-2), ALICE (LLL-3), SECDIST (KFK).

Gamma-ray data are calculated by the codes:

STAPRE (IRK), STAPRE (LLL-1), GNASH (LAS), EMPIRE (IBJ), TNG (ORL),
PEQGM (SLO).

The same reactions as considered in this paper have recently been studied in other references, e.g. in [65] by Reffo et al. (IDA-PENELOPE), in [64] by Marcinkowski et al., in [67] by Strohmaier (STAPRE), and very recently in [68] by Herman et al.

3 Angle- and energy-integrated cross sections

The calculated angle- and energy-integrated cross sections at incident energies of 10, 14.6, 20 and 25.7 MeV are given in Tables 1A, B, C to 4A, B, C, respectively, where A, B and C indicate the classification given in the previous section. The numbers in parentheses represent the results from the full equilibrium calculation. For further details concerning the data, we refer to the "Notes to Tables 1-4", Sect. 11. In tables 1D to 3D, we give some results from experimental data without allowance for pre-equilibrium contributions. This survey is far from being complete: the experimental data have been taken from references or graphs that were easily available. Their purpose is only to give some impression of the experimental values.

Some observations of tables 1-4 are:

1. There are no serious problems in the optical-model calculations ($\sigma_t, \sigma_{el}, \sigma_r$).
2. There is quite good agreement in the calculation of σ_{nnx} (maximum standard deviation is at 25.7 MeV: $\pm 4.4\%$). The PREM results show the largest deviation, at least at 25.7 MeV (-8.7%). The ALICE results are inconsistent with σ_r . Note that the equilibrium results are in excellent agreement, except for the HAUSER-V results at low energy.
3. With respect to the σ_{npx} data, there is not much agreement; the standard deviation is 37% to 50%. However, the equilibrium calculation is also quite uncertain: $\pm 50\%$ at low energies up to 30% at 25.7 MeV.
4. For the calculation of σ_{nax} , the situation is still worse: the standard deviations range from 30% to 60%; for the equilibrium results they vary from 30% to 70%. Extremely low cross sections are calculated by PREANG1.
5. In view of the large discrepancies in the proton and α -particle data we do not discuss further the cross sections in which these particles are involved ($np\gamma, npn\gamma, n\alpha\gamma, n\alpha n\gamma, npem, n\alpha em$) and restrict ourselves to the neutron and photon data. For more information we refer to literature: e.g. [67].
6. For the calculations of $\sigma_{nn'\gamma}, \sigma_{n2n\gamma}$ and $\sigma_{n3n\gamma}$ (without the results indicated by an asterisk in Tables 1-4), we find quite acceptable results, with a standard deviation of less than 10% for high values of these cross sections (>500 mb), except at $E=10$ MeV. In general the codes of Class A are superior, although reasonably good results can also be obtained with codes of Class B as follows from the tables. We note that the difference between the PERINNI results and the other codes at 10 MeV is partly due to the use of the back-shifted Fermi-gas formula, rather than the Gilbert-Cameron level density. This follows from additional information provided by the participants.
7. The standard deviation of the calculated total neutron-production cross sections is less than 5%. However, the pre-equilibrium contribution in this quantity is rather small (at most 23% at 25.7 MeV). Note that the hybrid model codes also give good results.

8. With respect to the total photon-production data, we notice reasonably good agreement between the class A codes that calculate these quantities: STAPRE, GNASH, TNG and EMPIRE. The results of PEOGM are much higher. Again, the pre-equilibrium effect is not large in this lumped quantity.
9. Some codes also calculate cross sections for the population of isomeric states; see Table 5.

Some conclusions are as follows:

The calculation of σ_{nnx} is generally satisfactory, although in some codes there is no consistency with the total reaction cross section (the codes should automatically check and eventually correct this discrepancy). The calculation of the much weaker σ_{npx} and σ_{nox} cross sections is unreliable. In particular the treatment of the α -emission needs more care. The calculation of multi-particle emission cross sections is difficult near thresholds: the energy grid is not always fine enough and perhaps no appropriate corrections are made if only part of a "bin" can be further emitted.

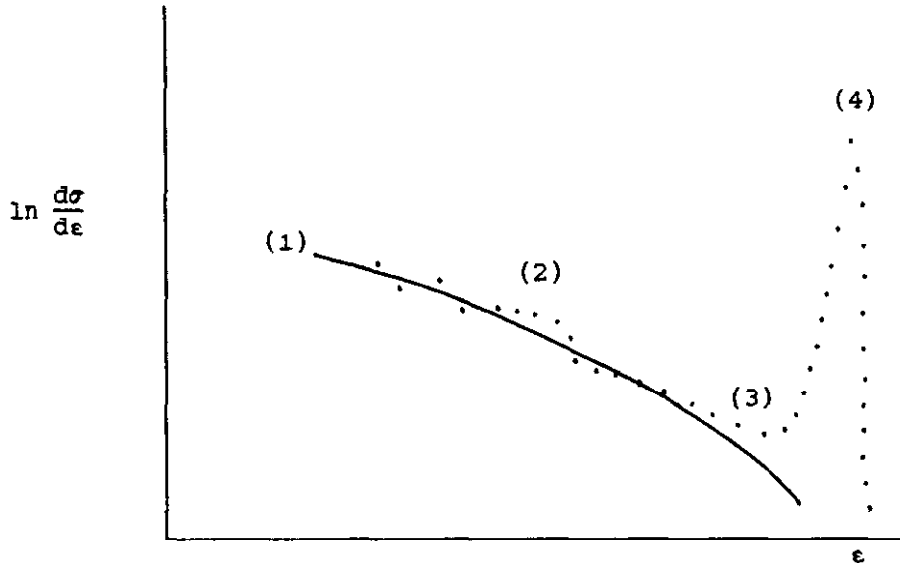
In codes of class B and some of class C, where the level density is described by a continuum over the whole energy range, it is important to utilise a realistic level-density expression at low energies, otherwise the (n,2n) and (n,3n) cross sections cannot be calculated with high accuracy. Again it is necessary to check the consistency of the multi-particle emission with the first-emission cross sections. Some results of 10 MeV need to be inspected more closely, mainly because the (n,2n) threshold is relatively low. Probably the γ -ray competition is important as well (it is neglected in most codes of classes B and C). We feel that most codes of classes B and C need further development in the following directions:

1. Refinement of multi-particle emission treatment with respect to energy mesh and integration.
2. More realistic description of the level density at low energies, in agreement with experimental level schemes (or introduction of discrete-level excitation).
3. Introduction of γ -ray competition.

Our impression is that the neglect of angular-momentum conservation is not the prime reason for some differences between the results of classes A and B+C. This follows for example from a comparison of PERINNI and PRANG results.

4 Angle-integrated total emission spectra

Before discussing the calculated results, the following general introduction is given.



The measured neutron spectrum at higher outgoing energies typically shows the following features illustrated in the above figure:

1. A uniform background attributable to pre-equilibrium emission. This may be calculated from the theories reviewed here, and the resulting cross section should always be on or below the data. If this is not the case it is an indication of a defect in the theory or in the (level-density) parameters used or in the data. Another possible cause of deviations between the background and the measured cross section is an abnormal fluctuation in the level density in a particular energy region, this could perhaps be found by a shell-model calculation.
2. Broad resonances attributable to giant collective states [74]. These are a feature of the target nucleus and show a systematic variation with the atomic number.
3. An excess of high-energy particles attributable to collective excitations of low-lying states. These are specific for the target nucleus and the corresponding cross sections may be calculated from the coupled-channels theory or DWBA.
4. A huge elastic peak appears at the highest energy end of the spectrum. Since the shape of this peak is not exactly known there may be elastic contributions to region (3).

There is some uncertainty about what exactly the various precompound models do calculate. By their nature, direct-collective excitations are not calculated explicitly by the precompound models, since only excitations of particles and holes are considered. Therefore, we expect that the precompound

models will underpredict the emission spectra at high energies, where other models are needed in addition to the exciton model. The excitation of giant collective states should also be calculated and added to the cross section. In the GDH models there is increased emission to simple states as compared with the exciton models, often giving better agreement with the experimental data. However, no collective excitations are included explicitly in the GDH model. If the parameters of the exciton model are obtained by fitting selected data, the calculated cross sections will include some of the effects of collective excitations, even though these are not included explicitly in the formalism. Due to the large number of approximations in both the exciton and the GDH model, it is difficult to draw firm conclusions about their domain of validity. We note that the parameters of the GDH/hybrid models are usually not varied.

Further progress could be achieved by using existing analyses of giant resonances excited by proton inelastic scattering, and by coupled-channels calculations of the contributions of low-lying collective states to the measured neutron inelastic cross section. This problem is encountered in all analyses of pre-equilibrium processes, including those using the fully quantum-mechanical theories. It will not, however, be possible to start this work in a meaningful way until the discrepancies in the existing data are resolved.

The angle-integrated total emission spectra of the codes mentioned in Section 2 (except for PERINNI and PRECO-D2) have been plotted in Figs. 1 to 4 for incident energies at 14.6 and 25.7 MeV. The results are displayed for each class A, B and C separately on linear-logarithmic and double-logarithmic scales. The results from one code, GNASH-LAS (because it represents a kind of "average") are connected by straight-line segments in Figs. 1 to 4 for interrelation purposes. Please note that in many cases the points refer to the mid-energies of bins (histogram). Some available experimental data have been plotted in Figs 1D, 2D, 3D and 4D, again together with the GNASH results.

Some observations of Figures 1 and 2 ($E = 14.6$ MeV) are:

1. There is good mutual agreement for outgoing energies from about $\epsilon = 1.5$ to 10 MeV, except for some results of class C. We note that the participants were free to adjust a parameter to fit data in the range from 6 to 9 MeV (see Fig. 1D). It seems that most participants have used their default values for C or K (Table 6), whereas the (geometry-dependent) hybrid-models have essentially no free parameters. The last-mentioned codes (class C) give lower cross sections near 8 MeV. We also note that the experimental data of Hermsdorf et al., as specified in the exercise, are rather high compared with other experimental data (Fig. 1D).
2. The problems at low energies ($\epsilon < 1.5$ MeV) are threefold:
 - a. there is a considerable spread in the calculated results, with maximum values for AMAPRE (Figs. 2A, 2B, 2C);
 - b. there is considerable spread in the experimental data as well (Fig. 2D);
 - c. below 0.5 MeV the mesh size is for most codes not fine enough to represent the left-energy tail of the evaporation peak. We note that the spread in the calculated data is related to the different shapes of the

spectra; The absolute values of $\sigma_{n\text{nem}}$ are in quite good agreement (Table 2).

Therefore, the differences are partly due to different pre-equilibrium fractions and also due to the choice of the mesh size that is usually equidistant (exception: PRANG code). We feel that for technological applications some special care is needed to represent the shape of the evaporation peak at the lowest energies.

3. At the high-energy end of the spectra ($\epsilon > 10$ MeV) there is considerable spread both in the calculated and in the experimental data (Fig. 1). The exciton-model codes (classes A and B without EMPIRE) give similar shapes, except that the end point of the spectrum is not the same. This could be related to the level density, in particular to the pairing-energy correction. As an example we refer to the results of STAPRE (LLL-1) with $P=0.72$ MeV and those of PRANG with a shift of opposite sign: $\Delta = -0.50$ MeV. This leads to (extrapolated) endpoints of 12.6 MeV and 14.5 MeV, respectively (see Figs 1A, 1B). This discrepancy could be avoided, because it is possible to adjust the summed (p,h) level densities to agree with the experimentally observed level density at low energies (from the level scheme). Such procedures have been followed in PRANG, TNG. In the last-mentioned code also a realistic pairing-energy correction was introduced [16].

The geometry-dependent hybrid models (EMPIRE, ALICE-LLL3, SECDIST) predict somewhat different shapes, with higher cross sections at high energies and lower values near 8 MeV (Fig. 1C). Comparison between the hybrid and geometry-dependent hybrid models (LLL-2, LLL-3) shows that the relatively high cross section at high emission energies is mainly due to the geometry effect included in the GDH model (and not primarily due to level density). It is quite difficult to compare the different shapes with the experimental data that are rather uncertain due to the subtraction of a huge elastic peak and background. Another point is that the precompound models do not claim to predict direct-collective excitations; these cross sections are usually calculated with a coupled-channels or DWBA model. Direct single-particle excitations are, however, included in the precompound models, though in a statistical way. These excitations ($n=3$) are enhanced in the GDH model at the highest emission energies.

Next we discuss the results at 25.7 MeV incident energy (Figs. 3 and 4). For these calculations the same parameters were used as for the 14.6 MeV results. Hence, the predictive power of the models is tested to a certain extent. Unfortunately there is only one set of experimental data (Fig. 3D) with data points only above $\epsilon = 12$ MeV [38]. We have made the following observations:

1. There is considerably more spread in the calculated spectral shapes compared with the calculation at 14.6 MeV. The GDH-results show a flatter shape at high outgoing energies, where the other codes give generally lower values. Again this is ascribed to geometry effects included in the GDH model. Differences between the various exciton-model codes are probably due to the adopted (p,h) level densities, including pairing-energy corrections and due to differences in the predicted precompound fractions.

2. Comparisons with experimental data [38] in between $\epsilon = 12$ and 17 MeV shows that for most codes there is agreement within 25% (except SECDIST, ALICE-LLL2), whereas at higher energies most calculations underpredict the measurements. The best results at high energies are given by the GDH models EMPIRE and ALICE-LLL3. From the other models the results of PRANG and PREM are relatively high, though below the experimental values. The experimental data show some structure, perhaps indicating direct-collective enhancements [64]. The geometry effects introduced in the GDH model enhance the high-energy part of the spectrum. However, this range is also quite sensitive to the shape of the (p,h) state density for the most simple excitations. A rather simple formula has been used for these densities, and more realistic expressions may give different outcomes.
3. At the lowest excitation energies it is again the representation of the evaporation peak that needs further attention (see below).

Although we feel that more care is needed to represent both the low-energy and the high-energy parts of the spectra as discussed before, we do not see clear advantages in the use of the more expensive codes from class A as compared to application of codes B+C for the calculation of the total neutron-emission spectra.

Relatively simple improvements are possible if the grid size is decreased at low energies and if the pairing energy is calculated more realistically [16] in addition to a fit of the sum of all (p,h) level density at low excitation energy. Another point to consider is whether geometry effects should be included in the exciton model (cf. [79]) to enhance the high-energy part of the $n=3$ component, as in the GDH model, or whether other codes should be used to calculate the excitation of collective states.

5 Angular distributions

The angular distributions of the emitted neutrons as a function of incident and outgoing energy reflect the changing proportions of the compound and multi-step-direct processes. At low incident energies compound processes dominate and the angular distributions of the outgoing neutrons are symmetric and usually nearly isotropic. As the incident energy increases the proportion of multi-step-direct processes rises, and this predominantly affects the more energetic outgoing neutrons. These changes in the character of the angular distributions may be conveniently displayed by plotting the relative coefficients

$$f_{\ell} = \frac{a_{\ell}}{a_0(2\ell+1)}$$

of the Legendre-polynomial expansion of the angular distributions. A symmetric distribution has all coefficients with ℓ odd identically zero, and if it is nearly isotropic all f_{ℓ} for $\ell > 0$ are small. Approximate expressions for f_{ℓ} at low emission energies are given in Refs. [48, 49, 76] for multi-step-compound reactions. As the outgoing energy increases, so does the proportion of multi-step-direct processes (and so f_1 and f_2 increase as well). This is shown in Fig. 5. At a high incident energy we expect the f 's to be larger, and this is

shown in Fig. 6. It should be noted that the absence of experimental data at small and large angles leads to considerable statistical uncertainties in the values of the f -coefficients. Furthermore, there are notable inconsistencies between the cross sections measured by different observers and this further increases the difficulty of comparing the experimental and theoretical angular distributions.

Any giant resonances that are superposed on the pre-equilibrium background have characteristic angular distributions that could produce localised peaks in the f -coefficients. For the reasons already mentioned, these would be difficult to observe. The collective states at lower energies in the final nucleus have much smaller widths and their characteristic angular distributions are observed if the experimental resolution is adequate.

The four main approaches are:

1. Systematics of Kalbach and Mann [15], in which a separation is made between multi-step direct processes and multi-step compound processes (assuming a symmetric distribution for MSC). This method has been applied in the codes PRECO-D2, GNASH. The systematics is based upon a large number of different experimental data, although relatively few neutron data have been used. At low incident and outgoing energies, the results could be uncertain. In PRECO-D2 the (MSC) systematics is also used for the compound part. In GNASH the systematics has been modified at low emission energies in such a way that each coefficient is forced to go linearly to 0 as E' goes to 0 for emission energies E' below 6 MeV (the original KM equations produce coefficients that are non-zero at $E'=0$). This is of great importance to the behaviour of f_2 at low emission energies (see below; Figs 5B, 6B). A somewhat more refined modification scheme is given in Ref. [66].
2. Generalized HF theory [16] that uses the rigorous expressions for the angular distribution in the limit of no precompound effects. A parametrization has been used to estimate the fraction of precompound angular distribution. This method has been applied in the code TNG.
3. (a) The approach of Mantzouranis et al., [17, 18] in which the "fast" particle is followed on its way through the nucleus, using the angular distribution of free nucleon-nucleon scattering in the nucleus. This method has been applied in the code PREANG1. In addition refraction effects have been introduced in the code PREANG1, i.e. maximum refraction of the incoming beam [18]. This large refraction is only possible at low energies. In Ref. [18] also adjusted coefficients of the scattering kernel were used with some success. This method was also followed by Marcinkowski et al. [64] in the analysis of 25.7 MeV data. Non-adjusted coefficients were used in the contribution by Garg and Sinha, presented in this report (TRM-2).

(b) Angle-energy correlated intra-nuclear scattering models [19, 20] are in fact a generalisation of the model of Mantzouranis et al., using the Kikuchi-Kawai expression [45] for nucleon-nucleon scattering in nuclear matter. This method has been applied in the codes PRANG, AMAPRE, ALICE/LIVERMORE. In PRANG (and AMAPRE) the KK expression is used only for the first collision; it is shown [19] that this approximation is well justified. Although refraction effects should be treated with quantum-mechanical theory, quasi-classical estimates have been made in Refs. [19,20]. Diffraction effects are not accounted for. The PRANG and

AMAPRE results include refraction (although different values are used). Blann has supplied results with and without refraction (and diffraction); most results shown in Figs. 7-16 are without refraction (the effect of refraction is to reduce the forward peaking and to enhance the backward angle cross sections, see Figs. 13 and 14). We note that refraction and finite-size effects are treated differently in PRANG and ALICE. In PRANG a truncated Legendre-polynomial expansion ($L \leq 6$) is adopted. Furthermore an adjustment has been made to obtain f_2 -values that are in agreement with the systematics; see dashed curves in Figs. 5 and 6. This adjustment ensures that the scattering kernel remains positive at all backward angles [76]. Other applications of this theory have been reported by Reffo et al. [65].

4. Angular distribution from direct reaction models using PWBA have been applied in the code SECDIST [14, 46, 47]. With this method isotropy is assumed for all contributions with $n > 5$, whereas for $n = 3$ the angular distribution from a simple PWBA model is used for one value of L ($L = 3$ was selected in the present exercise), see Refs. [46, 47]. The contributors claim that this choice is based upon shell-model considerations. This approximation was made as a first attempt to solve the benchmark problem within the limited time available. Related methods have been proposed by Sal'nikov [70] and Luk'yanov et al. [71].

The results of the calculations are displayed in a series of figures (5-16). First we discuss the figures where reduced Legendre coefficients have been plotted. This method of representation separates the angle-integrated and angular distribution parts of the cross section. Unfortunately, we have not in all cases the data expressed in this representation. In Figs. 5A and 6A the results of the first three approaches are given (codes GNASH, TNG, PRANG). Figs. 5B and 6B give a detailed comparison between the original Kalbach-Mann systematics (used in PRECO-D2) and the results of GNASH and PRANG. We note that there is a quite good agreement with the f_1 and f_2 coefficients, indicating that the models describe the multi-step direct part of the cross section surprisingly well (note that there are no fit parameters used in the PRANG code for the odd-order Legendre coefficients). For the second-order coefficient f_2 , there are some problems, in particular at low outgoing energies (see results at 25.7 MeV), but also with regard to the absolute values. The (adopted) PRANG curve labelled "adj" has been adjusted to "systematics", with a renormalisation factor (actually a different value of μ_2' , see Ref. [19]). It is interesting to note that the (multi-step) compound contribution at low outgoing energies is relatively high in the code TNG for the incident energy at 25.7 MeV (Fig. 6), in contrast to the situation at 14.6 MeV (Fig. 5). Since the TNG code should give rather exact results at low outgoing energies, it seems that this is some failure of the other models (in the original KM systematics the MSC angular distribution is probably overestimated at low outgoing energies; see Figs. 5B, 6B).

Our preliminary observation is that a multi-step compound component might be needed to increase the values of the even-order coefficients at low emission energies. This increase should probably be much less than predicted by the original (unmodified) Kalbach-Mann systematics (see Figs. 5B and 6B). On the difference (at low emission energies) of the TNG results at 14.6 and 25.7 MeV the readers should inspect the notes to table 6 (TNG), which indicate that f_2 might be overestimated by TNG at both incident energies. We conclude the additional MSC-compound is probably quite small.

Next we discuss the graphs (Figs. 7-12), where the double-differential cross sections are given for three different outgoing energies and two different incident energies. It has to be noted that the outgoing energies may not be exactly the same and that they may also represent an average over some outgoing energies. Furthermore, as the angle-integrated cross sections are not the same, the absolute values are different. Therefore we restrict ourselves to discuss here only the shape of the curves.

The results of the codes PRECO-D2, TNG, PRANG with adjusted kernel for f_2 , (see Figs. 5A, 6A), PREANG1, ALICE, AMAPRE and GNASH are indicated in Figs. 7 to 12. The GNASH results (modified KM systematics) are indicated by a full curve.

In the codes PREANG1 and PRECO-D2 (option TNL-2 has not been plotted) only first-emitted neutrons are considered; therefore the E' -range has been restricted to high values. The ALICE (LLL3) data are only given for the pure n-n scattering (no refraction nor finite-size effects; see below). The SEC-DIST results are not available in this form; they are discussed in the last paragraph of this section, see Fig. 18.

The experimental data in Figs 7 to 12 are from the recent measurements of Takahashi et al. [37] at 14.15 MeV and of Marcinkowski et al. [38] at 25.7 MeV. No corrections have been made for the elastic peak. Corrections for multiple scattering have only been made in the 25.7 MeV data; important corrections for this effect are needed in the 14.6 MeV data at low emission energies.

We conclude from Figs. 7 to 12 that the calculated shapes of most calculations are in good mutual agreement (the ALICE data have a different shape; no refraction effects have been included; the PREANG1 data are systematically too low at backward angles). The comparison with experimental data is difficult, in particular at 14.6 MeV. The fact that the angle-integrated data were (in most cases) fitted to the systematically higher data of Hermsdorf et al. [39] has to be considered. Still, the angular dependence is roughly reproduced by most codes, except for the PREANG1 results (corresponding to an early model), and the ALICE results (without refraction).

Finally, we inspect the angular distributions as given in Figs. 13 to 16 at two incident energies and two outgoing energies in the precompound range. The effect of refraction to the ALICE results is shown in Figs. 13 and 14. The same symbols are used as before. The experimental data in Figs. 13 to 16 were obtained by the compilers by averaging over intervals of 5-7 MeV and 7-9 MeV, respectively. The "error bars" are very conservative: they indicate the minimum and maximum values in the intervals. Please note that the incident energies in Figs. 13 and 14 vary by angle: at 15° the value of E' is 14.85 MeV, leading to relatively high cross section values; at 143° the value of E' is 13.47 MeV, probably leading to too low cross section values. Furthermore, there is some structure in the data at 7-9 MeV (a "peak" appears at 30° and 37°). The experimental data in Figs. 15 and 16 are from Marcinkowski et al. [38] without further corrections.

The calculated data are different in absolute value. This is partly due to differences in the value of E' (a low value of E' means a higher cross section) and partly due to differences in the angle-integrated cross sections. The shapes of the PRANG, AMAPRE, TNG, GNASH and PRECO-D results are quite consist-

ent (Figs. 13-16), in agreement with the picture given in Figs. 5, 6 (Legendre coefficients). The PREANG1 (TRM2) results show low backward-angle values. The ALICE (LLL3) results are clearly different in shape compared to all other results: there is considerably more forward-peaking whereas the backangle cross sections are too low. Quite similar results are obtained with the PRANG code if pure n-n scattering without refraction is adopted and if a large number of Legendre polynomial coefficients are used (not shown in figures). However, in the results with refraction effects and finite-size effects included (LLL4) the forward-peaking is very much decreased, whereas the backward-angle contribution is increased; see Figs. 13 and 14.

Comparison with experimental data is difficult because there are serious discrepancies, in particular between the data of Hermsdorf et al. [39] and those of Takahashi et al. [37] and Kammerdiener [73], see Fig. 17, suggested by Bahn and Jahn. Still, some conclusions are possible. First of all we note that at backward angles most theories are probably not too bad (PREANG1 is too low). At forward angles the experimental data at high outgoing energies might indicate that improvements are necessary (Figs. 15, 16). We feel that the forward peaking of ALICE (LLL3) is far too much whereas that of the other codes could be somewhat too small. In fact, the ALICE results agree better with data measured by Takahashi et al. (or Kammerdiener's data) than with those of Hermsdorf et al. The results of the other codes are in better agreement with the data of Hermsdorf et al. It is of prime importance to find the reason for the discrepancy in the experimental data (Fig. 17).

The results of SECDIST (KfK) are given on a separate graph (Fig. 18), provided by the participants. The calculations are based upon a PWBA method, where one value of L (transferred angular momentum) has been selected (L=3), as shown in Fig. 18. The 25.7 MeV results are preliminary. The contributor remarks that these results show a diffraction pattern typical of PWBA approximations; for L=3 also a minimum at forward angles appears.

We note that the PWBA method has some well-known deficiencies and in most applications the PWBA is replaced by the DWBA method. We also note that from experimental evidence the cross section is high in the forward direction.

6 Photon-production spectra

Total photon-production spectra have been calculated at E=14.6 MeV by the codes STAPRE (IRK, LLL-1), GNASH (LAS, JAE), TNG (ORL), EMPIRE (IBJ) and PEQGM (SLO).

The first two codes are well-known and are documented in Refs. [1-3]; they include angular-momentum conservation and follow the γ -ray cascade until eventually discrete levels with known branching ratios are reached. The photon emission spectra from the continuum and from the discrete levels are accumulated from all reactions. In the continuum E1, M1 and E2 transitions are considered. The γ -ray emission is treated as in the compound model: no n-dependent γ -ray emission rates are used. Pre-equilibrium effects are the result of different populations of the states. In these codes the spin-populations of the states that emit γ -rays (or particles) are not affected by pre-equilibrium emission. No direct and semi-direct γ -emission is calculated.

In the codes TNG [7] and EMPIRE [4] similar methods are followed for the calculation of γ -ray emission data (as compared to STAPRE and GNASH), except that the spin-populations are affected by pre-equilibrium excitation. However, no n-dependent γ -ray emission rates have been introduced.

The last-mentioned code PEQGM [9] does not account for angular-momentum conservation nor for excitation of discrete levels. It has, however, the interesting feature that precompound γ -ray emission is considered. This is important for the (n,γ) reaction at high energies. In the model of Bětáček and Dobeš [62] there is an n-dependence in the γ -emission rates; furthermore only transitions with $\Delta n = 0$ or -2 are allowed. The Brink-Axel estimate has been generalised to include an n-dependence. This leads to enhanced γ -ray emission from simple states; no external calculation of direct and semi-direct reactions seems to be required [63], cf. [76],[83].

The results of the photon-production spectra at $E=14.6$ MeV are displayed in Fig. 19. The γ -ray data in Tables 2 and 5 are also relevant in the discussion. Details about the calculational methods and constants are given in the participants' notes to Table 6.

From Fig. 19 it is seen that there is good agreement between the various codes at emission energies above 2.5 MeV except for the results of PEQGM (JAERI results have not been plotted, since there seems to be an error in the results). The PEQGM results show the giant-dipole resonance in the (n,γ) -spectrum and are also higher at most other energies. Please note that also the equilibrium results are much higher than corresponding values calculated by other codes (Tables 2A, B). Furthermore, the $(n,\gamma x)$ cross section calculated by PEQGM seems to be too high compared with experimental data (see Tables 2B and 2D).

At low energies (below 1.34 MeV) the γ -rays from discrete inelastic scattering contribute. Please note that the data plotted are actually grouped into bins of different sizes for the various contributions.

7 Model description and intercomparison

The codes reviewed in this comparison are divided into three classes, broadly described as Hauser-Feshbach with precompound option, Exciton model, and (Geometry-Dependent) Hybrid model. Within each class the codes differ in the ways summarised in Table 6 (see also participants' notes to Table 6), and in the following discussion.

We do not discuss here the fully quantum-mechanical theories of pre-equilibrium reactions as proposed recently by Feshbach et al. [50] and by Tamura et al. [51, 52]. These models have recently been reviewed at a conference [61]. Also not discussed is the much simpler model for direct reactions proposed by Luk'yanov et al. [71]. The last-mentioned authors neglect emission from states with exciton number larger than 3 ($n = 3$ is in all models the most important pre-equilibrium component). We refer to a review by Sal'nikov [70] for further discussions on this model. A critical review of precompound models has recently been given by Jahn [47].

A. Hauser-Feshbach codes with precompound option

These use the Hauser-Feshbach formalism which ensures angular-momentum conservation and allows the cross sections of reactions to discrete final states to be calculated. They are applicable over a large energy range (at low energies a width-fluctuation correction is applied) but are expensive to run because of the imposition of angular-momentum conservation and the large memory required. The angular distribution to continuum states is calculated only by TNG ("generalised" HF theory) and in the GNASH-contribution (modified KM systematics). All codes except EMPIRE use the exciton model for the pre-equilibrium part (EMPIRE uses the GDH model, see below). Pre-equilibrium is treated as a correction in all codes except PERINNI where there is no separation between equilibrium and pre-equilibrium. The spin-parity population is assumed to be unaffected by precompound effects, except in the TNG, PRANG and EMPIRE codes. Most codes give the energy- and angle-integrated cross sections, the angle-integrated particle spectra, multi-particle emission and gamma-ray cascades. Level densities are obtained from the Gilbert and Cameron or backshifted Fermi-gas formulae [21, 22], and the particle-hole density from the formula of Williams [23] with various corrections. The cross sections to discrete levels may always be calculated, but not always their pre-equilibrium contribution. Internal transition rates are obtained by the formulae of Williams [23] or of Oblozinsky [24]. The R- and Q-factors in the emission rates are usually normalised to unity for large n , and the special case of alpha-emission is treated in a variety of ways. Inverse reaction cross sections are used in the pre-equilibrium part (except for PERINNI, TNG and EMPIRE). Gamma-ray emission is included using specific expressions for the E1, M1 and E2 emission rates, where the E1-emission is based upon the Brink-Axel estimate. The spin-parity population is assumed to be unaffected by pre-compound effects, except in the TNG code.

B. Exciton model codes

These codes do not include explicit angular-momentum conservation and have no large memory requirements and so are simple and fast, although there is more sophistication in the precompound aspects of these codes than introduced in most of the class A codes. The Weisskopf-Ewing model is used, extended to include pre-equilibrium. It therefore does not give cross sections to discrete final states, and so is restricted to higher energies ($> 5\text{MeV}$). These codes are particularly suitable for phenomenological studies, studies on the effect of various model assumptions, and parameter search, in particular at energies high enough above thresholds (due to level-density breakdown). They may be less useful for a complete data evaluation, although recent improvements (level density, γ -ray competition, multi-particle emission, angular distribution) are very promising and it is expected that in the near future these codes may successfully compete with those of class A, at energies above 5 MeV [76]. It also seems very well possible to introduce discrete-level excitation (without accounting for spins and parities). Most exciton codes use a master equation and treat equilibrium and pre-equilibrium in a "unified" way. In general they still have less options than codes of class A. The level-density formula of Williams [23] is used, often with $g = A/13 \text{ MeV}^{-1}$ (which is rather too simple). Except for PEQGM there is no gamma emission included. In the last-mentioned code exciton-number dependent γ -ray emission rates have been introduced [62]. Angular distributions are calculated by several of these codes, using the

method of Mantzouranis et al., [45], recently improved by using the angle-energy correlated intra-nuclear scattering kernel [19], or by using systematics (separating multistep compound and multi-step direct contributions) [15].

C. (Geometry-Dependent) Hybrid Model Codes

These models originate from the work by Blann, see for example the review [34] and the recent paper [13]. The "hybrid" model is intended as a combination of the exciton model and the Harp-Miller-Berne model (see [34]). Its structure is very similar to the "never-come-back" approximation of the exciton model; however, different expressions for the mean lifetimes are used. In particular, the mean lifetime of the hybrid model refers to the particle under consideration and hence depends upon outgoing energy ϵ , whereas in the usual exciton model it is related to the nuclear system as a whole and is only a function of n . This results in a different expression for the internal transition rate $\lambda^+(\epsilon)$ that is derived from the concept of mean free path, rather than by a parametrization of the average transition matrix element $\langle M^2 \rangle$ and also in a different expression for the emission rate $\lambda_c^+(\epsilon)$ occurring in the mean lifetime. These different points of view have given rise to ample debate (see for example [35, 36]). Very recently the differences between the hybrid and exciton model have been discussed in Refs. [77,84]. For the present purpose it is important to note that the different ϵ -dependence causes differences in the shape of the emission spectra of the two models, see Figs. 1, 2 (LLL-2 is a hybrid model).

In the geometry-dependent versions of the model (LLL-3, KfK, IBJ) a decomposition is made according to incoming orbital angular momentum ℓ in order to account for the effects of the nuclear-density distribution [34]. This leads to increased emission from the surface region of the nucleus, and thus to increased emission of high-energetic particles, as can be clearly seen from Figs. 1 and 2. It seems not necessary to adjust the parameters in the expression for λ_c^+ in the reported GDH applications. This may give some confidence in their predictions.

The (GD)H models need to be supplemented with an evaporation model for the equilibrium part. Recently, the precompound part has been revised to describe multi-particle emission [13]. It has to be noted that the (geometry-dependent) hybrid model basically is an inclusive model, in contrast to the exclusive exciton model; see e.g. [77]. No angular-momentum conservation nor γ -ray competition is included in the pre-equilibrium part of the original model of Blann, also used at KfK [47]. These features are however introduced in the EMPIRE code (IBJ), that belongs to class A. At KfK a separate HF code HAFKA4 is used for the equilibrium part.

Recently, Blann et al. [20] have extended the GDH model with angular distributions, using the Kikuchi-Kawai expression [45], folded using the method of Mantzouranis et al. [17]. Basically, the approaches [19] and [20] are equivalent, though there are mathematical differences and the GDH model is used rather than the exciton model. At KfK the PWBA model is used to fit angular distributions by selecting a value L (transferred angular momentum), see [47] and Sect. 5.

8 Conclusions

In the present exercise the following codes were intercompared:

(A)	(B)	(C)
<u>HF + precompound</u>	<u>Exciton model</u>	<u>GDH model</u>
STAPRE (IRK,LLL)	PREM (TOH)	ALICE/LLL84 (LLL)
GNASH (LAS,JAЕ)	PRECO-D2 (TNL)	SECDIST/HAFKA (KFK)
HAUSER*V (TRM)	PREANG1 (TRM)	EMPIRE (IBJ)
PERINNI (ECN)	PRANG (ECN)	
TNG (ORL)	PEQGM (SLO)	
EMPIRE (IBJ)	AMAPRE (TUD)	

A comparison of the basic assumptions in these models was made. Promising new developments are the attempts to "unify" the precompound and compound models (PERINNI, TNG, PREANG1, PRANG, PEQGM), to include multi-particle emission (almost in all codes) and γ -ray emission (class A and PEQGM) and to describe angular distributions of continuum-particle emission (see below).

The overall results of the calculations of angle- and energy-integrated cross sections are quite consistent for the neutron-scattering reactions (n,n') and ($n,2n$). For the much smaller (n,p) and (n,α) cross sections large deviations were found. There are no distinct differences between the results of the much more expensive codes of class A and those of classes B and C (at energies above 10 MeV). This statement is true for the main quantities in the comparisons; it is not true in the sense that the class A codes provide more information than many of the smaller codes (e.g. discrete level excitation data, discrete γ -ray cross sections, isomeric state data). Action is needed to check the internal consistency of multi-particle emission in the codes, to improve the α -particle emission cross sections, to check the energy mesh and integration procedures in the codes and to assure correspondence between level density and experimentally observed level schemes (in classes B+C). Angular-momentum conservation and γ -ray competition are probably less important at high energies (for the main quantities in this comparison).

The calculated angle-integrated neutron emission spectra at 14.6 MeV incident energy are consistent from emission energies of 1.5 to 10 MeV, but there are problems at the lowest emission energies (evaporation peak) and at the highest emission energies (direct excitation of collective states). At low emission energies the grid size needs to be finer in general; at high emission energies level-density effects (pairing), geometry effects (GDH models give highest distributions) and effects of "discrete" level excitation (CC or DWBA) play a role. More problems were generally encountered at higher incident energies, where most codes underpredict the experimental data at high emission energies, indicating the presence of direct-collective excitations. In this respect the GDH codes give a better shape than most other codes, probably due to the "geometry effects". Again, no clear preference for the use of class A, B or C followed from the calculated results as compared to experimental data.

Finally, the angular distributions of continuum neutron emission were intercompared. The four methods used are:

- 1) Systematics of Kalbach and Mann (PRECO-D2; GNASH)
- 2) Generalised HF (TNG)
- 3a) Fast-particle method of Mantzouranis et al. (PREANG1)
- 3b) Angle-energy correlated intra-nuclear scattering (PRANG; AMAPRE, ALICE/LLL84).
- 4) PWBA (SECDIST/HAFKA).

The results of GNASH, PRECO-D (method 1), TNG (method 2) and PRANG, AMAPRE (method 3b) are quite consistent for the odd-order (reduced) Legendre coefficients. For the even-order coefficients methods 1 and 2 give higher values at low emission energies. This last-mentioned divergence of method 3 is due to the neglect of the anisotropy effect of multi-step compound processes. We note, however, that the magnitude of this effect at low energies is quite uncertain and might be overestimated in methods 1 and 2; see also [76]. The angular distributions of methods 1-3 at high emission energies are similar in shape, except for the ALICE results which are much more forward-peaked, at least when refraction effects are not considered in the calculations. Comparison with experimental data, though difficult, suggests that forward peaking might be somewhat underpredicted by most codes, whereas the ALICE results are probably too high at 0° .

The results of the present exercise are too limited to draw firm conclusions on the domain of validity of the models. In general the extrapolation from 14.6 MeV to 25.7 MeV gave acceptable results, without the need to change any internal parameter.

In recent years fully quantum-mechanical theories of pre-equilibrium reactions have been formulated e.g. by Feshbach, Kerman and Koonin [50] and by Tamura et al. [51, 52] and applied to analyse experimental data (Avaldi et al. [53]; Bonetti et al. [54, 57]; Udagawa [58, 59]; Herman et al. [68]). These theories may be used to calculate the contribution of pre-equilibrium processes to the reactions described in this report, and encouraging results have already been obtained [60,68]. A detailed comparison with unified, exciton and hybrid models is in progress [61] and this should make it possible to improve the approximations made in these theories so that they can be used to calculate with rapidity and adequate accuracy the wide range of cross sections needed in practical applications. Some examples of this feedback are given in Ref. [61].

Finally, we hope that in the near future new high-quality (n,n') measurements will become available in extended mass and energy regions. Such data will be very helpful to check whether the physics of the models is correct.

Acknowledgement Thanks are due to all participants (see Sect. 2) for providing the compilers with all the information to perform the intercomparison. The authors are very grateful to Prof. P.E. Hodgson for his help in the interpretation of the differences between the various nuclear model codes.

9 References

- [1] B. Strohmaier, M. Uhl, Proc. Winter Course on Nuclear Theory for Applications - 1978, IAEA-SMR-43 (1980) p.313.
- [2] Lawrence Livermore National Laboratory 1983 - version of STAPRE code.
- [3] P.G. Young and E.D. Arthur, Los Alamos Scientific Laboratory Report LA-6947 (1977).
- [4] M. Herman, A. Marcinkowski, K. Stankiewicz, Comp. Phys. Comm. 33 (1984), p373.
- [5] H. Gruppelaar, unpublished. (The code is a modified version of ERINNI by F. Fabbri and G. Reffo, RT/FI(77)4).
- [6] F.M. Mann, HEDL-TME-78-83 (1979)
- [7] C.Y. Fu, unpublished, see also Ref. [16] and Proc. Int. Conf. on Nuclear Cross sections for Technology (Knoxville 1979), NBS-SP594 (1980) p. 757.
- [8] H. Gruppelaar, J.M. Akkermans (unpublished). See also Refs. Phys. Rev. C22 (1980) p.73; Z. Phys. A300 (1981) p.345; Phys. Rev. C28 (1983) p.587. An updated code version will be published [76].
- [9] E. Běták and J. Dobeš, PEOGM: A pre-equilibrium computer code with gamma emission and multiple particle emission included, Report of the Institute of Physics (Bratislava, August 1983); see also [62, 63].
- [10] G. Keeni and S. Yoshida, PREM, Science Reports of the Tohoku University, Series 8, Vol. 3, no.1, June 1982, p.41.
- [11] J.M. Akkermans and H. Gruppelaar, Netherlands Energy Research Foundation Report ECN-60 (1979).
- [12] C. Kalbach, PRECO-D2: Program for calculating pre-equilibrium and direct reaction double differential cross sections, Los Alamos National Laboratory Report LA-10248-MS; see also Refs. [15, 43, 44].
- [13] M. Blann and J. Bisplinghoff, Code ALICE/LIVERMORE 82, UCID-19614 (1982) and update UCID-20169(1985);
M. Blann and H.K. Vonach, Phys. Rev. C28 (1983) p. 1475.
- [14] I. Broeders, U. Fischer, H. Jahn, E. Wiegner, unpublished (contr. to this exercise). See also Refs. [46, 47].
- [15] C. Kalbach and F.M. Mann, Phys. Rev. C23 (1981) p.112; C. Kalbach, *ibid* 23 (1981) p. 124; see also Ref. [12].
- [16] C.Y. Fu, Symp. on neutron cross sections from 10 to 50 MeV, Brookhaven 1980, BNL-NCS-51245, Vol. 2 (1980) p. 675; Nucl. Science and Eng., 86 (1984) p. 344.

- [17] G. Mantzouranis, D. Agassi and H.A. Weidenmuller, Phys. Lett. 57B (1975) p. 220; G. Mantzouranis, H.A. Weidenmuller and D. Agassi, Z. Phys. A276 (1976) p. 145.
- [18] J.M. Akkermans, H. Gruppelaar and G. Reffo, Phys. Rev. C22 (1980) p. 73.
- [19] C. Costa, H. Gruppelaar and J.M. Akkermans, Phys. Rev. C28 (1983) p. 587.
- [20] M. Blann, W. Scobel and E. Plechaty, Phys. Rev. C30 (1984), p. 1493.
- [21] A. Gilbert and A.G.W. Cameron, Can. J. of Phys. 43 (1965) p. 1446.
- [22] W. Dilg et al., Nucl. Phys. A217 (1973) p. 269.
- [23] F.C. Williams, Nucl. Phys. A166 (1971) p. 231.
- [24] P. Oblozinsky, I. Ribansky and E. Běták, Nucl. Phys. A226 (1974), p. 347.
- [25] C. Kalbach, Z. fur Physik A287 (1978) p. 319.
- [26] C.K. Cline, Nucl. Phys. A193 (1972) p. 417.
- [27] C. Kalbach, Z. fur Physik A283 (1977) p. 401.
- [28] E. Gadioli, E. Gadioli-Erba and P.G. Sona, Nucl. Phys. A217 (1973) p. 589.
- [29] L. Millazzo-Colli and G.M. Braga-Marcazzan, Nucl. Phys. A210 (1973) p. 297.
- [30] G. Mantzouranis et al., Phys. Lett. 57B (1975) p. 220.
- [31] S.K. Gupta, Z. Phys. A303 (1981) p. 329.
- [32] D.G. Gardner, Proc. of NEANDC/NEACRP Specialists' meeting on Fast Neutron capture cross sections, Argonne, 1982; NEANDC(US)214/L; ANL-83-4 (1983) p. 67; UCRL-87438 (1982).
- [33] W. Augustyniak and A. Marcinkowski, Acta Physics Polonica 4 (1979) p. 357.
- [34] M. Blann, Ann. Rev. Nucl. Science 25 (1975) p. 123.
- [35] M. Blann, Phys. Rev. C17 (1978) p. 1871.
- [36] E. Gadioli, E. Gadioli-Erba and G. Tagliaferri, Phys. Rev. C17 (1978) p. 2238.
- [37] A. Takahashi et al., Double differential neutron emission cross sections, Numerical tables and figures (1983), A-83-01, Oktavian report. Osaka University, Japan.
- [38] A. Marcinkowski et al., Nucl. Science and Eng. 83 (1983) p. 13.

- [39] D. Hermsdorf et al., Differentielle Neutronenemissionsquerschnitte $\sigma_{NM}(E_o, E, \epsilon)$ bei 14.6 MeV..., ZfK-277 (1974) Rossendorf bei Dresden.
- [40] H. Kalka, D. Hermsdorf and D. Seeliger, contribution to the pre-compound-model intercomparison. The code AMAPRE is an extension of the code AMALTHEE [41] with the angular-distribution model of Ref. [19].
- [41] O. Bersillon and L. Faugere, AMALTHEE, A Fortran code for spectra and cross sections calculations within the exciton model, NEANDC(E)191"L", INDC(FR)26/L (1977) Bruyeres-le-Chatel.
- [42] E. Gadioli et al., Phys. Rev. C16 (1977) p. 1404.
- [43] C. Kalbach, Phys. Rev. C24 (1981) p. 819.
- [44] C. Kalbach, Phys. Rev. C23 (1981) p. 124.
- [45] K. Kikuchi and M. Kawai, Nuclear Matter and Nuclear Reactions, North-Holland, Amsterdam, 1968, p. 33.
- [46] H. Jahn, C. Broeders and I. Broeders, Proc. Int. Conf. on Nuclear Cross sections and Technology, Washington, D.C., 1975, NBS-SP-425, p. 350.
- [47] H. Jahn, Critical Review of precompound models with consideration of the contribution to the "International Nuclear Model and Code Comparison on Pre-equilibrium Effects", organised by the NEA Data Bank 1983/84, KfK-3646, August 1984.
- [48] V.A. Plyuiko, Sov. J. Nucl. Phys. 27 (1978), p. 623.
- [49] H. Gruppelaar, Model calculations of double-differential cross sections, Consultants Meeting on Nuclear Data for Structural Materials, IAEA, Vienna, Nov. 83 (ECN-84-003).
- [50] H. Feshbach, A. Kerman and S. Koonin, Am. Phys. (New York), 125 (1980) 429.
- [51] T. Tamura and T. Udagawa, Phys. Lett. 71B (1977) p. 273.
- [52] T. Tamura, T. Udagawa and H. Lenske, Phys. Rev. C26 (1982) p. 379.
- [53] L. Avaldi, R. Bonetti and L. Colli-Milazzo, Phys. Lett. 94B (1980) p. 463.
- [54] R. Bonetti, M. Camnasio, L. Colli-Milazzo and P.E. Hodgson, Phys. Rev. C24 (1981) p. 71.
- [55] R. Bonetti and L. Colombo, Phys. Rev. C28 (1983) p980.
- [56] R. Bonetti, L. Colli-Milazzo, M. Melanotte, A. de Rosa, G. Inghima, E. Perillo, M. Sandoli, V. Russo, N. Saurier and F. Shakin, Phys. Rev. C25 (1982), p. 717.

- [57] R. Bonetti, L. Colli-Milazzo, I. Doda and P.E. Hodgson, *Phys. Rev. C* 26 (1982), 2417.
- [58] T. Udagawa, T. Tamura and B.T. Kim, *Phys. Lett.* 82B (1979), p. 349.
- [59] T. Udagawa, D. Price and T. Tamura, *Phys. Lett.* 116B (1982), p. 311.
- [60] G.M. Field, R. Bonetti and P.R. Hodgson (1984) (Private communication).
- [61] P.E. Hodgson, G.M. Field, H. Gruppelaar and P. Nagel, Invited paper presented at the International Conference on Nuclear Data for Basic and Applied Science, Santa Fe, USA, May 1985; extended paper to be published.
- [62] E. Běták and J. Dobeš, *Phys. Lett.* 84B (1979), p. 368.
- [63] B. Basarragtscha et al., *J. Phys.* G8 (1982), p. 275.
- [64] A. Marcinkowski et al., *Nucl Phys.* A402 (1983), p. 220.
- [65] G. Reffo, F. Fabbri and C. Costa, Angular momentum conservation in precompound decay, RT/FI(83)10, ENEA (1983).
- [66] D.G. Foster and E.D. Arthur, Average neutronic properties of "prompt" fission products, LA-9168-MS, UC-34C, Feb. 1982, Los Alamos National Laboratory Report.
- [67] B. Strohmaier, *Ann. Nucl. Energ.* 9 (1982), p. 397.
- [68] M. Herman, A. Marcinkowski and K. Stankiewicz, *Nucl. Phys.* A430 (1984), p. 69.
- [69] D. Schmidt, Data file EXFOR 32001, Feb. 1982, Technical University Dresden.
- [70] O.A. Sal'nikov, Inelastic scattering of neutrons, translated by IAEA, INDC(CCP)-223/L, June 1984.
- [71] A.A. Luk'yanov et al., *Yad. Fiz.* 21 (1975), p. 67, translated in *Sov. J. Nucl. Phys.* 21 (1975), p. 35.
- [72] S.P. Simakov et al., *Yad. Fiz.* 38 (1983), p. 801.
- [73] J.L. Kammerdiener, Report UCRL-51232 (1972).
- [74] J. Speth and A. van der Woude, Giant resonances in nuclei, *Rep. progr. Phys.* 44 (1981) p. 46.
- [75] J.M. Akkermans and H. Gruppelaar, *Z. Phys.* A300 (1981) p. 345.
- [76] H. Gruppelaar and J.M. Akkermans, Paper presented at the International Conf. on Nuclear Data for Basic and Applied Science, Santa Fe, USA, May 1985; ECN-164, report with code manual is in press.

- [77] J.M. Akkermans, Paper presented at the International Conf. on Nuclear Data for Basic and Applied Science, Santa Fe, USA, May 1985.
- [78] E. Bahm and H. Jahn, private communication, 1985.
- [79] C. Kalbach, to be published (1985).
- [80] H.P. Degtyarev et al., Sov. J. Nucl. Phys. 34 (1981) p. 169.
- [81] H. Vonach et al., Symp. on Neutron Cross Sections from 10 to 50 MeV, Brookhaven (1980), BNL-NCS-51245, Vol. 1, p.343.
- [82] O.A. Sal'nikov, Sov. J. Nucl. Phys. 122 (1971) p.620 and Report YK-7 (1972).
- [83] J.M. Akkermans and H.Gruppelaar, Phys. Lett. 157B(1985) p. 95.
- [84] J. Bisplinghoff, to be published (1985).

Table 1A
 Angle- and energy-integrated cross sections at 10 MeV
 with pre-equilibrium and equilibrium components
 HF models, unified models

Quantity	STAPRE IRK	STAPRE LLL-1	GNASH LAS	EMPIRE IBJ	PERINNI ECN-1	HAUSER-V TRM-1	TNG ORL	GNASH JAE
total	4294.	4294.7	4294.7	-	4290.6	4294.2	4304.	4294.4
elastic	2472.	2473.1	2473.2	-	2467.5	2489.1	2444.	2472.7
reaction	1823. 1835.6 ²	1821.6 1841.6 ²	1821.6	1824.	1823.1	1796.1 1814.1 ²	1860.	1821.7
nnx	1817.	1822.1 1834.2 ¹	1802. 1817. ¹	1799.	1795.1 1814.5 ¹	1747.7 1748.9* ¹	1846. 1853. ¹	1795.0 1821.0 ¹
np _x	14.9	15.6 5.6 ¹	12.9 2.4 ¹	23.0	17.1 5.6 ¹	5.6 1.6 ¹	11.3 4.7 ¹	21.3 7.0 ¹
nα _x	3.7	3.9 1.9 ¹	6.2 1.2 ¹	-	10.2 2.6 ¹	1.7 1.7 ¹	2.7 2.6 ¹	3.7 1.2 ¹
nγ _x	-	-	-	-	0.67 0.89 ¹	41.1 61.6 ¹	-	-
nn'γ	1298.	1249.0 1153.3 ¹	1298. 1202. ¹	1200.	1403.1* 1332.1* ¹	1676.8* 1700.7* ¹	1065.* 1008. ¹	1258.3 1181.0 ¹
n2nγ	520.6	571.7 679.3 ¹	503. 613.8 ¹	595.	391.8* 481.6 ¹	70.9* 48.2* ¹	780.* ² 844. ¹	529.7 623.0 ¹
n3nγ	0.	0. 0. ¹	0. 0. ¹	0.	0. 0. ¹	0. 0. ¹	0. 0. ¹	0. 0. ¹
nnpγ	0.76	0.70 0.81 ¹	0.53 0.63 ¹	2.6	0.14 0.20 ¹	0.005 0.003 ¹	0.18 0.63 ¹	4.3 4.9 ¹
npγ	14.8	15.5 5.5 ¹	12.8 2.4 ¹	23.0	17.1 5.6 ¹	5.6 1.6 ¹	11.2 4.6 ¹	21.2 6.9 ¹
npnγ	0.067	0.079 0.084 ¹	0.04 0.04 ¹	0.046	0.02 0.01 ¹	0.013 0.002 ¹	0.054 0.15 ¹	0.08 0.09 ¹
nαγ	3.7	3.9 1.9 ¹	6.2 1.2 ¹	-	10.2 2.6 ¹	1.7 1.7 ¹	2.70 2.55 ¹	3.6 1.2 ¹
nαnγ	0.0089	0.0079 0.0095 ¹	0.57 0.66 ¹	-	0. 0. ¹	0.002 0.002 ¹	0. 0. ¹	0.0050 0.0054 ¹
n nem	2341.	2393.9 2513.6 ¹	2305. 2431. ¹	2394.	2187.5 2296.4 ¹	1818.6* 1797.1* ¹	2626. 2697. ¹	2325. 2435. ¹
n pem	15.7	20.1 6.4 ¹	13.4 3.0 ¹	25.7	17.3 5.8 ¹	5.6 5.6 ¹	11.5 5.4 ¹	25.6* 12.0* ¹
n αem	4.5	4.6 2.7 ¹	6.8 1.9 ¹	2.8	10.2 2.6 ¹	1.7 1.7 ¹	3.0 3.1 ¹	6.4 4.3 ¹
n γem	-	-	4520. 4442. ¹	4220.	-	-	-	4253.0 4210.0 ¹

* Data not used in average (Table 1D).

¹ Results of calculations without allowance for pre-equilibrium effects

² See notes after Tables 1-4.

Table 1B
 Angle -and energy-integrated cross sections at 10 MeV
 with pre-equilibrium and equilibrium component²
 Exciton models

Quantity	PRANG ECN-2	PEQGM SLO	PREM TOH	PREANG1 TRM-2	PRECO-D2 TNL-1	PRECO-D2 TNL-2	AMAPRE (TUD)
total elastic reaction	- - 1823.4	- - 1821.2	- - 1823.4	- - -	- - 1817.	- - 1817.	- - -
nnx	1800.9 1817.7 ¹	1808.6 1816.3 ¹	1799.8 1821.8 ¹	- -	1704.*	1700.*	-
npx	16.7 4.3 ¹	10.1 2.7 ¹	23.1 1.1 ¹	-	20.3	23.9	-
nax	5.8 1.4 ¹	-	-	-	3.7	3.8	-
nγx	-	4.1 2.7 ¹	-	-	-	-	-
nn'γ	1293.4 1212.4 ¹	1808.5* 1815.5* ¹	1162.6 1073.3 ¹	-	-	-	-
n2nγ	506.5 605.4 ¹	0.* 0.* ¹	633.8 744.9 ¹	-	-	-	-
n3nγ	0.	0. 0. ¹	0. 0. ¹	-	-	-	-
nnpγ	0.	0.67 0.80 ¹	0. 0. ¹	-	-	-	-
npγ	16.7 4.2 ¹	10.1 2.6 ¹	23.0 1.1 ¹	-	-	-	-
npnγ	0.03 0.03 ¹	0.05 0.06 ¹	0. 0. ¹	-	-	-	-
nαγ	5.77 1.36 ¹	-	-	-	-	-	-
nanγ	0. 0. ¹	-	-	-	-	-	-
n nem	2307.5 2423.1 ¹	1808.6* 1816.3* ¹	2430.2 2562.8 ¹	-	-	-	-
n pem	16.7 4.3 ¹	10.8 3.5 ¹	23.0 1.1 ¹	-	-	-	-
n αem	5.77 1.36 ¹	-	-	-	-	-	-
n γem	-	6755.* 7049.* ¹	-	-	-	-	-

* Data not used in average (Table 1D).

¹ Results of calculations without allowance for pre-equilibrium effects.

² See notes after Tables 1-4.

Table 1C
 Angle- and energy-integrated cross sections at 10 MeV
 with pre-equilibrium and equilibrium component²
 (Geometry-dependent) Hybrid models

Quantity	ALICE LLL-2	ALICE LLL-3	SECDIST KFK
total	-	-	4446.
elastic	-	-	2590.
reaction	1789.9	1789.9	1856.
nnx	1694.*	1648.*	1870.
np α	39.	46.	-
n α x	43.5*	44.8*	-
n γ x	-	-	-
nn' γ	1480.*	1440.*	1338.
n2n γ	213.*	205.*	532.
n3n γ	0.	0.	0.
nnp γ	1.1 ³	3.0 ³	-
np γ	38.	43.	-
npn γ	1.1 ³	3.0 ³	-
n α γ	43.5	44.8	-
n α n γ +nn α γ	0.	0.	-
n nem	1920.*	1920.*	2402.
n pem	38.9	43.9	2525. ¹
n α em	50.8	52.0	-
n γ em	-	-	-

* Strongly deviating from average values; inconsistencies.

¹ Results of calculations without allowance for pre-equilibrium effects.

² See notes after Tables 1-4.

³ $\sigma_{nnp} + \sigma_{npn}$.

Table 1D
Experimental data at about 10 MeV

Quantity	Experimental value in mb; Reference (CINDA)	Average* calculated
total elastic reaction	4300 Foster and Glasgow (1971); 10MeV - -	- - -
nnx	-	1808 ± 28
npX	-	1824 ± 12 ¹
nαX	-	20.0 ± 10.2
nγX	-	3.9 ± 1.9 ¹
		4.4 ± 2.3
		1.8 ± 0.6 ¹
		-
nn'γ	-	1262 ± 54
n2nγ	320 Fréhaut et al. (1980); 10MeV	1138 ± 74 ¹
n3nγ	0	549 ± 44
nnpγ	-	656 ± 107 ¹
		-
npγ	-	-
npnγ	-	-
nαγ	4±1 Tewes et al. (1980)	-
nαnγ	-	-
n nem	-	2371 ± 107
n pem	-	2485 ± 111 ¹
n αem	-	-
n γem	-	-

* Average of results given in Tables 1A, 1B, 1C excluding data indicated by a *; the uncertainty represents the standard deviation.

¹ Results of calculations without allowance for pre-equilibrium effects.

Table 2A
 Angle- and energy-integrated cross sections at 14.6 MeV
 with pre-equilibrium and equilibrium components

Quantity	STAPRE IRK	STAPRE LLL-1	GNASH LAS	EMPIRE IBJ	PERINNI ECN-1	HAUSER-V TRM-1	TNG ORL	GNASH JAE
total	4020.	4020.4	4020.4	-	4020.5	4020.3	3961.0	4018.2
elastic	2264.	2265.1	2265.4	-	2264.0	2296.3	2199.	2265.0
reaction	1756.	1755.3	1755.3	1750.	1756.4	1724.0	1762.	1753.2
	1771.1 ²	1769.1 ²			1750.6 ^{1,2}			
nnx	1711.	1702.2	1708.	1689.	1685.7	1685.7	1710.	1682.
		1755.3 ¹	1749.1	1735.1	1740.5 ¹	1721.7 ¹	1746.1	1738.1
np _x	50.6	55.9	35.7	58.9	54.5	19.4	44.4	60.9
	12.1 ¹	5.2 ¹	12.3 ¹	11.5 ¹	4.4 ¹	12.1 ¹	13.1	
n α x	9.50	11.0	10.8	-	15.9	4.5	7.3	9.8
		1.6 ¹	1.2 ¹	2.6 ¹	3.8 ¹	2.2 ¹	4.0 ¹	1.1 ¹
n γ x	-	-	-	-	0.34	14.4	-	-
				0.56 ¹	22.2 ¹			
nn' γ	266.6	342.9	332.8	287.	384.4	966.4*	250.	251.0
		101.4 ¹	97.3 ¹	63.9 ¹	71.7 ¹	932.4* ¹	25.0 ¹	69.3 ¹
n2n γ	1441.	1352.1	1369.	1396.	1332.8	718.4*	1448.	1421.0
	1644.2 ¹		1644.1	1663.1	1662.4*	788.3* ¹	1706.1	1657.0
n3n γ	0.	0.	0.	0.	0.	0.	0.	0.0
		0.1	0.1	0.1	0.1	0.1	0.1	0.1
nnp γ	2.8	4.5	3.3	3.3	1.9	0.89	8.8	5.5
		6.2 ¹	4.3 ¹	-	2.8 ¹	0.95 ¹	11.1 ¹	6.5
np γ	38.0	42.9	28.2	37.0	46.0	14.9	25.9	50.9
		4.5*	1.9 ¹	-	6.3 ¹	3.3 ¹	2.6 ¹	7.1
npn γ	12.2	13.0	7.5	12.3	8.0	4.53	18.5	9.9
		7.7 ¹	3.4 ¹	12.3 ¹	5.0 ¹	1.1 ¹	9.5 ¹	6.0 ¹
n α γ	7.9	9.7	9.1	-	12.0	4.10	6.0	9.8
		0.9 ¹	0.6 ¹		2.5 ¹	2.0 ¹	2.5 ¹	0.7 ¹
n α n γ	1.6	1.3	1.7	-	3.8	0.42	1.3	1.1
		0.75 ¹	0.6 ¹		1.3 ¹	0.24 ¹	1.5 ¹	0.5 ¹
n nem	3166.	3068.6	3086.	3096.	3031.1	2409.0*	3178.	3114.
		3408.0 ¹	3396.1	-	3412.3 ¹	2511.3* ¹	3463.1	3401.0 ¹
n pem	53.5	56.6	39.1	62.2	56.4	20.3	53.2	66.4
		18.3 ¹	9.6 ¹	-	14.4 ¹	5.4 ¹	23.2 ¹	19.6
n α em	11.1	13.7	13.4	5.1	16.7	4.5	10.4	14.2
		5.1 ¹	4.5 ¹	-	5.0 ¹	2.2 ¹	8.0 ¹	6.3
n γ em	4130.	3736.	3675.	3483.	-	-	4203.	3041.0*
		3075.1	3523.	-			-1	2916.0 ¹

* Data not used in average (Table 1D).

¹ Results of calculations without allowance for pre-equilibrium effects.

² See notes after Tables 1-4.

Table 2B
 Angle- and energy-integrated cross sections at 14.6 MeV
 with pre-equilibrium and equilibrium component²

Quantity	PRANG ECN-2	PEQGM SLO	PREM TOH	PREANG1 TRM-2	PRECO-D2 TNL-1	PRECO-D2 TNL-2	AMAPRE (TUD)
total	-	-	-	-	-	-	3968.
elastic	-	-	-	-	-	-	2214.
reaction	1755.8	1754.0	1749.3	1752.1	1755.	1755.	1754.
nnx	1697.9 1744.4 ¹	1721.9 1744.3 ¹	1660.0 1744.0 ¹	1735.3	1608.*	1597.*	-
npx	47.7 8.8 ¹	29.7 7.5 ¹	89.4 5.5 ¹	15.7	53.0	63.1	-
nax	10.2 2.6 ¹	-	-	0.38*	10.0	10.4	-
nγx	-	5.6 1.6 ¹	-	-	-	-	-
nn'γ	359.4 99.6 ¹	420.2 159.3 ¹	244.0 23.7 ¹	185.6*	-	-	-
n2nγ	1336.7 1642.4 ¹	1274.7 1552.1 ¹	1399.6 1659.2 ¹	1549.7*	-	-	-
n3nγ	0. 0. ¹	0.	0. 0. ¹	0.	-	-	-
nnpγ	1.7 2.3 ¹	27.1 33.6 ¹	0.77 1.03 ¹	-	-	-	-
npγ	34.4 1.9 ¹	19.1 1.0 ¹	64.3 0.79 ¹	9.5	-	-	-
npnγ	13.2 6.9 ¹	10.6 6.6 ¹	26.8 4.8 ¹	6.2	-	-	-
nαγ	6.9 1.4 ¹	-	-	0.22	-	-	-
nαnγ	3.3 1.1 ¹	-	-	0.16	-	-	-
n nem	3051.1 3394.8 ¹	3007.2 3303.6 ¹	3070.8 3343.1 ¹	3291.4*	-	-	-
n pem	49.4 11.1 ¹	56.8 41.1 ¹	81.1 5.6 ¹	15.7	-	-	-
n αem	10.3 2.7 ¹	-	-	-	-	-	-
n γem	-	4490. 4293. ¹	-	-	-	-	-

* Data not used in average (Table 2D).

¹ Results of calculations without allowance for pre-equilibrium effects.

² See notes after Tables 1-4.

Table 2C

Angle- and energy-integrated cross sections at 14.6 MeV
with pre-equilibrium and equilibrium component²

quantity	ALICE LLL-2	ALICE LLL-3	SECDIST KFK
total elastic reaction	- - 1741.9	- - 1741.9	4025. 2280. 1745.
nnx npx n α x n γ x	- - - -	- - - -	1740. 1740. ¹ - -
nn' γ n2n γ n3n γ nnp γ	195.* 1370. 0. 53 ³	222. 1340. 0. 47.5 ³	472.* 1268.* 0. -
npr γ nprn γ	31 53 ³	44.7 47.5 ³	- -
n α γ n α n γ +nn α γ	30.5 40.6	31.3 41.4	- -
n nem n pem n α em n γ em	3060. 86.5 78.3 -	3010. 97.6 79.9 -	3007.8 3440. ¹ - -

* Strongly deviating from average values; inconsistencies.

¹ Results of calculations without allowance for pre-equilibrium effects.

² See notes after Tables 1-4.

³ $\sigma_{nnp} + \sigma_{npr}$.

Table 2D
Experimental data at 14-15 MeV

Quantity	Experimental value in mb; Reference (CINDA)	Average* calculated
total elastic reaction	4000 Foster and Glasgow (1971); 14.5 MeV -	- - -
nnx	-	1702 ±21
np α	-	1741 ± 8 ¹
n α x	51±8.0 Grimes et al. (1978); 15 MeV	48 ±18 9.2± 3.2 ¹
n γ x	2 Prokopets	9.9± 2.7
nn' γ	1300 Fréhaut et al. (1980); 14.7 MeV	2.4± 1.0 ¹ - 305 ±62 79 ±39 ¹
n2n γ	1290 Veesser et al. (1977); 14.5 MeV	1373 ±48 1647 ±38 ¹
n3n γ	0	-
nnp γ	-	-
np γ	51.0±8.0 Grimes et al. (1978); 15 MeV	-
npn γ	45 Koori et al. (1984); 14.1 MeV	-
n α γ	39±2 Traxler et al. (1984); 14.1 MeV	-
n α n γ	14±3 Grimes et al. (1978); 15 MeV	-
n α n γ	9.9±0.8 Fischer et al. (1982); 14.1 MeV	-
n nem	3150±300 Hermsdorf et al.; 14.6 MeV	3072 ±53 3396 ±45 ¹
n pem	-	-
n α em	9-14	-
n γ em	-	-

* Average of results given in Tables 2A, 2B, 2C excluding data indicated by a *; the uncertainty represents the standard deviation.

¹ Results of calculations without allowance for pre-equilibrium effects.

Table 3A
 Angle- and energy-integrated cross sections at 20 MeV
 with pre-equilibrium and equilibrium component

Quantity	STAPRE IRK	STAPRE LLL-1	GNASH LAS	EMPIRE IBJ	PERINNI ECN-1	HAUSER-V TRM-1	TNG ORL	GNASH JAE
total	3374.	3372.2	3372.2	-	3377.5	3372.5	3323.	3374.2
elastic	1696.	1695.2	1695.5	-	1699.2	1724.8	1625.	1695.5
reaction	1678. 1692.7	1677.1 1702.1	1677.1	1678.	1678.3	1647.7 1683.2 ¹	1698.	1678.7
nnx	1571. 1679.3 ¹	1561.2 1667. ¹	1599.	1580. 1655.5 ¹	1559.0 1661.8 ¹	1595.2 1670. ¹	1598. 1659.0 ¹	1502.0
npx	102.3 21.7 ¹	119.0 8.6 ¹	66.0	69.1 18.0 ¹	103.1 9.6 ¹	41.2 23.9 ¹	85.1 18.1 ¹	147.7
nax	18.4	22.0 1.2 ¹	11.7 0.9 ¹	-	16.0 4.4 ¹	6.7 2.1 ¹	14.4 4.9 ¹	28.8 0.9 ¹
nγx	-	-	-	-	0.18 0.42 ¹	4.6 9.7 ¹	-	-
nn'γ	172.2	185.8 7.3 ¹	180.2 7.8 ¹	200.	203.3 3.5 ¹	579.2* 518.8* ¹	157. 0.63 ¹	192.9 5.2 ¹
n2nγ	1142.	1081.7 1128.8 ¹	1123. 1189. ¹	1114.	1073.5 1142.3 ¹		745.* ² 588.* ¹	1122.9 1285.8 ¹
n3nγ	254.6	267.7 502.8 ¹	271.9 435.9 ¹	207.	254.3 465.2 ¹	1006.1* 1131.6* ¹	658.* 1027.* ¹	155.1 317.2 ¹
nnpγ	18.5	19.2 30.2 ¹	16.3 23.4 ¹	41.8 ² nnpγ	18.0 29.3 ¹	9.9 11.4 ¹	29.9 42.7 ¹	25.0 41.1 ¹
npγ	39.2	45.8 0.35 ¹	28.6 0.20 ¹	40.	46.9 0.4 ¹	19.1 2.5 ¹	21.7 0.3 ¹	75.8* 1.4 ¹
npnγ	59.0	72.8 20.9 ¹	37.4 8.2 ¹	43.	55.1 17.2 ¹	22.1 7.1 ¹	63.4 23.6 ¹	71.7* 16.5 ¹
nαγ	8.1	11.2 0.04 ¹	5.0 0.03 ¹	-	16.0	4.1 1.2 ¹	4.6 0.3 ¹	15.5 0.08 ¹
nαnγ	10.3	10.7 1.1 ¹	6.7 0.9 ¹	-	4.4 ¹	2.6 0.9 ¹	9.7 4.6 ¹	13.3 0.8 ¹
n pem	3297.	3262.7 3837.0 ¹	3311. 3739. ¹	3158.	3201.6 3749.2 ¹	-	3732. 4340. ¹	3020. 3598.0 ¹
n pem	123.0	138.9 53.2 ¹	83.4 33.6 ¹	139.	121.9 49.3 ¹	51.1 21.0 ¹	115. 67. ¹	172.8* 60.3 ¹
n αem	24.1	27.6 9.2 ¹	18.2 9.7 ¹	15.5	21.6 13.2 ¹	6.7 2.1 ¹	22. 15.0 ¹	34.8 9.5 ¹
n γem	-	-	3928. 3800. ¹	3156.	-	-	-	3450. 3557.0 ¹

* Data not used in average (Table 3D).

¹ Results of calculations without allowance for pre-equilibrium effects.

² See notes after Tables 1-4.

Table 3B
 Angle- and energy-integrated cross sections at 20 MeV
 with pre-equilibrium and equilibrium component

Quantity	PRANG ECN-2	PEQGM SLO	PREM TOH	PREANG1 TRM-2	PRECO-D2 TNL-1	PRECO-D2 TNL-2	AMAPRE (TUD)
total elastic reaction	- - 1678.6	- - 1677.4	- - 1678.6	- - -	- - 1673.	- - 1673.	- - -
nnx	1577.1 1661.7 ¹	1616.3 1660.9 ¹	1492.2 1663.9 ¹	- -	1484.*	1464.2*	-
npx	90.0 13.6 ¹	58.8 15.3 ¹	186.4 14.2 ¹	- -	95.1	113.7	-
nax	11.5 3.4 ¹	-	-	-	16.2	17.4	-
nγx	-	3.4 1.2 ¹	-	-	-	-	-
nn'γ	202.4 3.0 ¹	147.2* 0.* ¹	144.5* 0.3* ¹	-	-	-	-
n2nγ	1083.8 1168.6 ¹	1327.7* 1522.3* ¹	927.1* 937.5* ¹	-	-	-	-
n3nγ	272.5 463.6 ¹	81.3* 123.5 ¹	353.7* 509.1 ¹	-	-	-	-
nnpγ	16.4 23.4 ¹	60 74 ¹	14.1 20.3 ¹	-	-	-	-
npγ	34.5 0.089 ¹	16.5 0. ¹	58.5 0.015 ¹	-	-	-	-
npnγ	55.2 13.2 ¹	42 15 ¹	132.2 14.0 ¹	-	-	-	-
nαγ	0.9 0.12 ¹	-	-	-	-	-	-
nαnγ	10.6 3.3 ¹	-	-	-	-	-	-
n nem	3272.8 3775.3 ¹	3149.8 3447.1 ¹	3197.1 3422.9 ¹	-	-	-	-
n pem	106.8 37.7 ¹	118.9 90.0 ¹	181.7 14.0 ¹	-	-	-	-
n αem	13.0 5.7 ¹	-	-	-	-	-	-
n γem	-	5359.* 5677.* ¹	-	-	-	-	-

* Data not used in average (Table 3D).

¹ Results of calculations without allowance for pre-equilibrium effects.

² See notes after Tables 1-4.

Table 3C
 Angle- and energy-integrated cross sections at 20 MeV
 with pre-equilibrium and equilibrium component²

Quantity	ALICE LLL-2	ALICE LLL-3	SECDIST KFK
total elastic reaction	- - 1634.6	- - 1634.6	3295. 1620. 1675.
nnx np α n α x n γ x	- - - -	- - - -	1670. - - -
nn' γ n2n γ n3n γ nnp γ	82.* 1070. 224. 118. ³	126.* 1020. 214. 111. ³	- - - -
np γ npn γ	21.6 118. ³	40.7 111. ³	- -
n α γ n α n γ +nn α γ	2.7 100.	2.8 101.	- -
n nem n pem n α em n γ em	3130. 144. 110. -	3040. 161. 111. -	2838.* 3440. ¹ - -

* Strongly deviating from average values; inconsistencies.

¹ Results of calculations without allowance for pre-equilibrium effects.

² See notes after Tables 1-4.

³ $\sigma_{nnp} + \sigma_{nnpn}$.

Table 3D
Experimental data at about 20 MeV

Quantity	Experimental value in mb; Reference (CINDA)	Average* calculated
total elastic reaction	- - -	- - -
nnx	-	1576 ±45
np _x	-	1664 ±7 ¹
nα _x	-	98 ±37
nγ _x	-	15.9±4.8 ¹
		16.3±5.8
		2.5±1.6 ¹
nn'γ	-	187 ±15
n2nγ	1200±100 Veaser et al. (1977)	4.6±2.5 ¹
n3nγ	-	1092 ±35
nnpγ	-	1183 ±55 ¹
		236 ±37
		402 ±128 ¹
npγ	-	-
npnγ	-	-
nαγ	7±1 Bayhurst and Prestwood (1961)	-
nαnγ	-	-
n nem	-	3185 ±93
n pem	-	3626 ±159 ¹
n αem	-	-
n γem	-	-

* Average of results given in Tables 3A, 3B, 3C excluding data indicated by a *; the uncertainty represents the standard deviation.

¹ Results of calculations without allowance for pre-equilibrium effects.

Table 4A
 Angle- and energy-integrated cross-sections at 25.7 MeV
 with pre-equilibrium and equilibrium component

Quantity	STAPRE IRK	STAPRE LLL-1	GNASH LAS	EMPIRE IBJ	PERINNI ECN-1	HAUSER-V TRM-1	TNG ORL	GNASH JAE
total	2922.	2919.8	2919.8	-	2925.8	2920.1	2896.	2916.5
elastic	1311.	1309.4	1309.6	-	1314.6	1352.9	1289.	1309.8
reaction	1611. 1624.6	1610.3 1625.5	1610.3	1608.	1611.2	1567.2 1610.3 ¹	1607.	1606.7
nnx	1445.	1418.1 1594.5 ¹	1509. 1598. ¹	1468.	1451.3 1582.7 ¹	1493.2 1587.0 ¹	1465. 1564. ¹	1389.0 1582.0 ¹
npx	152.	175.9 30.3 ¹	90.6 11.3 ¹	138.	151.7 23.8 ¹	64.2 16.1 ¹	121. 37.3 ¹	175.1 23.9 ¹
nax	27.6	31.5 0.75 ¹	10.3 0.61 ¹	-	8.0 4.3 ¹	7.6 1.8 ¹	21.4 4.9 ¹	42.0 0.7 ¹
nγx	-	-	-	- 0.36 ¹	0.11 5.4 ¹	2.2	-	-
nn'γ	98.1	123.1 0.8 ¹	111.2 1.1 ¹	186.	142.9 0.46 ¹	368.5* 303.7* ¹	90.6 0.* ¹	120.0 0.6 ¹
n2nγ	445.6	511.0 159.1 ¹	454.9 183.1 ¹	480.	452.7 140.1 ¹	1083.6* 1232.3* ¹	363. 57. ¹	601.2 242.0 ¹
n3nγ	815.0	736.1 1349.7 ¹	874.3 1310. ¹	673.	780.0 1309.3 ¹		923. 1372. ¹	583.8 1184.0 ¹
nnpγ	24.2	16.9 19.9 ¹	23.6 30.8 ¹	98.3 ² nnpx	16.3 19.0 ¹	41.1 51.0 ¹	77.6 122. ¹	45.7 71.9 ¹
npγ	31.5	36.4 0.02 ¹	21.3 0.005 ¹	40.1	40.4 0.02 ¹	15.9 1.0 ¹	14.8 0.3 ¹	52.6* 0.24 ¹
npnγ	89.3	112.2 11.7 ¹	57.4 5.4 ¹	74.7	76.9 6.0 ¹	48.3 15.1 ¹	106. 37. ¹	104.6 13.9 ¹
nαγ	6.4	9.2 0.002 ¹	2.1 0.001 ¹	-	3.0 8.0	2.2 0.51 ¹	11.0 0. ¹	0.007 ¹
nαnγ	20.9	22.1 0.70 ¹	8.0 0.56 ¹	-	4.3 ¹	4.6 1.3 ¹	19.1 4.9 ¹	31.0* 0.6 ¹
n nem	3674.	3570.9 4501.9 ¹	3837. 4480. ¹	3405.	3652.9 4477.6 ¹		3798. 4407. ¹	3358.0 4294.0 ¹
n pem	216.1	210.4 89.8 ¹	148.8 101.1 ¹	36.	151.8 41.5	105.3 82.0 ¹	199. 159. ¹	249.0 164.0 ¹
n αem	36.4	37.1 8.3 ¹	20.7 14.8 ¹	18.7	20.6 25.5 ¹	7.6 1.8 ¹	31.6 18.8 ¹	52.1* 15.9 ¹
n γem	-	-	4184. 4326. ¹	2943.(?)	-		-	2091.0* 944.2 ¹

* Data not used in average (Table 4D).

¹ Results of calculations without allowance for pre-equilibrium effects.

² See notes after Tables 1-4.

Table 4B
 Angle- and energy-integrated cross sections at 25.7 MeV
 with pre-equilibrium and equilibrium component

Quantity	PRANG ECN-2	PEQGM SLO	PREM TOH	PREANG1 TRM-2	PRECO-D TNL-1	PRECO-DG TNL-2	AMAPRE (TUD)
total	-	-	-	-	-	-	2895.
elastic	-	-	-	-	-	-	1293.
reaction	1610.3	1610.0	1610.3	1610.3	1606.	1606.	1602.
nnx	1496.6 1589.2 ¹	1521.5 1584.9 ¹	1328.4 1581.7 ¹	1542.7	1380.	1352.	-
npx	134.3 17.5 ¹	86.3 24.0 ¹	282.2 25.5 ¹	59.0	134.	160.	-
nαx	6.4 3.7 ¹	-	-	0.5	19.1	21.2	-
nγx	-	2.6 1.1 ¹	-	-	-	-	-
nn'γ	134.7 0.11 ¹	75.0 0.* ¹	101.1 0.05 ¹	69.4*	-	-	-
n2nγ	472.4 169.8 ¹	495.7 257.1 ¹	371.2	-	-	-	-
n3nγ	806.5 1332.1 ¹	856.5 1280.4 ¹	804.5 1414.3 ¹	1473.5*	-	-	-
nnpγ	20.4 18.7 ¹	100.1 +n _p nγ ²	19.3	-	-	-	-
npγ	25.6 0.003 ¹	11.9 0. ¹	45.0 0.0002	6.9	-	-	-
npnγ	82.3 5.1 ¹	100.1 +n _p nγ ²	186.2 6.6 ¹	52.1	-	-	-
nαγ	0.12 0.006 ¹	-	-	0.006	-	-	-
nαnγ	6.18 3.5 ¹	-	-	0.5	-	-	-
n nem	3727.8 4518.1 ¹	3873.7 4524.8 ¹	3586.2 4355.9 ¹	-	-	-	-
n pem	186.0 97.1 ¹	180.7 141.7 ¹	261.3 22.6 ¹	-	-	-	-
n αem	10.8 11.3 ¹	-	-	-	-	-	-
n γem	- 4515. ¹	4553.	-	-	-	-	-

* Data not used in average (Table 4D).

¹ Results of calculations without allowance for pre-equilibrium effects.

² See notes after Tables 1-4.

Table 4C
 Angle- and energy-integrated cross section at 25.7 MeV
 with pre-equilibrium and equilibrium component²

Quantity	ALICE LLL-2	ALICE LLL-3	SECDIST KFK
total elastic reaction	- - 1575.6	- - 1575.6	2879. 1330. 1549.
nnx npx nαx nγx	- - - -	- - - -	1540. - - -
nn'γ n2nγ n3nγ nnpγ	47.6* 313. 856. 120.	97.4 303. 802. 127.	- - - -
npy npnγ	14.2 120. ³	34.1 127. ³	- -
nαγ nαnγ+nnαγ	0.09 109.	0.09 108.	- -
n nem n pem n αem n γem	3670. 229. 13.3 -	3520. 250. 13.2 -	2520.* 3040.* ¹ - -

* Strongly deviating from average values; inconsistencies.

¹ Results of calculations without allowance for pre-equilibrium effects.

² See notes after Tables 1-4.

³ $\sigma_{nnp} + \sigma_{nnpn}$.

Table 4D
Experimental data at about 25.7 MeV

Quantity	Experimental data in mb	Average* calculated
total	-	-
elastic	-	-
reaction	-	-
nnx	-	1453 ±65
npX	-	1585 ± 9 ¹
nαX	-	137 ±54
nγX	-	23 ± 7.3 ¹
		18 ±11
		2.4± 1.7 ¹
		-
nn'γ	-	116 ±29
n2nγ	-	0.5± 0.4 ¹
n3nγ	-	438 ±83
nnpγ	-	172 ±61 ¹
		792 ±88
		1319 ±64 ¹
		56 ±40
		47 ±35 ¹
npγ	-	-
npnγ	-	-
nαγ	-	-
nαnγ	-	-
n nem	-	3639 ±154
n pem	-	4444 ±78 ¹
n αem	-	-
n γem	-	-

* Average of results given in Tables 4A, 4B, 4C excluding data indicated by a *; the uncertainty represents the standard deviation.

¹ Results of calculations without allowance for pre-equilibrium effects.

NOTES TO TABLES 1-4

All cross sections are given in mb. Data in parentheses refer to the equilibrium calculation without prior allowance for precompound contributions. Data indicated by an asterisk (*) are "probably wrong"; they have not been included in the average; see comments below. The uncertainty in the average represents one standard deviation.

The meaning of the quantities is as follows:

<u>Symbol</u>	<u>Meaning</u>
total	total cross section
elastic	shape-elastic cross section (the compound-elastic cross section is very small at these energies)
reaction	total reaction cross section (or compound-formation cross section)
nnx	first-neutron emission cross section
np α	first-proton emission cross section
n α	first-alpha emission cross section
n γ x	first- γ -ray emission cross section
nn' γ	inelastic-scattering cross section
n2n γ	(n,2n) cross section
n3n γ	(n,3n) cross section
nnp γ	(n,np) cross section
np γ	(n,p) cross section
npn	(n,pn)+(n,np) cross section
n α γ	(n, α) cross section
n α n γ	(n, α n)+(n,n α) cross section
n nem	total neutron-production cross section (without elastic scattering)
n pem	total proton-production cross section
n α em	total alpha-production cross section
n γ em	total photon-production cross section

STAPRE (IRK), S. Wilboolsak, B. Strohmaier, M. Uhl.

Two values of σ_{γ} are given; the second value corresponds to a slightly different incident energy at which the statistical precompound/compound calculations were performed. No equilibrium calculations have been submitted. Total γ -ray production data are given at 14.6 MeV.

Drs. B. Strohmaier and M. Uhl suggest that the different partition of neutron emission into (n,n' γ) and (n,2n γ) observed in the STAPRE-IRK and STAPRE-LLL1, GNASH-LAS results could be due to the pairing correction used for pre-equilibrium decay. "This pairing correction is certainly the reason that our neutron production spectra as displayed in the graphs is below the results of some other codes."

STAPRE (LLL-1), D.G. Gardner, M.A. Gardner.

Two values of σ_r are given; the second value corresponds to a slightly different incident energy at which the statistical precompound/compound calculations were performed. Total γ -ray production data are given at 14.6 MeV. Modified γ -ray strength functions were used, though with the same absolute values as stated in the specifications.

GNASH (LAS), P.G. Young

The data above 10 MeV have been revised by the author (new integration routine).

EMPIRE (IBJ), M. Herman.

Note that this code also belongs to class C. Total and elastic cross section not given. Equilibrium data given only for $E=14.6$ MeV. Note that σ_{nnpx} is given rather than $\sigma_{\text{nnp}\gamma}$.

The (n,α) cross sections are not given, because no pre-equilibrium mechanism is considered in the α -channel.

Please note small inconsistencies between σ_r and $\sigma_{\text{nnx}} + \sigma_{\text{np}\gamma}$, because of neglect of α -channel. The data in Tables 1-5 have been corrected according to a revision of the author (June 1984). The spectra have not been corrected because the changes were relatively small.

PERINNI (ECN-1), H. Gruppelaar, H.A.J. van der Kamp.

The calculation is based upon the level-density formula of Williams, renormalised to the back-shifted Fermi gas model, rather than the Gilbert-Cameron formula that is used in other codes for the calculation of the compound part. No photon-production data given.

HAUSER-V (TRM-1), S.B. Garg, A. Sinha

The value of σ_r in the equilibrium calculation is somewhat different from that used in the precompound/compound calculation. The values of σ_{nnx} , $\sigma_{\text{np}\gamma}$, $\sigma_{\text{n}\alpha\gamma}$, σ_{nnem} , σ_{npem} , $\sigma_{\text{n}\alpha\text{em}}$ were calculated from the other cross sections by compilers. Note that $\sigma_{\text{n}3\text{n}}$ is lacking; this leads to relatively low values of σ_{nnem} at 20, 25.7 MeV. No photon-production data given. The values of $\sigma_{\text{nn}\gamma}$ and $\sigma_{\text{n}2\text{n}}$ are quite different from the other data.

TNG (ORL), C.Y. Fu.

The angle-integrated cross sections were calculated with 1-MeV bins, which is apparently too wide for the $(n,2n)$ and $(n,3n)$ cross sections near thresholds (Tables 1A, 3A).

GNASH (JAE), K. Shibata.

Revised results (September 1984) have been displayed in the tables. The (n,p) cross sections are still relatively high and the photon-production cross section are relatively low.

PRANG (ECN-2), H. Gruppelaar, H.A.J. van der Kamp.

No γ -ray competition included (future option; see GRYPHON code [76] and [83]).

PEGM (SLO), E. Běták.

The γ -ray competition has been included, but α -emission has been suppressed. The values of σ_{nnp} and σ_{nnp} are not clearly separated at $E = 20$ and 25.7 MeV. The summed values are 101.5 (88.8) mb at 20 MeV and 100.1 (44.5) mb at 25.7 MeV.

At 10 MeV the (n,2n)-contribution is too small; the same holds for the (n,3n)-contribution at 20 MeV. Dr. Běták suggests that this is caused by the finite energy step used and by the use of $g = A/13$ MeV⁻¹ and no pairing corrections. These effects are important, especially when the energy available is not high enough above the threshold.

Please note high values of total γ -ray emission cross sections.

PREM (TOH), G. Keeni, S. Yoshida.

In this code no γ -ray competition nor α -particle competition has been taken into account.

The data have been renormalised by the compilers with factors 1.0422, 0.9596, 0.9206 at $E = 10, 20$ and 25.7 MeV to adjust the reaction cross sections.

The inconsistency problems between σ_{nnx} and $\sigma_{nn'\gamma} + \sigma_{n2n\gamma} + \sigma_{n3n\gamma} + \sigma_{nnp\gamma}$ have been reduced by adopting a smaller mesh size in the calculations with pre-equilibrium component (0.10 rather than 0.25 MeV). At 25.7 MeV there is also a contribution of 43.5 mb from σ_{npnn} and a contribution of 17.9 at σ_{nnpn} .

PREANG1 (TRM-2), S.B. Garg, A. Sinha

Calculations have only been performed at 14.6 and 25.7 MeV. The data for $\sigma_{nnx}, \sigma_{npx}, \sigma_{n\alpha x}, \sigma_{n2n\gamma}, \sigma_{nnp\gamma}, \sigma_{n\alpha n\gamma}, \sigma_{nnem}, \sigma_{npem}$ were obtained from the relevant particle-emission spectra by the compilers. These data are quite uncertain. The compilers have renormalised the data at 25.7 MeV by a factor 0.9191 to adjust the reaction cross section. No γ -ray competition was included.

The (n, α) cross sections seems too low.

PRECO-D2 (TNL), C. Kalbach.

The differences between the two PRECO-D2 calculations are in the Q-factor (see notes to Table 6).

Only first-particle emission has been considered.

The sum of σ_{nn} , σ_{np} and $\sigma_{n\alpha}$ is smaller than σ_r to allow for direct reactions producing other light ions, notably deuterons.

AMAPRE (TUD), H. Kalka, D. Hermsdorf, D. Seeliger.

No data given at 10 and 20 MeV (instead data were provided at 9 and 12 MeV). No angle- and energy-integrated reaction cross sections were given (only emission spectra and Legendre coefficients of angular distributions at 14.6 and 25.7 MeV). The secondary (n,2n) emission spectra were calculated by the STAPRE code.

ALICE (LLL-1,2), M. Blann

LLL-1 and -2 correspond to the hybrid and geometry-dependent hybrid models programmed in ALICE/LIVERMORES2. No γ -ray competition has been included. The values of σ_{nnx} , σ_{npx} , $\sigma_{n\alpha x}$ are not explicitly given.

There are inconsistencies between the sum of all cross sections and the total reaction cross section.

In the present results no inclusive reactions are included (σ_{nnx} , σ_{npx} , etc.). In general the code calculates and prints both the inclusive and the exclusive cross sections.

SECDIST (KFK), I. Broeders, U. Fischer, H. Jahn, E. Wiegner.

No p-, α - and γ -competition included. The division of σ_{nnx} between $\sigma_{nn'\gamma}$, $\sigma_{n2n\gamma}$, $\sigma_{n3n\gamma}$ could not be deduced from the contribution of the authors.

**Table 5a Cross sections for population of isomeric states
at 14.6 MeV (mb)¹**

Final state	STAPRE IRK	STAPRE LLL-1	GNASH ² LAS	EMPIRE IBM	TNG ORL
93m Nb	132.4	179.7 (76.8)	144.8 (60.4)	59.1 (31.1)	65. (-)
92m Nb	460.6	482.0 (584.6)	559.5 (674.0)	474.3 (586.)	691. (-)

**Table 5b Cross sections for population of isomeric states
at 25.7 MeV (mb)¹**

Final state	STAPRE IRK	STAPRE ² LLL-1	GNASH ² LAS	EMPIRE IBM
93m Nb	--	67.5	46.3 (0.7)	27.1 (0.9)
92m Nb	--	124.8 (19.5)	143.7	110.0 (40.1)
91m Nb	--	77.6 (140.4)	474.2 (749.4)	249.1

**Table 5c Experimental data for activation cross sections of
isomeric states at 14.6 MeV (mb)¹**

Final state	Experimental value in mb
93m Nb	135 Ryves and Kolkowski, 1981
92m Nb	460 Many data points

¹ It has been pointed out by D.G. Gardner that the branching ratio for the 13/2⁺ level of Nb-93 at 0.95 MeV as specified in the exercise is in error. Therefore, a comparison to experimental data for the population of Nb-93^m is not very relevant.

² Revised.

Table 6 Comparison of model codes¹

1 Class	2 Code	3 Equilibrium	4 Pre-equilibrium	5 Relation	6 Options	7 Level density	8 p-h level density	9 Discrete levels
(A)	STAPRE (IRK)	HF	RWM	COR ⁺	CP M,6	GC ⁺	WS,g=A/13 ⁺	YES ⁺
	STAPRE (LLL-1)	HF	RWM	COR ⁺	CP M,6	GC ⁺	WS ⁺	YES
	GNASH (LAS)	HF	ME,NCB	COR	CPA M,6 ⁺	GC ⁺	WS	YES ⁺
	GNASH (JAE)	HF	ME,NCB	COR	CP M,6	GC	+	YES ⁺
	EMPIRE (IBJ)	HF	GDH,NCB	COR,C ⁺	CP M,6	GC	g=A/13,σ ²⁺	YES ⁺
	PERINNI (ECN-1)	HF	ME ⁺	UM, C ⁺	C M,3	BF ⁺	+	EQ
	HAUSER-V (TRM-1)	HF	ME,NCB	COR	C M,2	GC	WS	EQ
	TNG (ORL)	HF	MEC	UM, C	CPA M,3	GC	WS,σ ²⁺	YES ⁺
(B)	PRANG (ECN-2)	WE	ME	UM ⁺	CPA M,6	BF ⁺	+	NO
	PEQGM (SLO)	WE	ME ⁺	UM ⁺	CP M,4 ⁺	W	W,g=A/13	NO
	PREM (TOH)	WE	ME	UM	CP M,2	W	W,g=A/13	NO
	PREANG1 (TRM-2)	WE	ME	UM	CPA 6	W	WS	NO
	PRECO-D2(TNL-1,2)	WE	NCB ⁺	COR ⁺	CPA 6		W,g=A/13 ⁺	NO
	AMAPRE (TUD)	WE	ME	UM	CPA M,2	BF	W	NO
(C)	ALICE (LLL-1,2)	WE	(GD)H,NCB	COR ⁺	CPA M,4	BF ⁺	WS ⁺	NO
	SECDIST (KFK)	HF	GDH,NCB	COR ⁺	CPA M,2	GC	+	EQ ⁺
	EMPIRE (IBM)	HF	GDH,NCB	COR,C ⁺	CP M,6	GC	g=A/13,σ ²	YES ⁺

1 Class	2 Code	10 Internal transition	$\langle M^2 \rangle$	R-factor	α-emission	Transmission coef.	12 Spectrum	13 Ang. dist.	14 γ-ray emission
(A)	STAPRE (IRK)	+	K=136.6	G	φ=0.11	I	TEG,EB	no	BWY ⁺
	STAPRE (LLL-1)	W	C=100	C	φ=0.25	I	TEG,EB	no	BWY ⁺
	GNASH (LAS)	W	K=150 ⁺		+	I	TEG,EB	KM ⁺	BWY ⁺
	GNASH (JAE)	+	+	-	-	I	TEG,EB	no	BWY ⁺
	EMPIRE (IBJ)	+	-	-	no	I,T	EG,EB	no	BW ⁺
	PERINNI (ECN-1)	O	C=650 ⁺	Q ⁺	γ=10 ⁺	Tj ⁺	no	no	B ⁺
	HAUSER-V (TRM-1)	W ⁺	K=135	Q	M ⁺	T(j) ⁺	F,EB	no	B ⁺
TNG (ORL)	O	C=?	Q ⁺	M	I,T	EG,EB	yes	BW ⁺	
(B)	PRANG (ECN-2)	O	C=650 ⁺	Q ⁺	γ=10 ⁺	I	TE,EP	KK ⁺	no
	PEQGM (SLO)	O	K=110	C	no	I	TEG,EP	no	B ⁺
	PREM (TOM)	W	+	+	no	+	TE,EP	no	no
	PREANG1 (TRM-2)	O	C=225	C	γ=.0002	I	F,EP	M	no
	PRECO-D2(TNL-1,2)	+	K=135	Q ⁺	+	I ⁺	F,EP	KM ⁺	no
	AMAPRE (TUD)	O	C=100	C	-	I	E,EB ⁺	KK ⁺	no ⁺
(C)	ALICE (LLL-1,2)	+	-	+	+	I,T ⁺	TE,EB	KK ⁺	no
	SECDIST (KFK)	+	-	-	no	I,T	TE,EP	PWBA	no
	EMPIRE (IBM)	+	-	-	no	I,T?	EG,EB	no	BW ⁺

¹ Extracted from questionnaire (Appendix B); see next pages for explanation of abbreviations.

+ See next pages for comments supplied by participants.

ABBREVIATIONS USED IN TABLE 6

(+ Means see detailed notes by participants given below)

3. Equilibrium

WE Weisskopf-Ewing (evaporation model)
HF Hauser-Feshbach

4. Pre-equilibrium Model Part

ME Master-equation approach without conservation of angular momentum and parity
MEC As ME with conservation of angular momentum and parity
NCB Never-come-back assumption
RWM Random-walk model up to equilibrium [1, 75]

5. Relation of equilibrium to pre-equilibrium parts

UM Unified model of pre-equilibrium and equilibrium emission
C With conservation of angular momentum
COR Pre-equilibrium is treated as a correction to the statistical model
H Hybrid model
GDH Geometry-dependent hybrid

6. Options for quantities calculated

C Cross-sections (angle and energy integrated)
P Particle spectra (angle-integrated)
A Angular distributions
M,n Multiparticle emission of up to n (different) outgoing particles

7. Total level density in equilibrium part

GC Gilbert-Cameron [21]
BF Back-shifted Fermi-gas model (Dilg. et al) [21]
W Williams [23]

8. Particle-hole density

WS Williams' state density with energy shift or pairing energy correction [23]
W As WS without energy shift or pairing energy correction
 $g=A/13$ $g=A/13 \text{ MeV}^{-1}$

σ^2 Williams' level density with n-dependent spin distribution

9. Discrete levels

Yes Included in equilibrium + pre-equilibrium calculation
EQ Included in equilibrium calculation only
No Not considered

10. Internal Transition Rates

Average transition probability $\lambda^{\pm} = \frac{4\pi}{h} \langle M^2 \rangle \omega_f^{\pm}$

Value of ω_f^{\pm} : W Williams [23]
O Oblozinsky et al. [24]

$\langle M^2 \rangle$ from : C=N $\langle M^2 \rangle = NA^{-3} E^{-1}$ [26]
K=k Kalbach formula [25]

11. Emission Rates

R-factor:

C Cline (without renormalisation to 1 at high values of n:
ref. [26])
Q Kalbach's Q-factor, normalised to 1 at high values of n:
ref. [27])
G Gadioli et al. ref [28]

Treatment of α -emission:

M α -particle emission rate according to ref. [29]
 $\gamma=N$ Form factors with $\gamma=N$.
 $\phi=p$ α -particle pre-formation probability p.
no α -emission not included.

Transmission Coefficients:

I Inverse reaction cross-sections used in pre-compound part
T Transmission coefficients used in compound and precompound
part without j-dependence
Tj As T but with j-dependence

12. Spectrum Calculations

Complexity:

F Only first-emitted particles calculated
T Total particle production spectra calculated
E Emission spectra are calculated for every reaction, and
for every outgoing particle (e.g. two spectra for n,2n)

G Gamma-ray calculation possible

Representation:

EB Spectrum is represented in energy bins of equal width
EP Spectrum is given by point data at equidistant energies
No No spectrum calculation

13. Angular Distribution Calculation

KM Systematics of Kalbach and Mann [15] for angular distributions
in precompound part
M Model of Mantzouranis et al., Ref. [17]
KK Kikuchi-Kawai expression [45], see implementation in exciton
model in [19] and in GDH model in [20].
PWBA PWBA type of calculation for emission from $n=n_0$ only.

14. Gamma-Ray Emission

B Brink-Axel formula
W Weisskopf formula for M1 and E2
Y Expression for Yrast line
no No gamma-ray emission

PARTICIPANTS' NOTES TO TABLE 6 (indicated by +)

STAPRE [1, 2]

Pre-equilibrium part (4)

The "random-walk" equation [1, 75] is solved rather than the master equation. The never-come-back assumption is not followed. Instead, the number of transitions is limited until the equilibrium population is reached (note from editors).

Relation of Equilibrium to Pre-equilibrium Parts (5)

The first-chance HF cross section is multiplied by the depletion factor resulting from the exciton model calculation. The depletion factors in the IRK calculation are: 0.819, 0.699, 0.569 and 0.455 for E=10, 14.6, 20 and 25.7 MeV, respectively. It is assumed that the spin-parity distribution is the population resulting from equilibrium emission. In the LLL version equilibrium is defined when the populations in the (n+2)th exciton state differ from those in the nth exciton state by less than 1 percent.

Total level density in equilibrium part (7)

The codes have different options. The option used was Gilbert and Cameron with $\sigma^2 = c \sqrt{aU} A^{2/3}$, $c=0.146$, $U=E-P$.

Comments (IRK):

σ^2 is linearly interpolated between σ_{exp}^2 and E_c and $0.146 \sqrt{aU} A^{2/3}$ at U_x .

In some cases large differences were found between the results with $c=0.146$ and $c=0.0888$. For instance, for the equilibrium contribution to σ_{nax} the results at 10 or 14.6 MeV differed nearly by a factor of 2.

For nuclei for which the level-density parameters were not specified, those of neighbouring nuclei of the same type were used (e.g. Nb-92 for Nb-90).

The first energy of the continuum is chosen by the code; it may differ by up to 0.25 MeV from the prescribed value.

In the LLL version the level density at low energies is normalised on an integer number of levels, rather than half integer values; an appropriate extrapolation has been made.

Particle-hole level density (8)

Williams' state density formula was used with pairing correction.

$$\text{IRK-contribution: } g = \frac{6}{\pi^2} \frac{A}{8} \approx A/13 \text{ MeV}^{-1},$$

$$\Delta = 12/\sqrt{A}.$$

LLL-1 contribution: $g = \frac{6}{\pi^2} a$, a, a as specified (GC),
P as specified (GC).

Discrete levels (9)

Comment by IRK:

Discrete levels are included in both equilibrium and pre-equilibrium calculations. For the spectra, the PE contribution is calculated for energy bins of size 0.25 MeV assuming the (p,h) state density holds for all excitation energies. For the population of the second compound nucleus the PE contribution is distributed among the levels in the corresponding energy bins; if a bin contains no level the contribution is assigned to the first level below it. If there are several levels in one bin, the weights of the contributions are chosen proportional to the results of the HF calculation.

Internal transition rates (10)

The IRK expression for the final state density is:

$$\omega_f^+ = \frac{1}{2(n+1)} g(gE - \frac{1}{2} ((p+1)^2 + (n+1)^2))^2$$

$$\text{with } g = \frac{6}{\pi^2} \frac{A}{8} \text{ MeV}^{-1}.$$

Gamma-ray emission (14)

The Brink-Axel formula for E1 radiation used at IRK is as follows:

$$T_{\gamma}^{E1}(\epsilon_{\gamma}) = 2\epsilon_{\gamma}^3 \cdot 26.02 \times 10^{-8} \sigma_r \frac{(\sigma_r^2)}{(\epsilon_r^2 - \epsilon_{\gamma}^2)^2 + \epsilon_{\gamma}^2 \Gamma_r^2} \times \frac{1}{3\epsilon_{\gamma}}$$

$$\text{with } \epsilon_r = 16.5 \text{ MeV}, \quad \Gamma_r = 5.0 \text{ MeV}, \quad \sigma_r = 16.2 \text{ mb.}$$

At LLL a modified shape was used, with $\sigma_r = 220.5 \text{ mb.}$

The Weisskopf formula for M1 radiation used at IRK is as follows:

$$T_{\gamma}^{M1}(\epsilon_{\gamma}) = 2\pi C^{M1} \epsilon_{\gamma}^3$$

$$\text{with } C^{M1} = 1.669 \times 10^{-9} \text{ MeV}^{-3}$$

At LLL a modified shape was used with $C^{M1} = 2.12 \times 10^{-9} \text{ MeV}^{-3}$

The Weisskopf formula for M2 radiation used at IRK is as follows:

$$T_{\gamma}^{E2}(\epsilon_{\gamma}) = 2\pi C^{E2} \epsilon_{\gamma}^5$$

$$\text{with } C^{E2} = 7.928 \times 10^{-12} \text{ MeV}^{-5}.$$

At LLL a modified shape was used with $C^{E2} = 1.04 \times 10^{-11} \text{ MeV}^{-5}.$

The yrast line expression used is:

$$25 \geq J_{\max} = \frac{2\pi}{h} 2 \sqrt{I_{\text{rigid}}(E-\delta)} \geq 6 \quad (\text{IRK}),$$

3 or 7/2 (LLL-1).

Comments (15)

1. The incident energies are slightly different (a bin structure is used also for incident energies)
2. Direct and semi-direct capture has not been included.
3. The different partition of neutron emission into $(n,n'\gamma)$ and $(n,2n\gamma)$ between the IRK and LLL-1 versions could, perhaps, be due to different pairing corrections used in pre-equilibrium decay. This pairing correction is certainly the reason of the different end points of the spectra.

GNASH (LAS) [3]

Options (6)

The maximum number of particles (60) depends only on the size of the computer (now CDC 7600). We will soon be increasing this capability by a factor of 10, when we move to a Cray.

Total level density in equilibrium part (7)

We use the Gilbert-Cameron prescription with $\sigma^2 = 0.0888 \sqrt{aU} A^{2/3}$ at all excitation energies above E_c .

We have the calculation capability to use level densities from any arbitrary level-density calculation by accessing precalculated tables.

Discrete levels (9)

We make a crude correction to the equilibrium discrete level cross-sections for pre-equilibrium effects.

Internal transition rates (10)

$$g_o = A/13 \text{ (composite)}; g_n = A/13 (=7.15); g_p = 6.50; g_\alpha = 6.10.$$

These values of g_o and g_p , which are our default options in GNASH, agree well with the three given Hermsdorf fit points. For protons and alphas, however, our default values for g_p and g_α ($A/13$) overpredict the precompound point of Grimes' data, so I decreased them slightly. The agreement with Grimes is still not good, but I believe the problem might be the proton and alpha transmission coefficients.

Emission rates (11)

Use Kalbach's expressions for pickup and knockout, reference [27].

Angular distribution (13)

The expressions of Kalbach and Mann have been used. These are modified at secondary neutron energies < 6.5 MeV, where the coefficients are forced to go to 0. (HF angular distributions with auxiliary code).

Gamma-ray emission (14)

Yrast expression used.

GNASH (JAE) [3]

Particle-hole density (8)

The particle-hole density is involved in the normalization factor α , i.e.

$$\alpha = |M|^2 g^4 / A.$$

Discrete levels (9)

Discrete levels were included both in equilibrium and pre-equilibrium calculations.

Internal transition rates (10)

$$\omega_f^+ = g^3 E^2 / (p+h+1). \text{ For } |M|^2 \text{ see (8) (above).}$$

EMPIRE [4]

Relation of equilibrium to pre-equilibrium parts (5)

Flux of projectiles of angular momentum L available for formation of

compound nucleus is reduced by factor $R^L = 1 - \sum_{x=0}^{E-Bx} P_x^L(\epsilon) d\epsilon$

where x denotes neutrons and protons, $P_x^L(\epsilon)$ is probability of finding particle x in channel of energy ϵ to $\epsilon + d\epsilon$.

Particle-hole density (8)

Ericson level density with standard spin distribution of n-exciton levels

$R_n(J) = (2J+1)(2\sigma^2)^{-1} \exp[-(J+1/2)^2/2\sigma_n^2]$ where $\sigma_n^2 = 0.28 A^{2/3} n$. Yrast

lines for n-exciton configurations $U_{\text{yrast}} = \frac{75J^2}{A^{4/3}(n-1/2)}$ taken into account.

Discrete levels (9)

Included in equilibrium as well as in pre-equilibrium calculation.

Internal transition rates (10)

Transition rates based on nucleon-nucleon scattering cross-section with lifetimes averaged over all excitons. Average nuclear matter density along trajectory has been selected.

Gamma-ray emission (14)

CM1 = 0.1, CE2 = 0.1.

$$T_{E1}^{\text{GDR}} = 5.46 \times 10^{-7} \sum_{i=1}^2 \frac{\sigma_i \Gamma_i^2 E_\gamma^4}{(E_\gamma^2 - E_i^2)^2 + \Gamma_i^2 E_\gamma^2}$$

$$T_{E2}^{\text{W}} = \text{CE2} \times 3.54 \times 10^{-13} A^{4/3} E_\gamma^5$$

$$T_{M1}^{\text{W}} = \text{CM1} \times 1.30 \times 10^{-7} E_\gamma^3$$

Additional comments (15)

The integration step 1 MeV was used for the calculations of reactions induced by 10 MeV and 14.6 MeV neutrons, while in the two remaining cases 2 MeV step was applied.

No transitions between discrete levels were considered, except those nuclei for which decay scheme was provided in the exercise specification.

Yrast lines were accounted for only in pre-equilibrium decay, see (8).

PERINNI [5]

Pre-equilibrium model part (4)

The solution of the (full) master equation is made in the PRANG code, i.e. the mean lifetimes $\tau(n)$ are calculated from a spin-independent exciton model for all values of n . The PERINNI code reads coefficients containing $\tau(n)$.

Relation of equilibrium to pre-equilibrium parts (5)

There is no separation between equilibrium and pre-equilibrium parts: for each value of n the contribution is calculated. In this exercise the spin distribution of the level density has been taken independent of n . There is no pre-equilibrium component for the excitation of discrete levels.

Total level density in equilibrium part (7)

There are several options in the code. For calculations with account of pre-equilibrium effects, the Williams' formula with a "renormalization" to the back-shifted Fermi gas formula of Dilg et al. [22] is employed (see below). At low excitation energies the value of σ^2 is calculated differently.

Particle-hole density (8)

A "renormalised" Williams' level-density formula was used:

$$\omega_n(U) = \sqrt{\frac{\pi}{3}} \frac{U}{a^{1/4}(U+t)^{5/4}} \omega_n^{\text{Williams}}(U)$$

$$a = \frac{\pi^2}{6} g; \quad U = E - \Delta; \quad \sigma^2 \text{ from expression of Dilg et al. with}$$

$$I_{\text{eff}} = I_{\text{rigid}}; \quad r_0 = 1.25 \text{ fm.}$$

Internal transition rates (10)

$$\langle M \rangle^2 = \frac{650}{(13g)^3 E} \text{ (for } g = A/13 \text{ this corresponds to } \langle M \rangle^2 = 650A^{-3} E^{-1} \text{)}.$$

This value is different from most other values, because a different level-density formula has been used.

Emission rates (11)

In addition $Q = 1$ exactly for $n \geq \bar{n}$.

For α -emission $\gamma_\alpha = 10$ at $n \leq \bar{n}$, and $\gamma_\alpha = 1$ at $n \geq \bar{n}$.

For the calculation of the mean life times (in PRANG) inverse reaction cross sections were used.

Gamma-ray emission (14)

The Brink-Axel formula was used for all nuclei, no M2 and E2 emission was included; no yrast line was used.

HAUSER-V [6]

Internal transition rates (10)

The average transition probability of Williams [23] has been modified to allow for the distinguishability between protons and neutrons.

Emission rates (11)

The α -particle emission is treated according to Ref. [27]. This includes a direct component. The j-dependent transmission coefficients yield a lower reaction cross section. The magnitude of difference varies from about 2 percent at 10 MeV to about 0.7 percent at 25.7 MeV. The j-dependence arises due to the inclusion of spin-orbit term in neutron and proton channels. The transmission coefficients have been obtained with the ELIESE-3 code and fed to HAUSER-V.

Gamma-ray emission (14)

The normalization varies smoothly with A as given in the HAUSER-V report [6].

TNG [7]

Particle-hole density (8)

$$\text{Energy shift} = \frac{1}{4} g (\Delta_o^2 - \Delta^2 (u,n)), \text{ see Ref. [16] ;}$$

$$\sigma_n^2 \text{ from pairing model.}$$

Discrete levels (9)

$$\text{Weighted by } \sigma_{\text{pre}} (E_{\text{cut}}).$$

R-factor (11)

Modified Q-factor of Kalbach.

Angular distribution calculation (13)

Generalised HF, see Ref. [16].

The f_2 and f_4 coefficients for $E = 25.7$ MeV are 96% HF for $E' = 0-4$ MeV and 67% HF for $E' = 4-8$ MeV under the following assumptions:

1. If the first collision does not involve the odd nucleon, then $I_0 = 9/2$ should not be used for calculating the formation stage ($n=3$) in the pre-compound part. Instead $I_0 = 1/2$ has been used.
2. If the first collision is uniformly probably inside the entire nucleus volume, then a smaller spin-cutoff parameter than prescribed should be used, at least for $n=3$. The adopted value is $c = 0.0888 a^{2/3}$.

Due to the way TNG was programmed, the same assumptions had to be used in both the precompound and compound parts of the calculation. Therefore, the f_2 and f_4 coefficients for small E' had to be too high, not only for the 25.7 MeV calculation, but for the 14.6 MeV calculation also.

Comments (15)

The angle-integrated cross sections were calculated with 1-MeV bins, which is apparently too wide for the $(n,2n)$ and $(n,3n)$ calculations near threshold.

PRANG [8]

Relation of equilibrium to pre-equilibrium part (5)

Combined treatment of pre-equilibrium and equilibrium contributions (master-equation approach).

Total level density in equilibrium part (7)

Williams' formula with a "renormalisation" to the back-shifted Fermi gas formula [23]:

$$\omega_n(U) = \sqrt{\frac{\pi}{3}} \frac{U}{a^{1/4}(U+t)^{5/4}} \omega_n^{\text{Williams}}(U)$$
$$a = \frac{\pi^2}{6} g; \quad U = E^2 - \Delta.$$

The parameters a and Δ have been fitted to the experimental level density information, as prescribed.

Particle-hole density (8)

See above.

Internal transition rates (10)

The expression for $\langle M^2 \rangle$ was:

$$\langle M^2 \rangle = \frac{650}{(13g)^3 E}$$

Note that the numerical value is larger than usual because a different level-density formula has been adopted.

Emission rates (11)

Kalbach's Q-factor has been used with $Q=1$ (exactly) at $n \geq \bar{n}$. For α -emission $\gamma_\alpha = 10$ at $n \leq \bar{n}$, and $\gamma_\alpha = 1$ at $n \geq \bar{n}$.

Angular distribution (13)

The "angle-energy correlated model" as described by C. Costa et al., [19], has been used. The f_2 - coefficient has been adjusted (renormalization) to fit the data of Hermsdorf et al. for a large class of elements; see dashed curves in Figs. 5A, 6A. Full curves represent unadjusted results in Figs. 5, 6.

Comments (15)

An updated version of PRANG, named GRYPHON, has been presented at the Santa Fe conference [76].

PEQGM [9]

Pre-equilibrium model part (4)

Master equations start with $n_0 = 1$ (1p0h). For the calculation of continuous particle emission, this is indistinguishable from $n_0 = 3$. Significant difference appears for gamma spectra where $n_0 = 1$ is essential [62], see Fig. 19.

Relation of equilibrium to pre-equilibrium part (5)

All the calculations are done within the pre-equilibrium formalism, without treatment of discrete levels and without any influence of angular momentum. The equilibrium is achieved only as a limit of the pre-equilibrium stage; no strict division between both parts is made. Master equations are firstly integrated in time (from 0 to ∞), all the rest of calculations deals only with the algebraic equations for time integrals (which contain both the parts, the pre-equilibrium and the equilibrium ones).

Options (6)

The number of particles can be easily increased by simple adjustment of arrays.

γ -ray emission (14)

See Refs. [9, 62, 63]. The E1 normalisation constant used for all nuclei was 1.79.

PREM [10]

Internal transition rates (10)

$$\begin{aligned} \langle M^2 \rangle &= \frac{\hbar/2\pi}{g_A^3} (1.6 \times 10^{21} E^{-1} - 6.0 \times 10^{18}) / C \downarrow \\ &= \frac{\hbar/2\pi G^3}{\pi} A^{-3} (1.6 \times 10^{21} E^{-1} - 6.0 \times 10^{18}) / C \downarrow \text{ MeV}^2 \end{aligned}$$

where $g_A = A/G$, $G=13$, $C \downarrow = 7.4$ and E the excitation energy in MeV.

Emission rates (1)

The expression for emission rates are given in Ref. [10].

Transmission coefficients: cross sections are approximated by the simple expressions

$$\sigma_n = \pi R^2, \quad \sigma_p = \begin{cases} 0 & \text{for } E < V_c \\ \pi R^2 (1 - V_c/E) & \text{for } E > V_c \end{cases}$$

where $R = r_0 A^{1/3}$ (r_0 , the nuclear radius parameter, was taken to be 1.647 fm). This value was chosen by comparing with the cross-section at 14.6 MeV obtained from optical-model calculations and

$$V_c = \frac{1.44(Z-1)}{r_0 (1+(A-1)^{1/3})} C \uparrow;$$

$C\uparrow$ is a correction factor taken to be 0.937 by comparing with the cross section at 14.6 MeV obtained from optical-model calculations.

PRECO-D2 [12]

Pre-equilibrium model part (4)

States which contain an unbound particle degree of freedom are differentiated from those that do not. The pre-equilibrium cross-section is divided into multi-step direct and multi-step compound parts ($n_0=3$). The closed-form reaction equations allow for λ^0 and λ^- transition which change the bound/unbound character of the state as well as for four types of λ^+ transitions. The closed-form equations are slightly modified from those in Ref. [44].

Relation of equilibrium to pre-equilibrium parts (5)

$$\sigma_{\text{PRE}} = \sum_{b=n,p,\alpha} \int_0^{E-B} \frac{d\sigma}{d\epsilon}(a,b)_{\text{PRE}} d\epsilon$$

$\sigma_{\text{CN}} - \sigma_{\text{PRE}}$ replaces σ_{CN} in Weisskopf-Ewing evaporation calculation.

For nucleon-induced reactions $\sigma_{\text{CN}} = 0.9 \sigma_{\text{RXN}}$ to allow for direct reactions involving complex particles.

Total level density in equilibrium part (7)

No angular momentum dependence is considered. The single Fermi gas (to be consistent with the one component exciton model for pre-equilibrium) state density is used:

$$\rho(E) = \frac{1}{E} \exp[2(aE)^{1/2}], \quad a = \pi^2 g/6,$$

where g is the value used in the pre-equilibrium calculations, namely $g = A/13$.

Particle-hole density (8)

Williams' state density is used but with a slightly different $A_{p,h}$:

$$A_{p,h} = \frac{p_m^2}{g} - \frac{p(p+1)+h(h+1)}{4g} \quad \text{with } p_m = \max(p,h).$$

This formula with finite-well depth corrections applied for $h = 1,2$ is the starting point for the derivation of the densities of bound and unbound configurations (i.e. states without and with unbound particle degrees of freedom). The state-density formulae (which also contain modifications to g for long range deviations from the equi-spacing model) are given in Ref. [43].

Internal transition rates (10)

Separate rates are used for $\lambda_+^{(uu)}$, $\lambda_+^{(ub)}$, $\lambda_+^{(bu)}$, $\lambda_+^{(bb)}$, $\lambda_0^{(ub)}$, $\lambda_0^{(bu)}$, $\lambda_-^{(ub)}$ and $\lambda_-^{(bu)}$. All are given in Ref. [43].

Emission rates (11)

In PRECO-D2 the Q-factor is either calculated according to Ref. [27] (as for the TNL-1 calculations) or (as for TNL-2) using the relation

$$Q_D^{(G)}(p) = \frac{\sum_{p_\pi=p_{\min}}^{p_{\max}} \left[\frac{Z}{A} \right]^{n_\pi - Z_D} \left[\frac{N}{A} \right]^{n_\nu - N_D} \frac{(p - A_D)!}{(p_\pi - Z_D)!(p_\nu - N_D)!} \cdot \frac{h!}{h_\pi! h_\nu!}}{\sum_{p_\pi=Z_a}^{p - N_D} \left[\frac{Z}{A} \right]^{n_\pi} \left[\frac{N}{A} \right]^{n_\nu} \frac{p!}{p_\pi! p_\nu!} \cdot \frac{h!}{h_\pi! h_\nu!}},$$

which is based on the assumption of Gadioli et al (Ref. [42]) that states are populated in proportion to their state densities.

Pre-equilibrium alpha emission is treated as the loss of four-particle degrees of freedom (two protons and two neutrons). No preformation or coalescence factor is used. Direct emission of alphas by knockout and three-nucleon pickup are calculated as in Ref. [27] with the modifications described in the PRECO-D writeup [12].

Transmission coefficients: inverse reaction cross-sections are also used in the compound part.

Angular distribution calculation

Kalbach-Mann systematics [15] are also used for the compound part.

Comments(15)

Recently, a paper on surface effects in the exciton model has been written by the contributor [79].

AMAPRE [40]

Spectrum calculations (12)

The spectrum is represented in energy bins of variable width. The data given are the mid-point values of the energy bins.

Angular distribution calculation

The method described in Ref. [19] has been adopted. Refraction of incoming and outgoing beam has been included (note of compilers: different coefficients ρ_i have been used as compared to the PRANG calculations; the graphs have not been included in this review, because they are difficult to read).

Comments(15)

The code AMAPRE is still under development. First results have been obtained for Nb-93, Pb-208 and Bi-209, see Proc. Conf. on Neutron Physics, Kiev, 1983.

Main points for future improvement:

- * description of multi-particle emission of neutrons and charged particles near the reaction thresholds;
- * γ -ray competition;
- * exciton-energy dependent level densities.

Note: The spectrum of secondary neutrons from (n,2n) at 14.6 MeV has been taken from the code STAPRE. The corresponding AMAPRE data are still in question.

ALICE-LIVERMORE (LLL-1,2) [13]

Pre-equilibrium model part (4)

Results sent for (a) GDH model, (b) Hybrid model.

Relation of equilibrium to pre-equilibrium parts (5)

Incoherent sum of P.E. + EQ. components, with σ_R depleted for P.E. prior to calculation of EQ. component.

Total level density in equilibrium part (7)

$$\rho(E) \sim (E-\Delta)^{-5/4} \exp(2\sqrt{a(E-\Delta)})$$

with option of Δ being defined as backshifted value or with odd-even reference surface as $\Delta = 0$. Results sent for backshifted option.

Particle-hole density (8)

Williams' expression with Pauli correction used, but $g = A/20$ at $E=E_s$ and energy dependent with Fermi-gas dependence on $E^{3/2}$.

Transition rates (11)

The internal transition rates are based on nuclear-nuclear scattering corrected for the Pauli exclusion principle; the initial exciton numbers are based on target N and Z, and on relative $\sigma_{nn}, \sigma_{pp}, \sigma_{pn}$. Emission rate into the continuum is based on simple phase space considerations.

α -emission (11)

Only equilibrium α 's in results submitted; we have not run QFS model for these cases.

Transmission coefficients (11)

T_ℓ enter GDH results via σ_ℓ of entrance channel.

Angular distribution (13)

Based on N-N scattering kernel for Fermi gas, folded using GDH model. Analytic expressions of Kikuchi and Kawai [45] used. A 3-dimensional folding method has been used, as discussed in Ref. [20]. Results have been submitted without and with refraction/diffraction (In Figs. 7-16 the results without refraction/diffraction are presented; in Figs. 13 and 14 a comparison is given of results with and without refraction).

SECDIST/HAFKA [14,47]

Relation of equilibrium to pre-equilibrium parts (5)

The total neutron emission cross-section (E = energy of the incident neutron; ϵ = energy of the emitted neutron) is calculated by:

$$\frac{d\sigma(E, \epsilon)}{d\epsilon} = \left[\frac{d\sigma(E, \epsilon)}{d\epsilon} \right]_{\text{eq.}} + \left[\frac{d\sigma(E, \epsilon)}{d\epsilon} \right]_{\text{pre-eq.}}$$

The equilibrium part is calculated by the Hauser-Feshbach code HAFKA4, the pre-equilibrium part is calculated by SECDIST without any adjustment (σ_r is depleted for the pre-equilibrium contribution prior to the calculation of the equilibrium part).

Particle-hole density (8)

For $n_0=3$ the geometry-dependent particle-hole densities of Blann, for $n \geq 5$ those of Ericson without any corrections, are used.

Discrete levels (9)

In the equilibrium calculation the discrete levels are considered as usual in Hauser-Feshbach calculations.

In the pre-equilibrium calculations, the discrete levels are not considered explicitly, but the high energy tail can be interpreted as the average over the DWBA-results for the first discrete levels, as shown by H. Jahn (Harwell Conference 1978) for Fe-56.

Internal transition rates (10)

The transition probability is calculated from the imaginary part of the optical potential. No fit parameter is used other than the optical model parameters.

Angular distribution (13)

A PWBA calculation was used for emission from $n=n_0=3$. This should be interpreted as an average direct component without collective excitation [47]. The compound part of the emission spectrum and the contributions of pre-equilibrium neutrons for $n \geq 5$ were assumed to be isotropic. See expression in Refs. [46, 47]. The value of L was selected to be equal to 3. Some graphs (provided by participants) are given in Fig. 18. Results at 25.7 MeV refer to preliminary work. No (n,2n) nor (n,3n) contributions have been taken into account in the angular distributions.

Comments (15)

The editors refer to Ref. [47], containing a critical review of precompound models.

Note discrepancies between experimental data of Refs. [37, 39], see Fig. 17, suggested by E. Bahm and H. Jahn [78]. The contributors stress that agreement between theory and experimental data is obtained without using fit parameters in the expression for $\lambda^+(\epsilon)$.

FIGURE CAPTIONS

- Fig. 1A** Calculated total neutron-emission spectra at E=14.6 MeV on a linear-logarithmic scale for class A codes. The points refer to bins. The GNASH results (LAS) are indicated by straight line segments in order to have a reference in the other figures.
- Fig. 1B** Calculated total neutron-emission spectra at E=14.6 MeV on a linear-logarithmic scale for class B codes. The GNASH results (LAS) are given for reference with other figures.
- Fig. 1C** Calculated total neutron-emission spectra at E=14.6 MeV on a linear-logarithmic scale for class C codes. The GNASH results (LAS) are given for reference with other figures.
- Figs. 1D,2D** Experimental values of total neutron-emission spectra at 14.6 MeV compared to the GNASH results (straight-line segments). The reference for the experimental data are given in the CINDA data index (see $\sigma_{n,em}$, exp. data). The angle-integrated data were obtained from a least-squares analysis on the original experimental values from TUB-75 (Hermsdorf et al. [39]) and LLL (Kammerdiener [73]) at ECN, Petten. Those of (Salnikov et al), KGU-81 (Degtyarev et al. [80]) and OSA-83 (Takahashi et al. [37]) were analysed at IRK, Vienna (courtesy of Prof. Dr. H. Vonach). The TUD-75 data at 6 to 9 MeV were the points at which the participants were asked to fit their data.
- Fig. 2A** Calculated total neutron-emission spectra at E=14.6 MeV on a double-logarithmic scale for class A codes. The points refer to bins. The GNASH results (LAS) are indicated by straight line segments in order to have a reference in the other figures.
- Fig. 2B** Calculated total neutron-emission spectra at E=14.6 MeV on a double-logarithmic scale for class B codes. The GNASH results (LAS) are given for reference with other figures.
- Fig. 2C** Calculated total neutron-emission spectra at E=14.6 MeV on a double-logarithmic scale for class C codes. The GNASH results (LAS) are given for reference with other figures.
- Fig. 3A** Calculated total neutron-emission spectra at E=25.7 MeV on a linear-logarithmic scale for class A codes. The points refer to bins. The GNASH results (LAS) are indicated by straight line segments in order to have a reference in the other figures.
- Fig. 3B** Calculated total neutron-emission spectra at E=25.7 MeV on a linear-logarithmic scale for class B codes. The GNASH results (LAS) are given for reference with other figures.
- Fig. 3C** Calculated total neutron-emission spectra at E=25.7 MeV on a linear-logarithmic scale for class C codes. The GNASH results (LAS) are given for reference with other figures.

- Figs. 3D,4D** Experimental values of total neutron-emission spectra at 25.7 MeV compared to the GNASH results (straight-line segments). The experimental points are from OHO (Marcinkowski et al. [38]).
- Fig. 4A** Calculated total neutron-emission spectra at $E=25.7$ MeV on a double-logarithmic scale for class A codes. The points refer to bins. The GNASH results (LAS) are indicated by straight line segments in order to have a reference in the other figures.
- Fig. 4B** Calculated total neutron-emission spectra at $E=25.7$ MeV on a double-logarithmic scale for class B codes. The GNASH results (LAS) are given for reference with other figures.
- Fig. 4C** Calculated total neutron-emission spectra at $E=25.7$ MeV on a double-logarithmic scale for class C codes. The GNASH results (LAS) are given for reference with other figures.
- Fig. 5A** Reduced Legendre coefficients f_1 and f_2 as a function of outgoing energy at incident energy of $E=14.6$ MeV. The angle integrated emission spectrum is given at the top of the figure. The calculated data are obtained with codes GNASH (modified KM systematics), TNG (generalised HF theory) and PRANG (angle-energy correlated model). Two PRANG results are given for f_2 , corresponding to a theoretical and an adjusted kernel (adjusted to systematics, see dotted curve). The experimental data are from various authors as indicated; see Refs. [37,39,73,80,81,82].
- Fig. 5B** Kalbach-Mann systematics compared to results of PRANG and GNASH (modified KM systematics). See further caption of Fig. 5A.
- Fig. 6A** Reduced Legendre coefficients f_1 and f_2 as a function of outgoing energy at incident energy of $E=25.7$ MeV. See further caption of Fig. 5A. The experimental data are from Marcinkowski et al. [38].
- Fig. 6B** Kalbach-Mann systematics [15] compared to results of PRANG and GNASH (modified KM systematics). See further caption of Fig. 6A.
- Fig. 7** Double-differential neutron-production cross section at $E=14.6$ MeV and $\theta \approx 20^\circ$ as a function of outgoing energy E' . The experimental data are from Takahashi et al. [37], without corrections for multiple scattering (at low E') and elastic scattering (at high E'). The calculated data of GNASH (LAS), TNG (LAS) and PRANG (ECN2) cover the full energy range; results from other codes are restricted to the high-energy part.
- Fig. 8** Double-differential neutron-production cross section at $E=14.6$ MeV and $\theta \approx 80^\circ$ as a function of outgoing energy E' . See further caption of Fig. 7.
- Fig. 9** Double-differential neutron-production cross section at $E=14.6$ MeV and $\theta \approx 140^\circ$ as a function of outgoing energy E' . See further caption of Fig. 7. Note that the measured data were obtained at $E=13.5$ MeV.

- Fig. 10** Double-differential neutron-production cross section at $E=25.7$ MeV and $\theta \approx 20^\circ$ as a function of outgoing energy E' . The experimental data are from Marcinkowski et al. [38], without correction for elastic scattering. See further caption of Fig. 7.
- Fig. 11** Double-differential neutron-production cross section at $E=25.7$ MeV and $\theta \approx 80^\circ$ as a function of outgoing energy E' . See further caption of Fig. 10.
- Fig. 12** Double-differential neutron-production cross section at $E=25.7$ MeV and $\theta \approx 80^\circ$ as a function of outgoing energy E' . See further caption of Fig. 10.
- Fig. 13** Angular-differential of neutron-production cross section at $E=14.6$ MeV and $E' \approx 6$ MeV. The experimental data are from Takahashi et al. [37], after averaging over the intervals 5-7 MeV; the uncertainties indicate maximum and minimum values in this range. Note that the data of Takahashi et al. correspond to different incident energies (14.85 MeV at $\theta = 15^\circ$ to 23.47 MeV at $\theta = 143^\circ$). There are two series of data points calculated with the ALICE/LIVERMORE code, with and without inclusion of refraction.
- Fig. 14** Angular distribution of neutron production cross section at $E=14.6$ MeV and $E' \approx 8$ MeV. Experimental data have been averaged over 7-9 MeV. See also caption of Fig. 13.
- Fig. 15** Angular distribution of neutron production cross section at $E=25.7$ MeV and $E' \approx 16$ MeV. The experimental data are from Marcinkowski et al. [38] (averaged over 16-17 MeV). Note that the values of E' are not exactly the same, leading to different absolute values of the cross sections.
- Fig. 16** Angular distribution of neutron-production cross section at $E=25.7$ MeV and $E' \approx 19$ MeV. See further caption of Fig. 15.
- Fig. 17** Discrepancies between experimental data on the angular distribution of the neutron-production cross section at $E=14-15$ MeV and $E' = 8-9$ MeV. The data shown are from Hermsdorf et al. [39], Kammerdiener [73] and Takahashi et al. [37] (Figure prepared by Bahm and Jahn [78]).
- Fig. 18** Angular distribution of neutron-production cross sections at $E=14.6$ MeV and $E=25.7$ MeV (preliminary results) for various outgoing energies according to a PWBA method as followed at KfK (code SECDIST). No $(n,2n)$ nor $(n,3n)$ contributions have been taken into account.
- Fig. 19** Calculated total photon-production spectra at $E=14.6$ MeV.

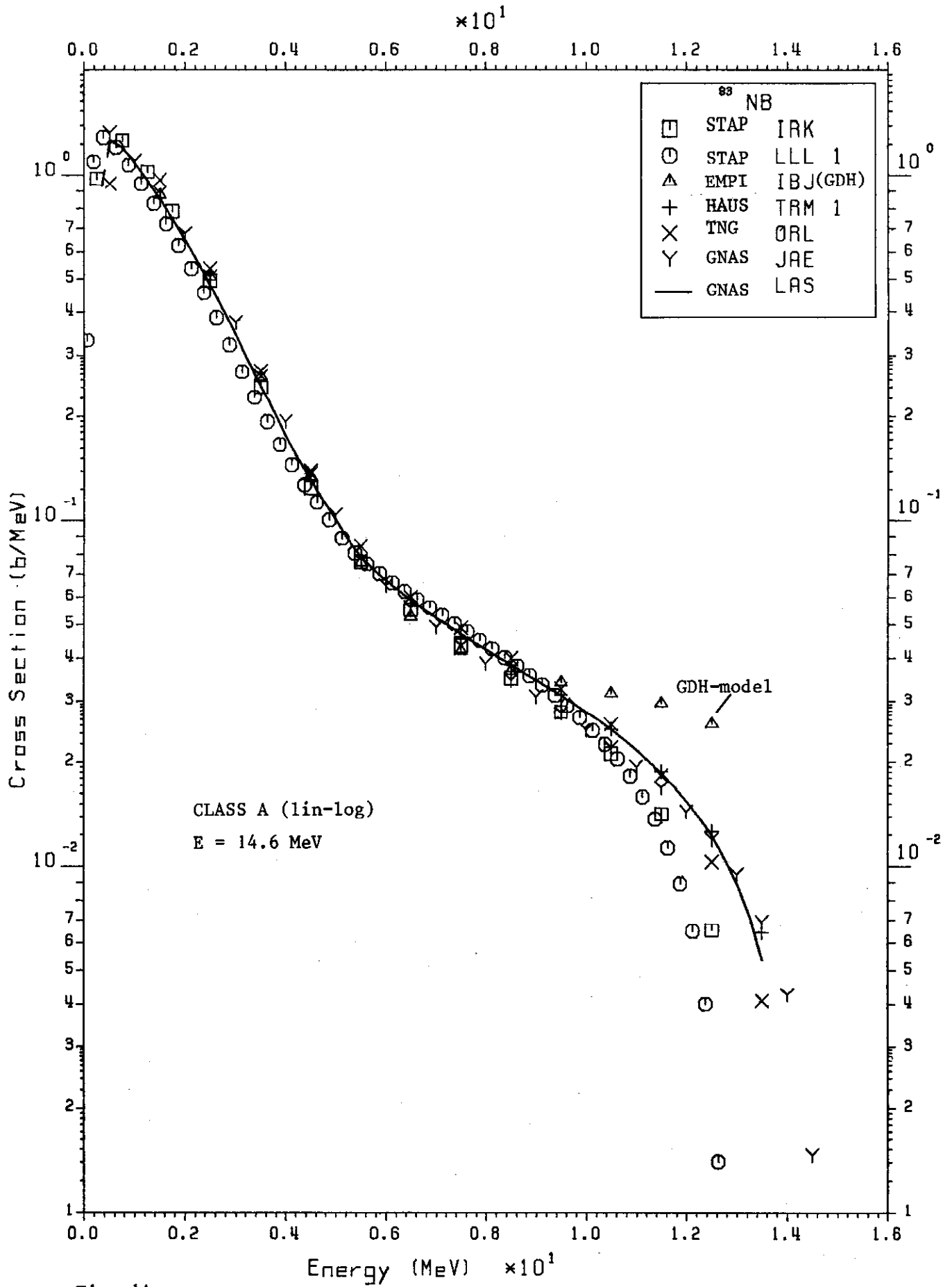


Fig. 1A.

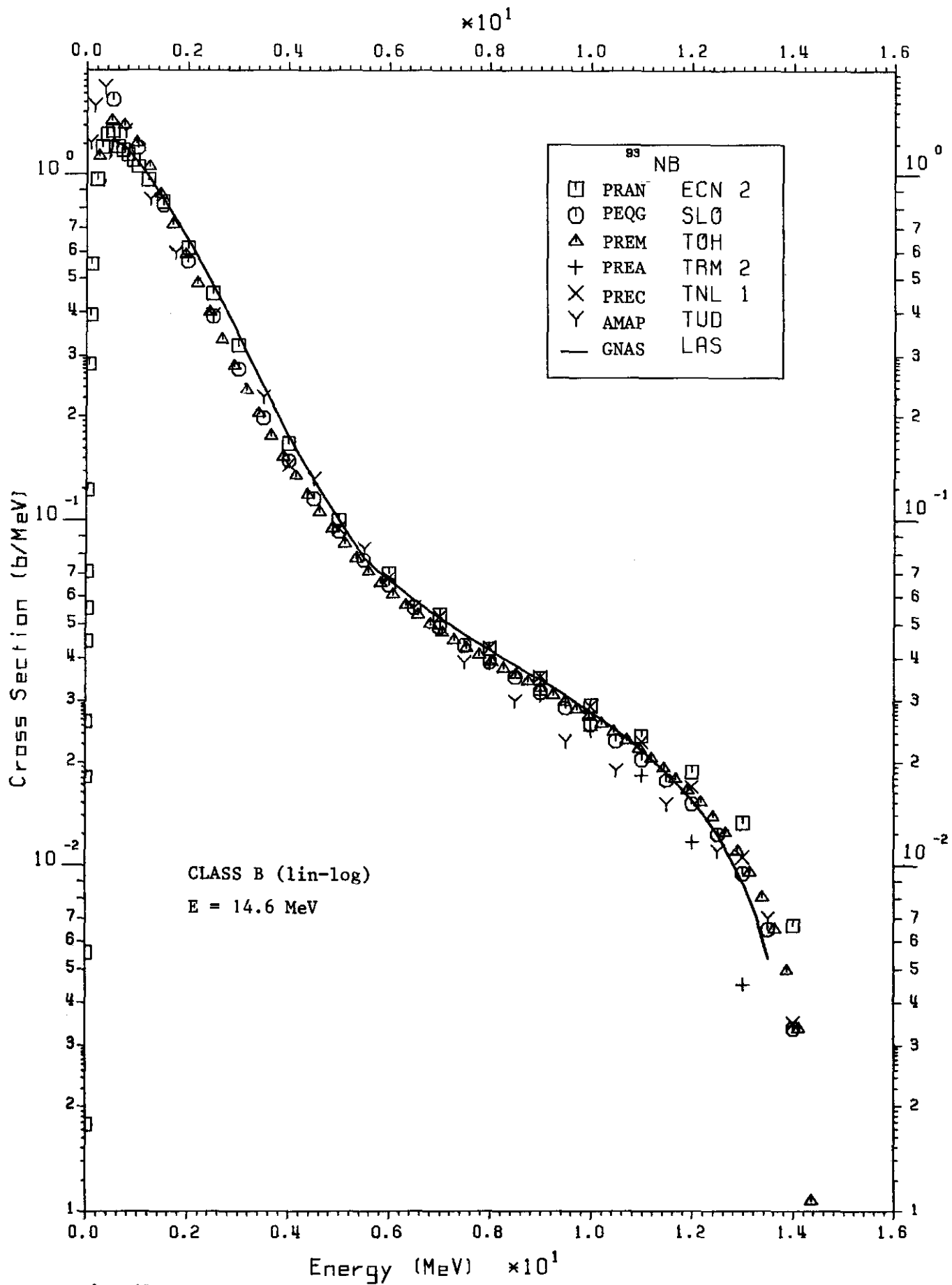


Fig. 1B.

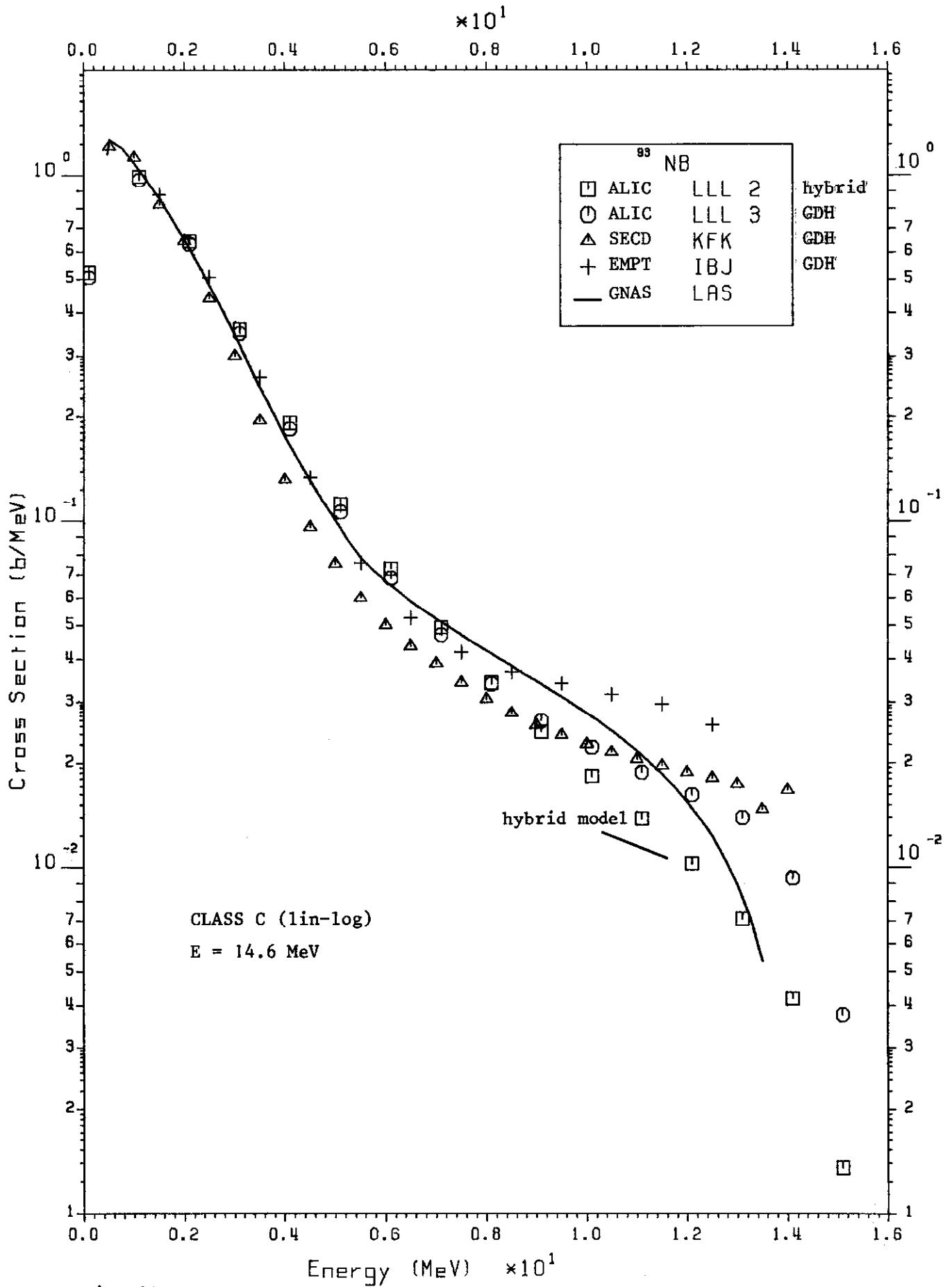


Fig. 1C.

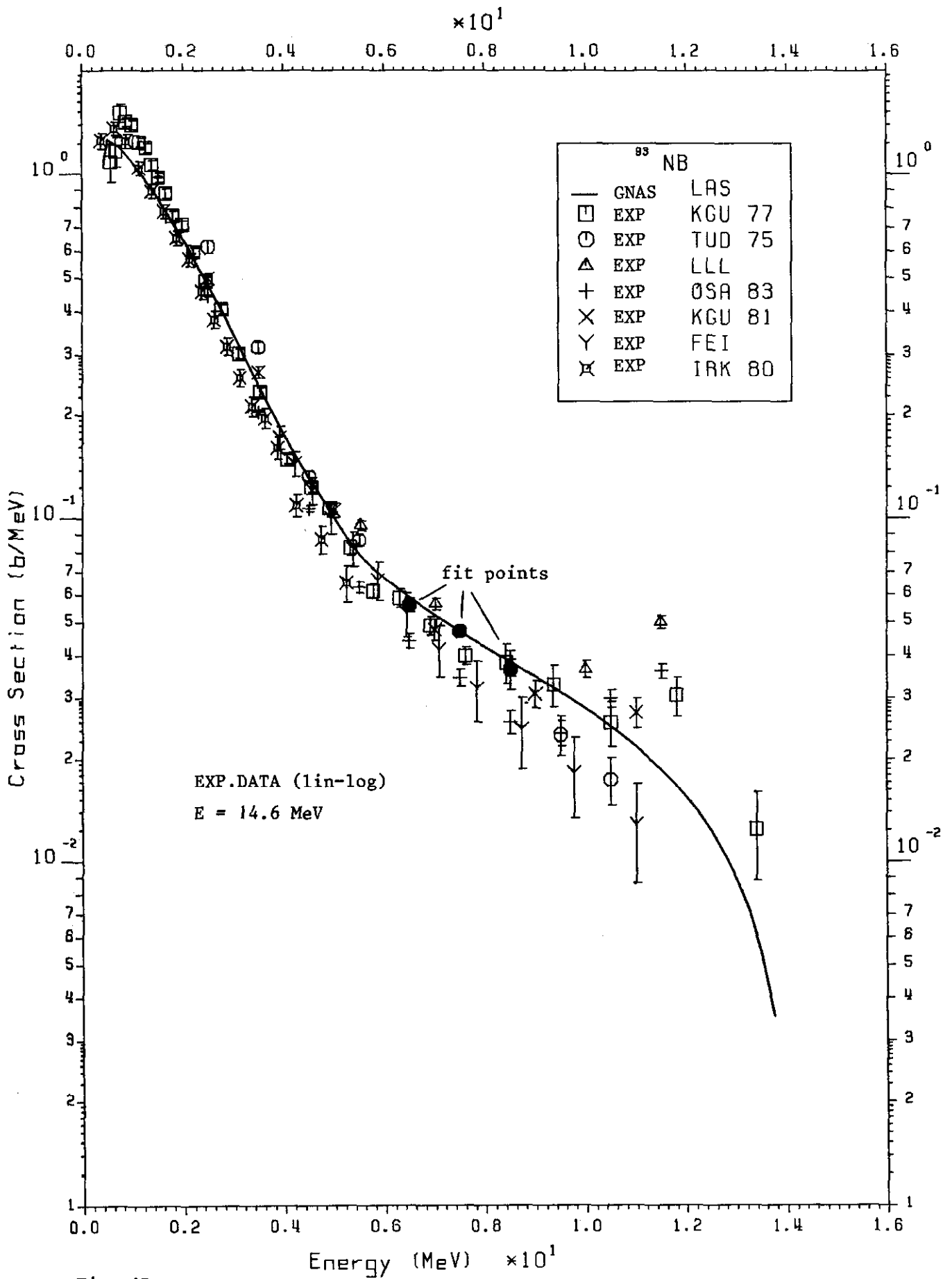


Fig. 1D.

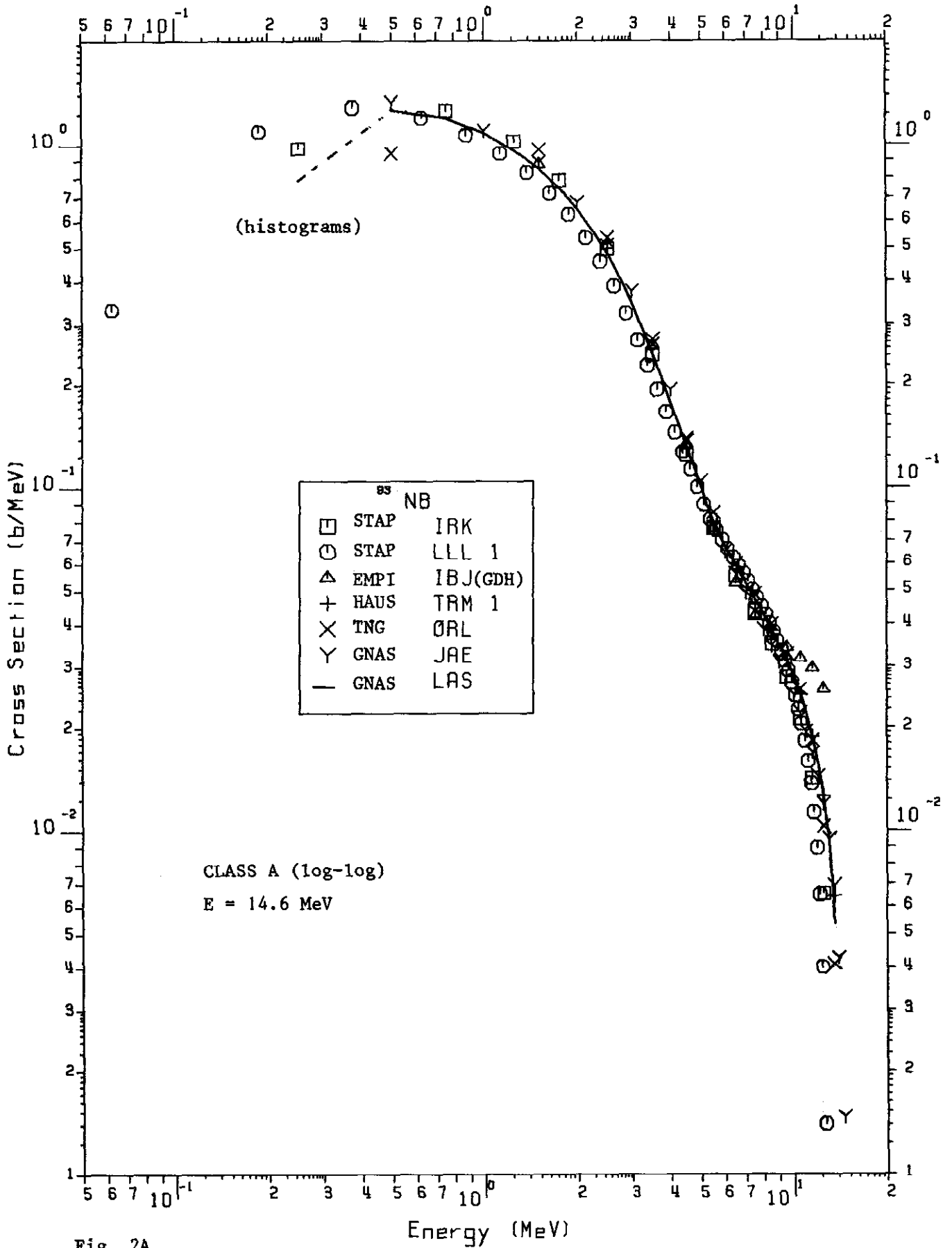


Fig. 2A.

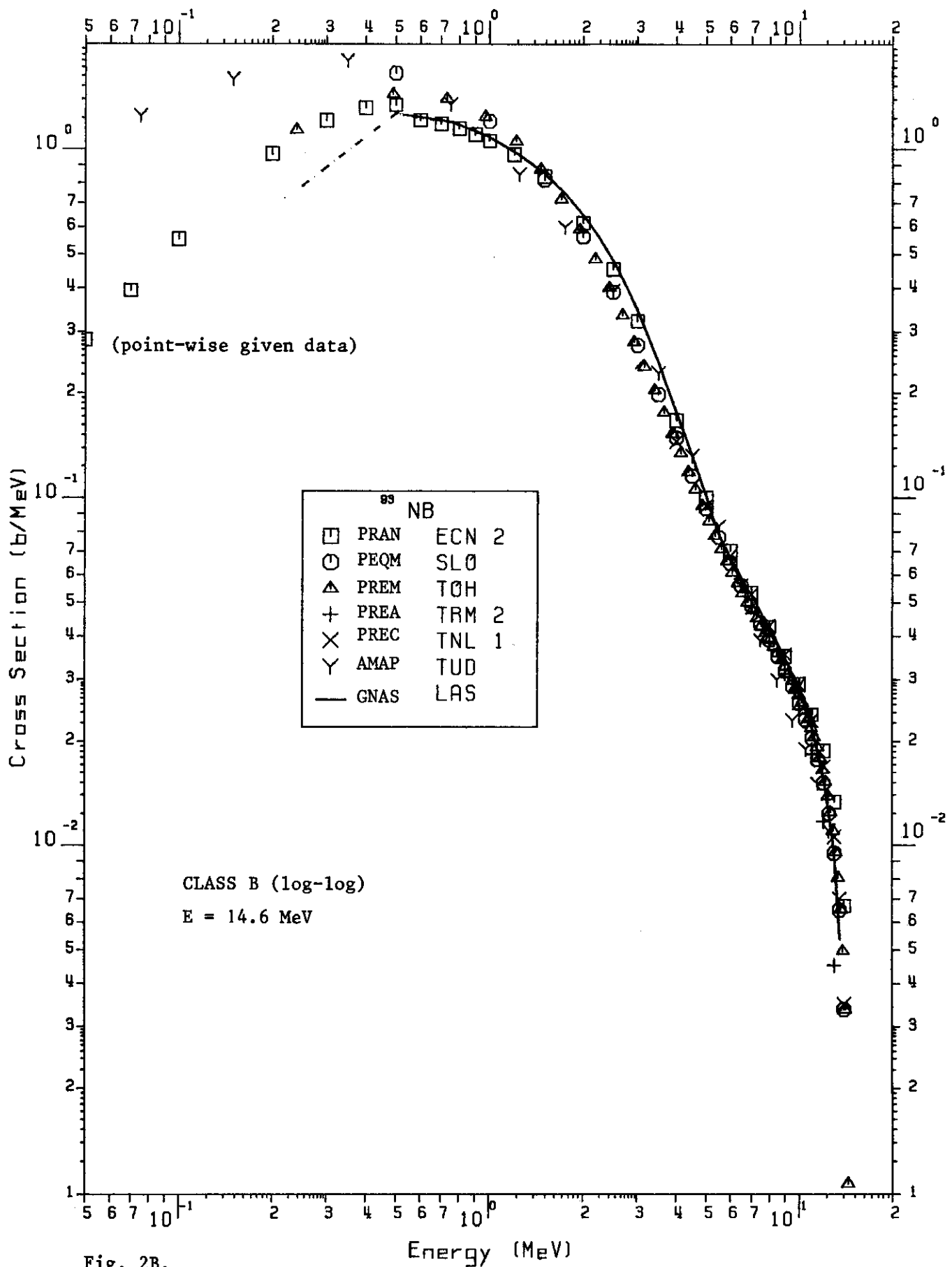


Fig. 2B.

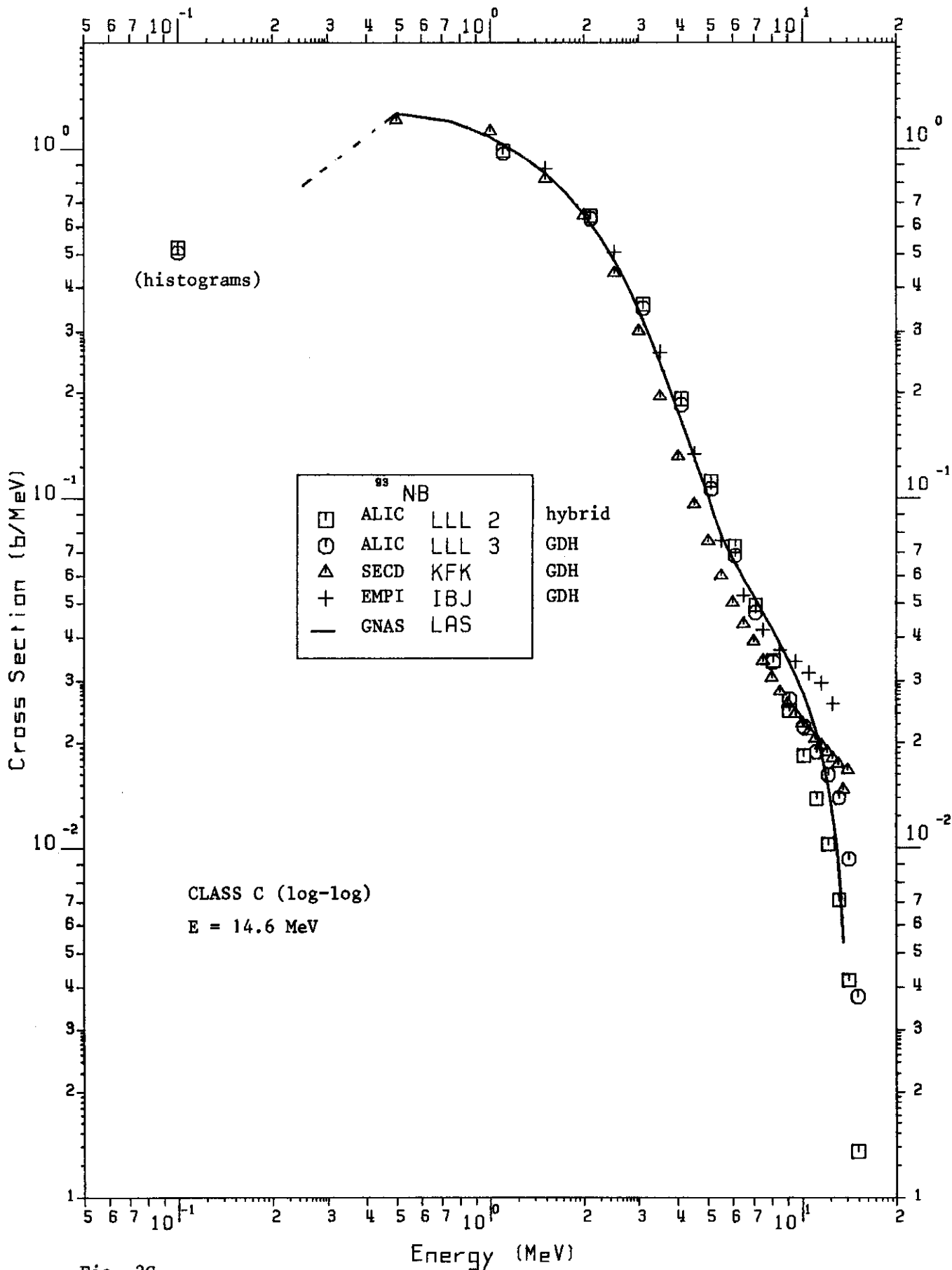


Fig. 2C.

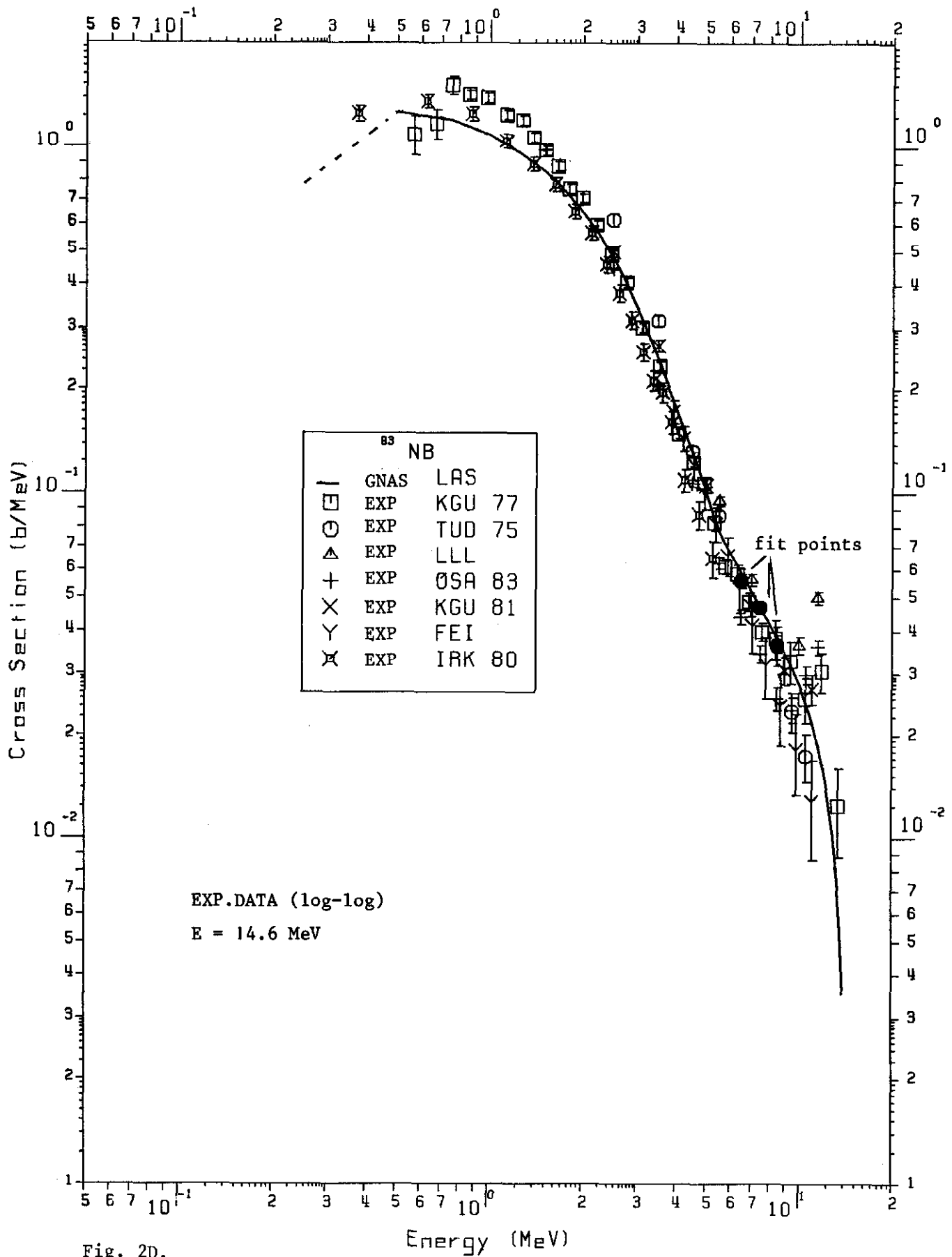


Fig. 2D.

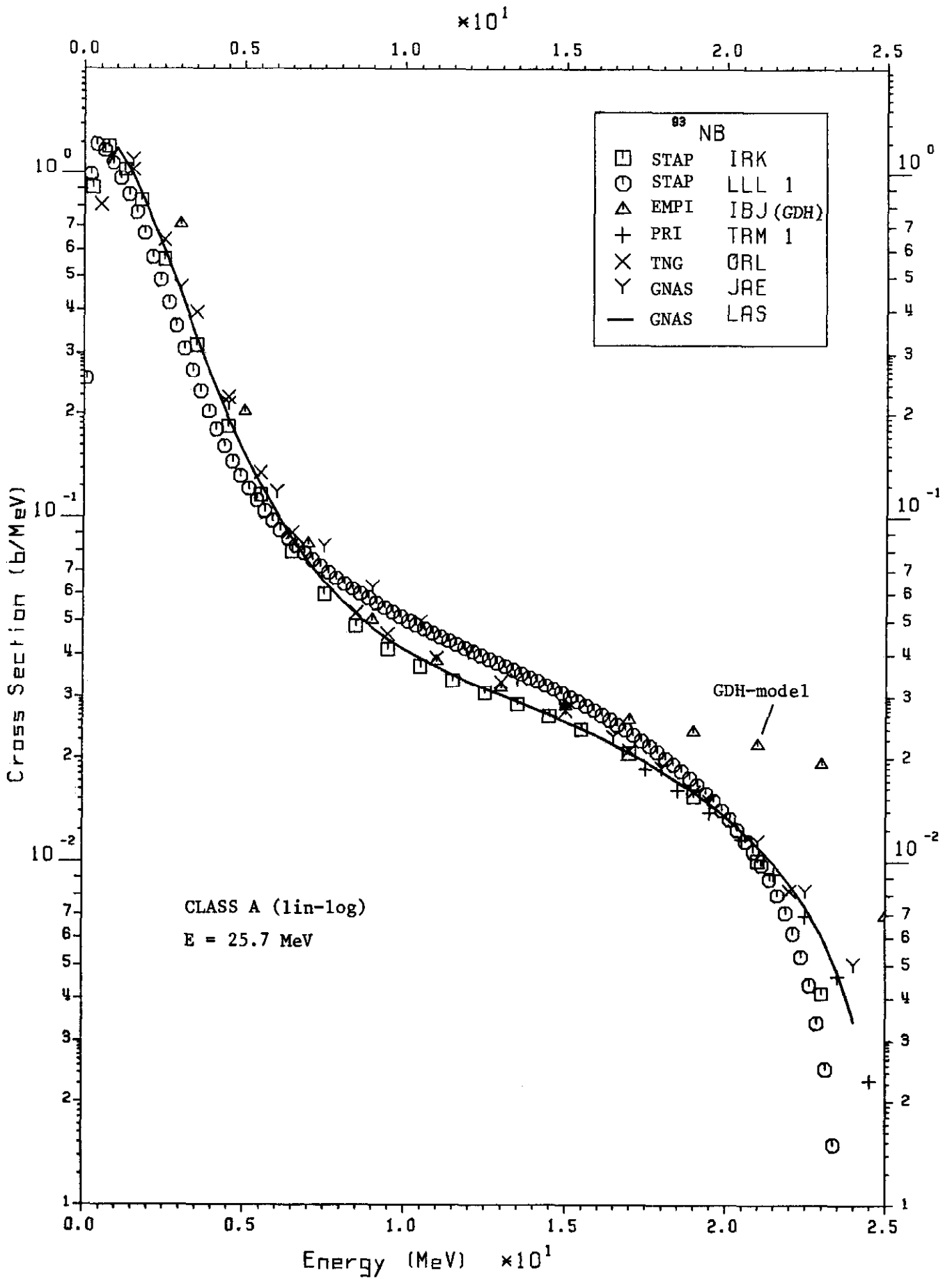


Fig. 3A.

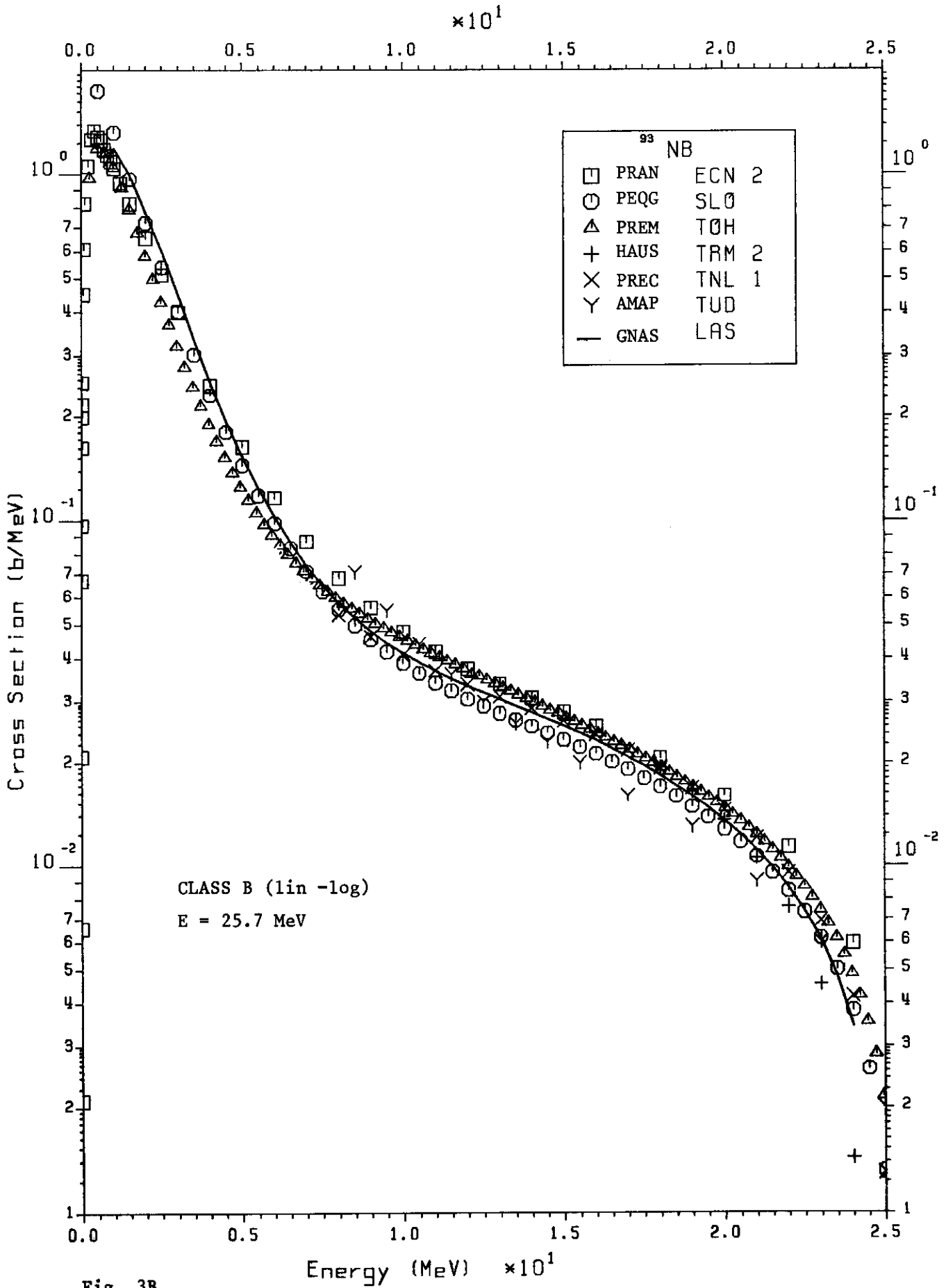
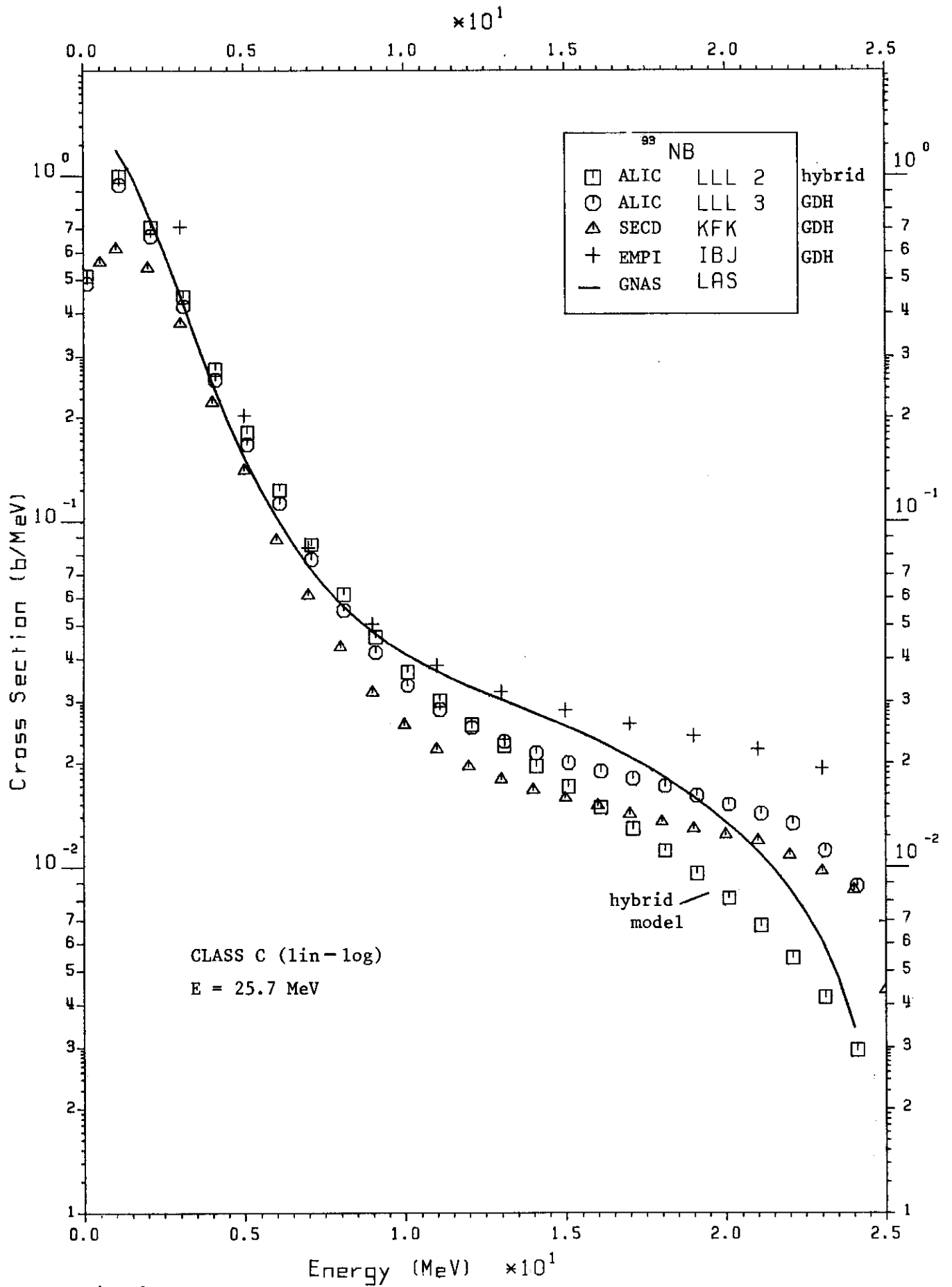


Fig. 3B.



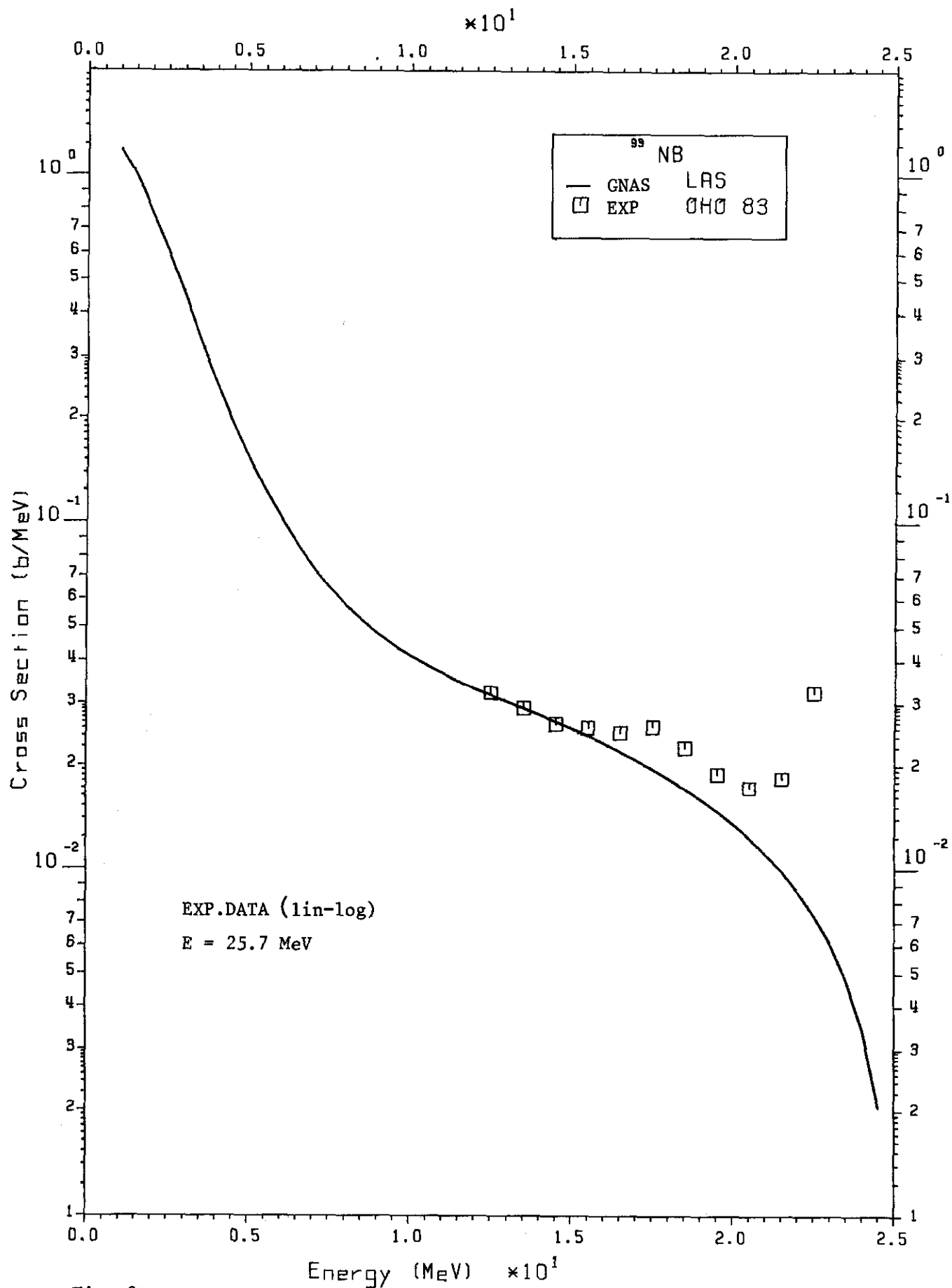


Fig. 3D.

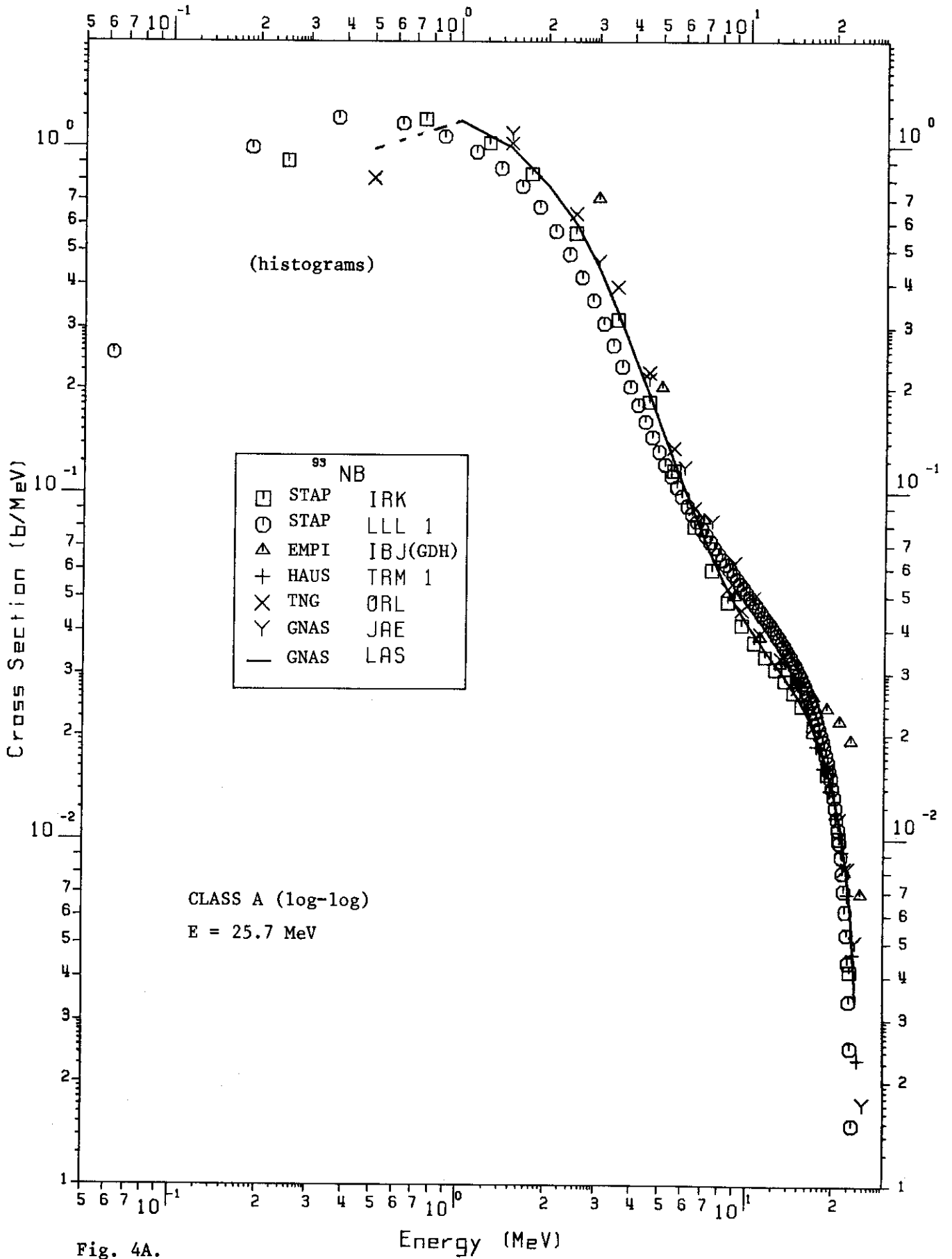


Fig. 4A.

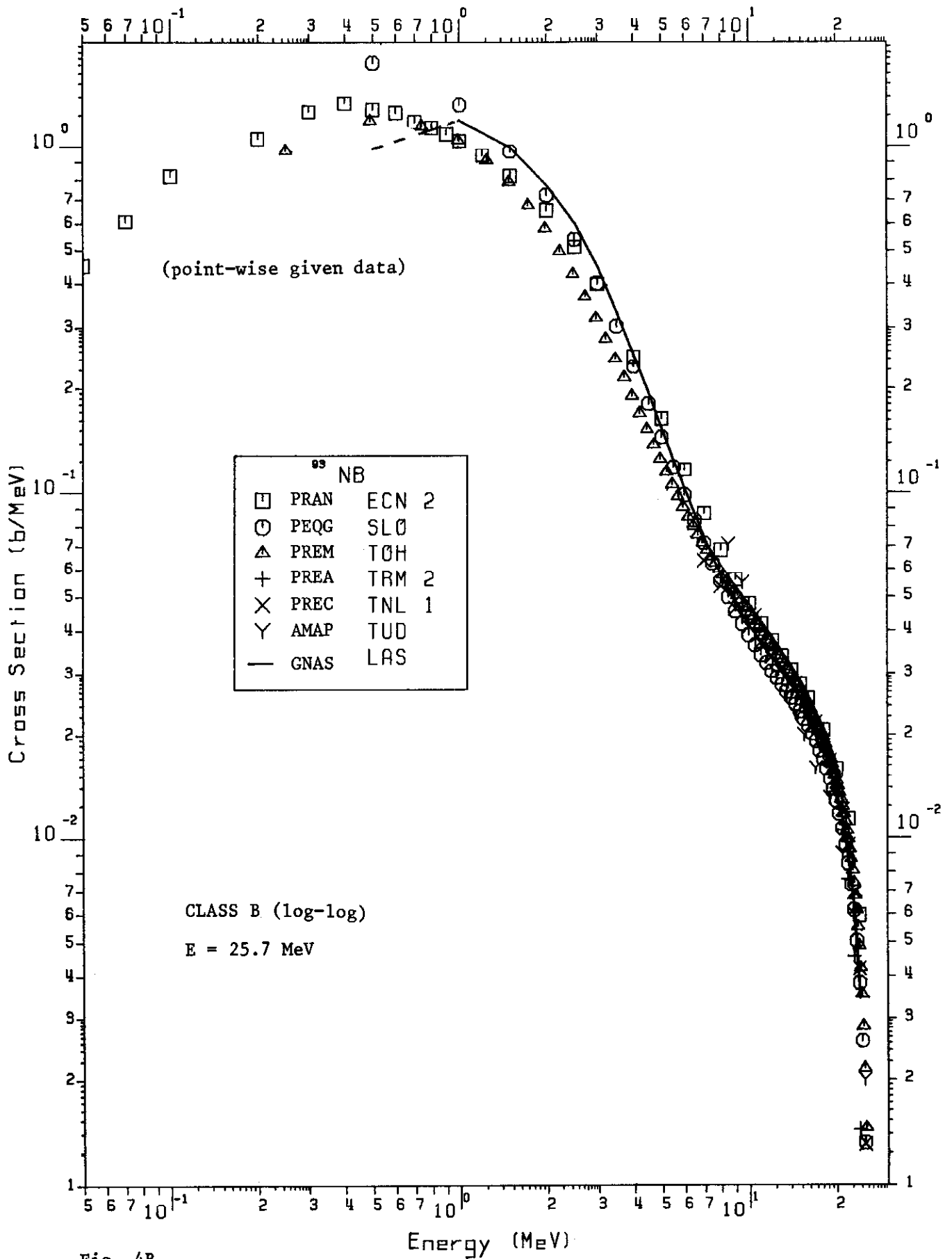


Fig. 4B

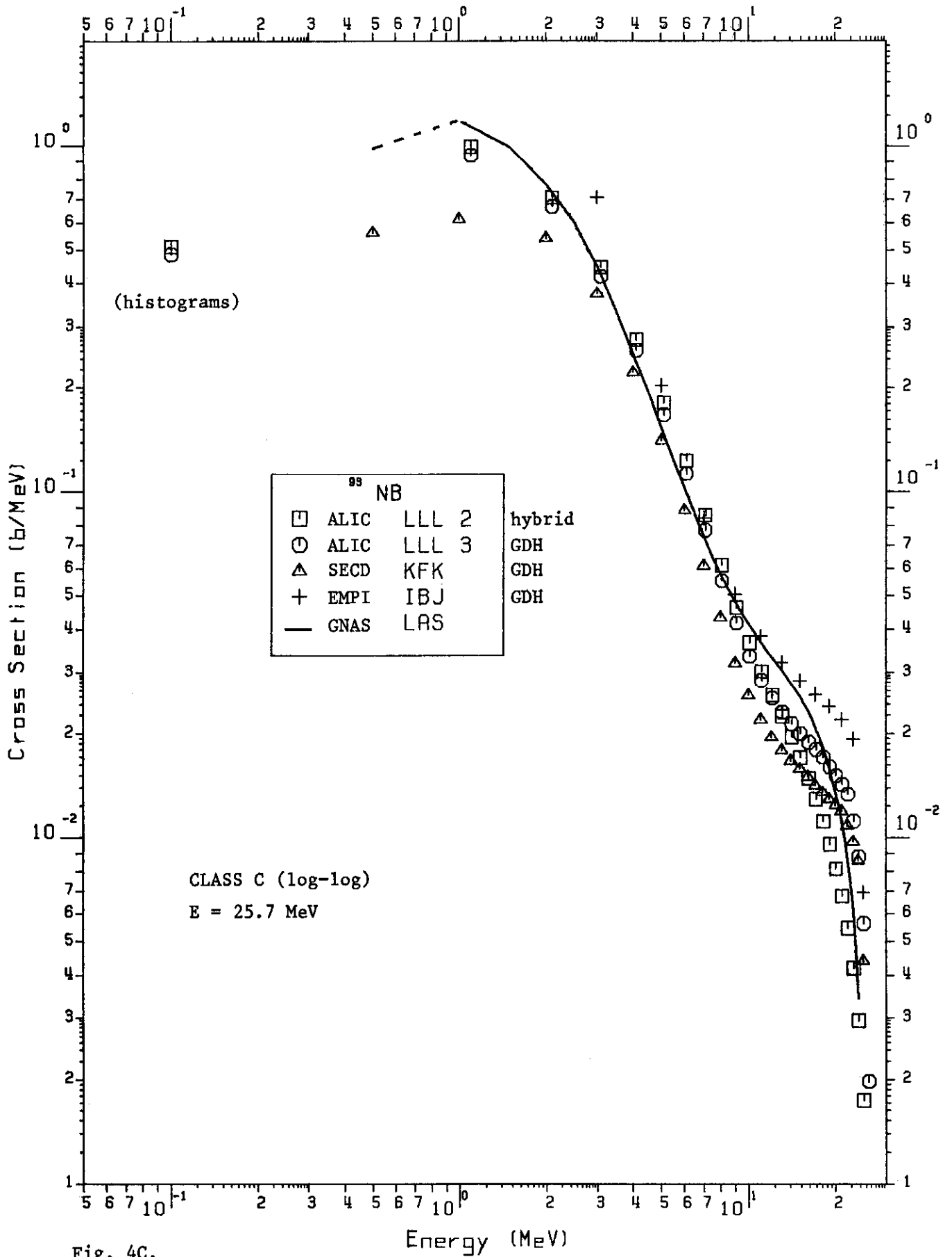


Fig. 4C.

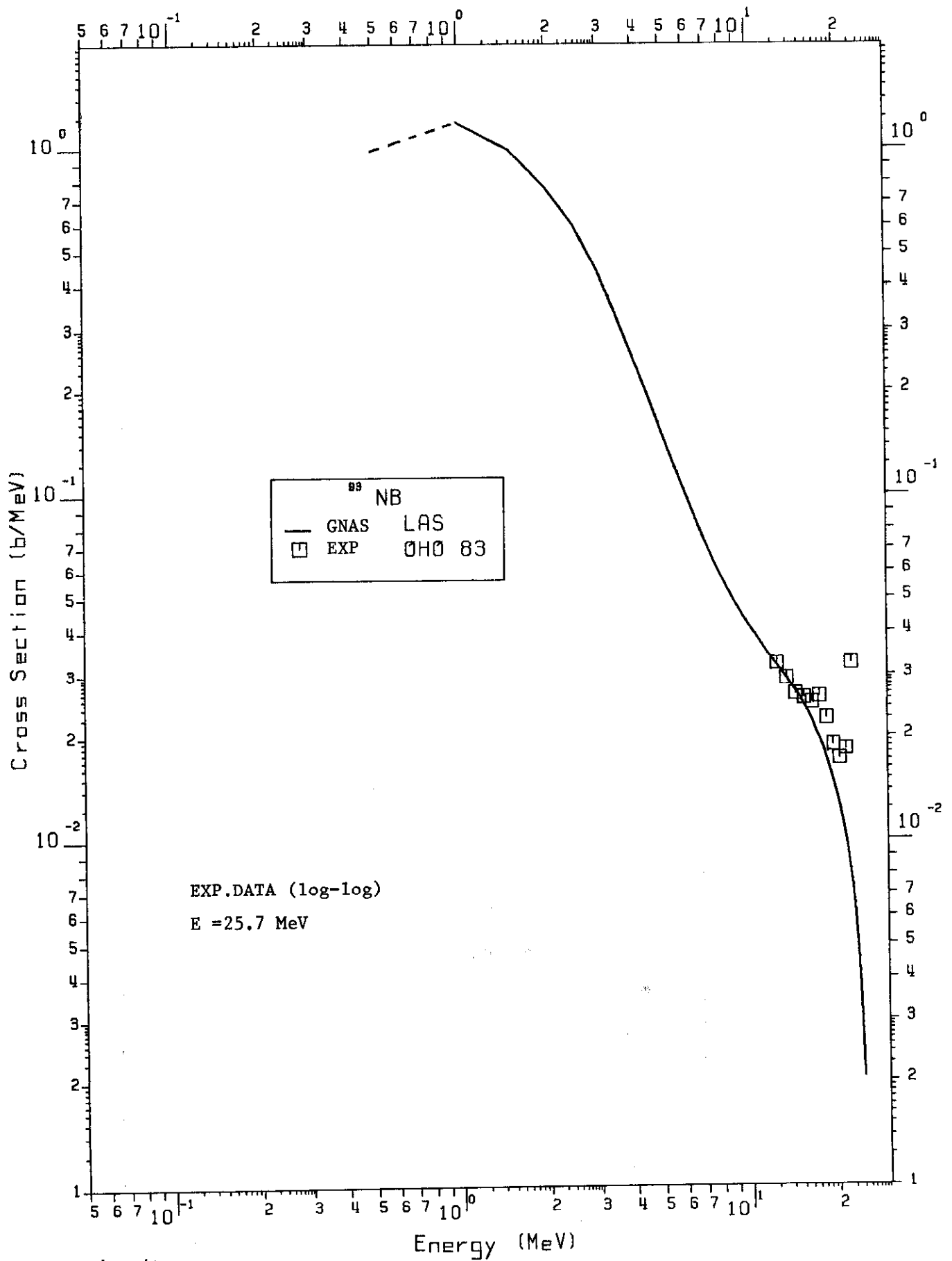


Fig. 4D

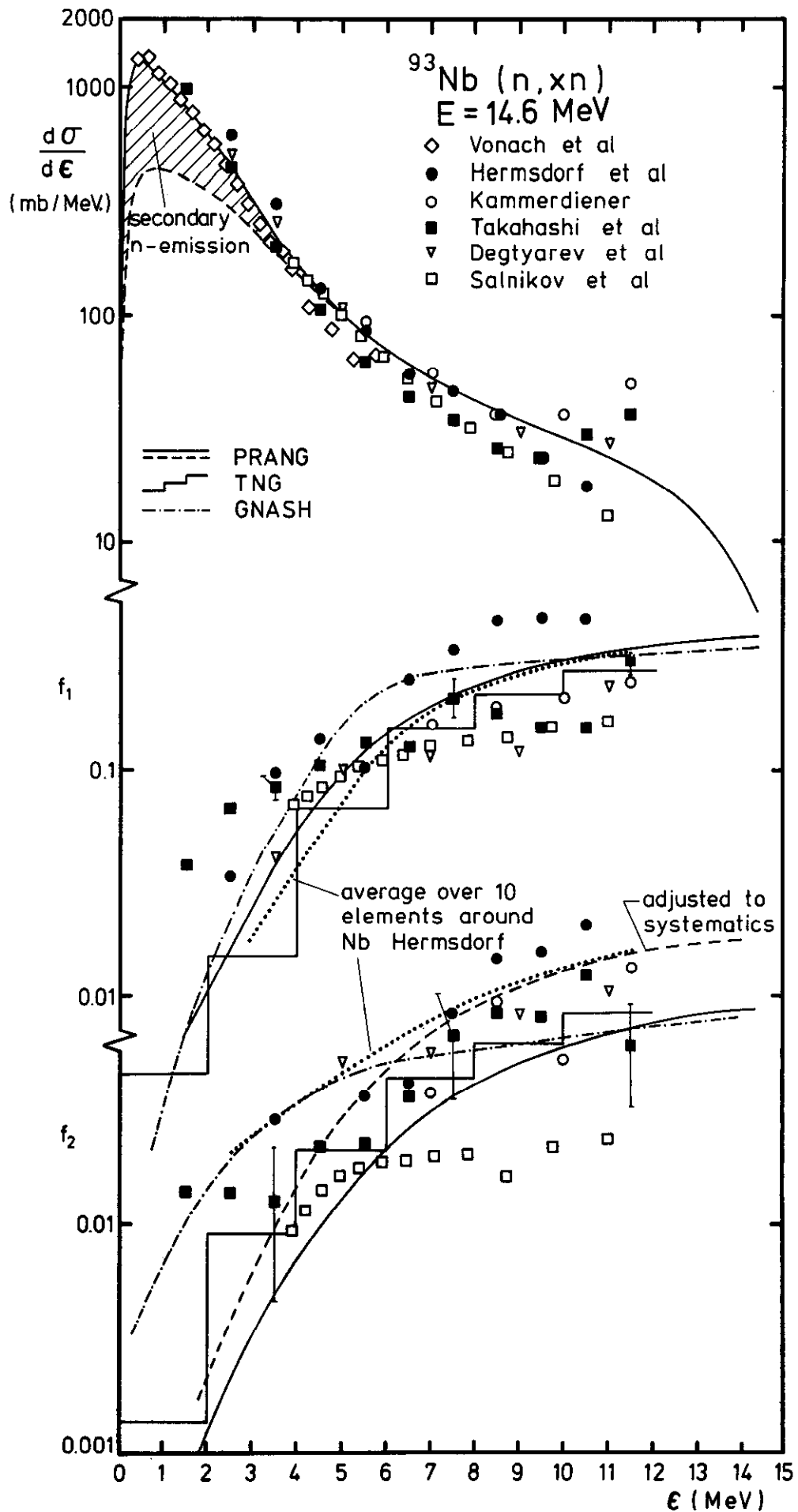


Fig. 5A.

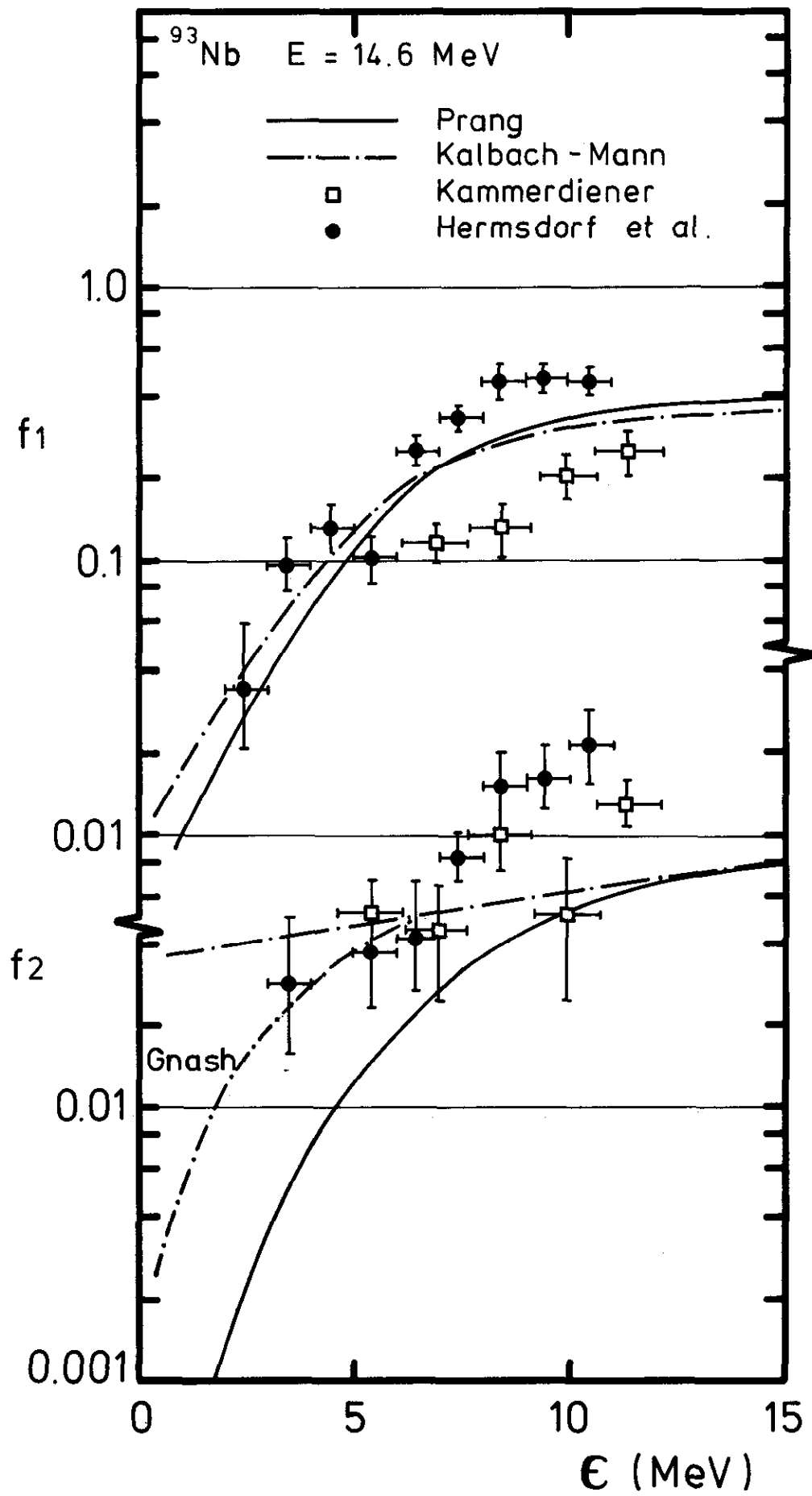


Fig. 5B.

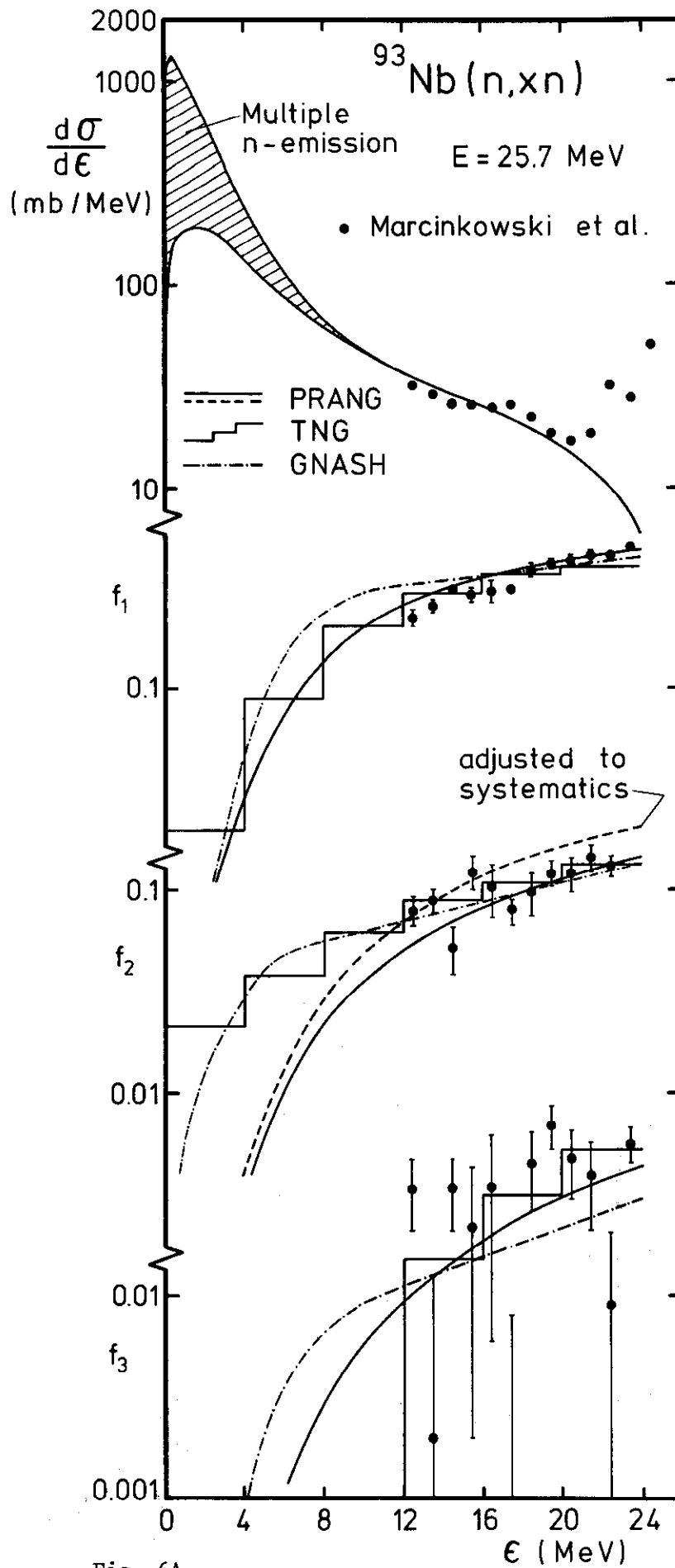


Fig. 6A.

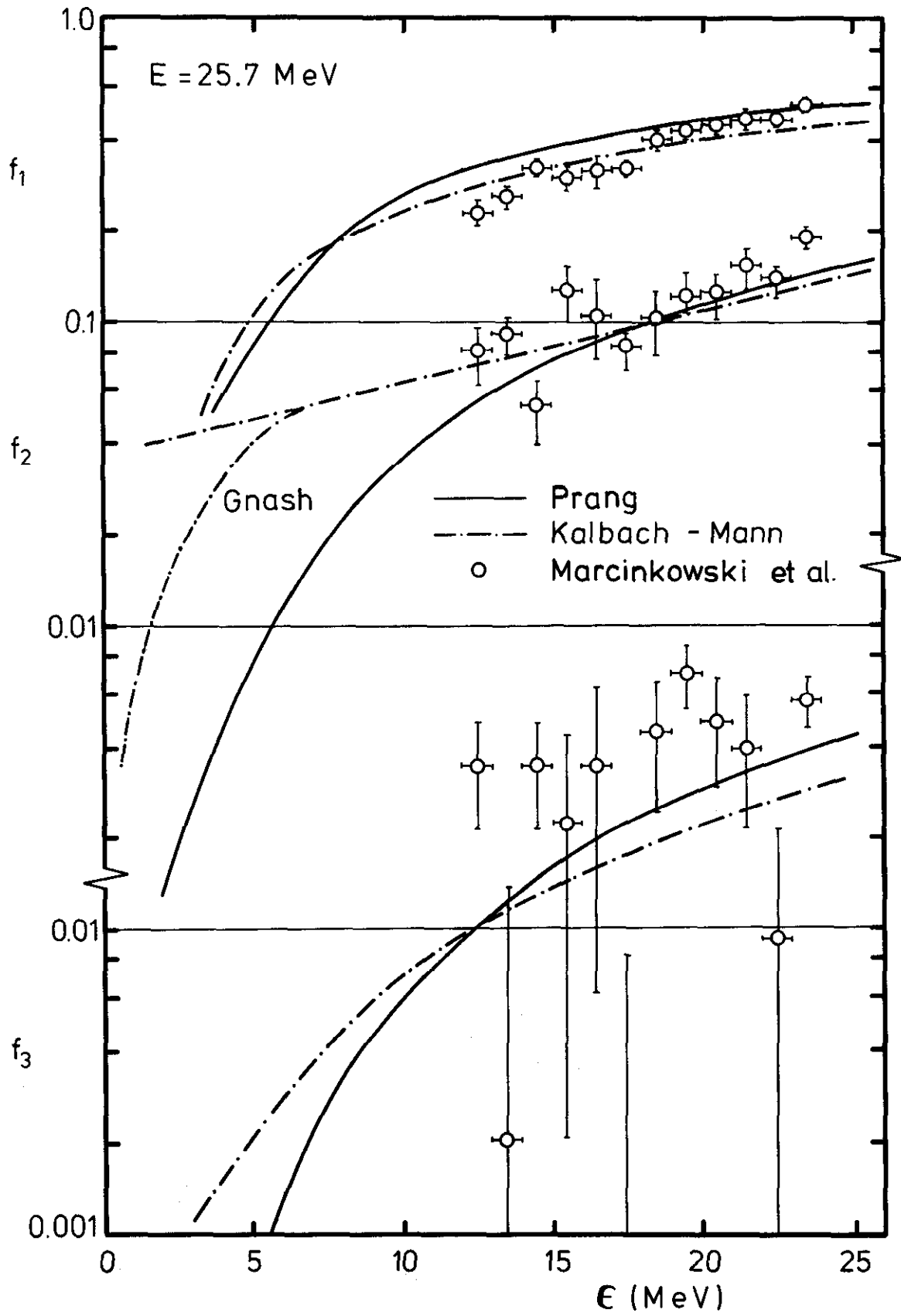


Fig. 6B.

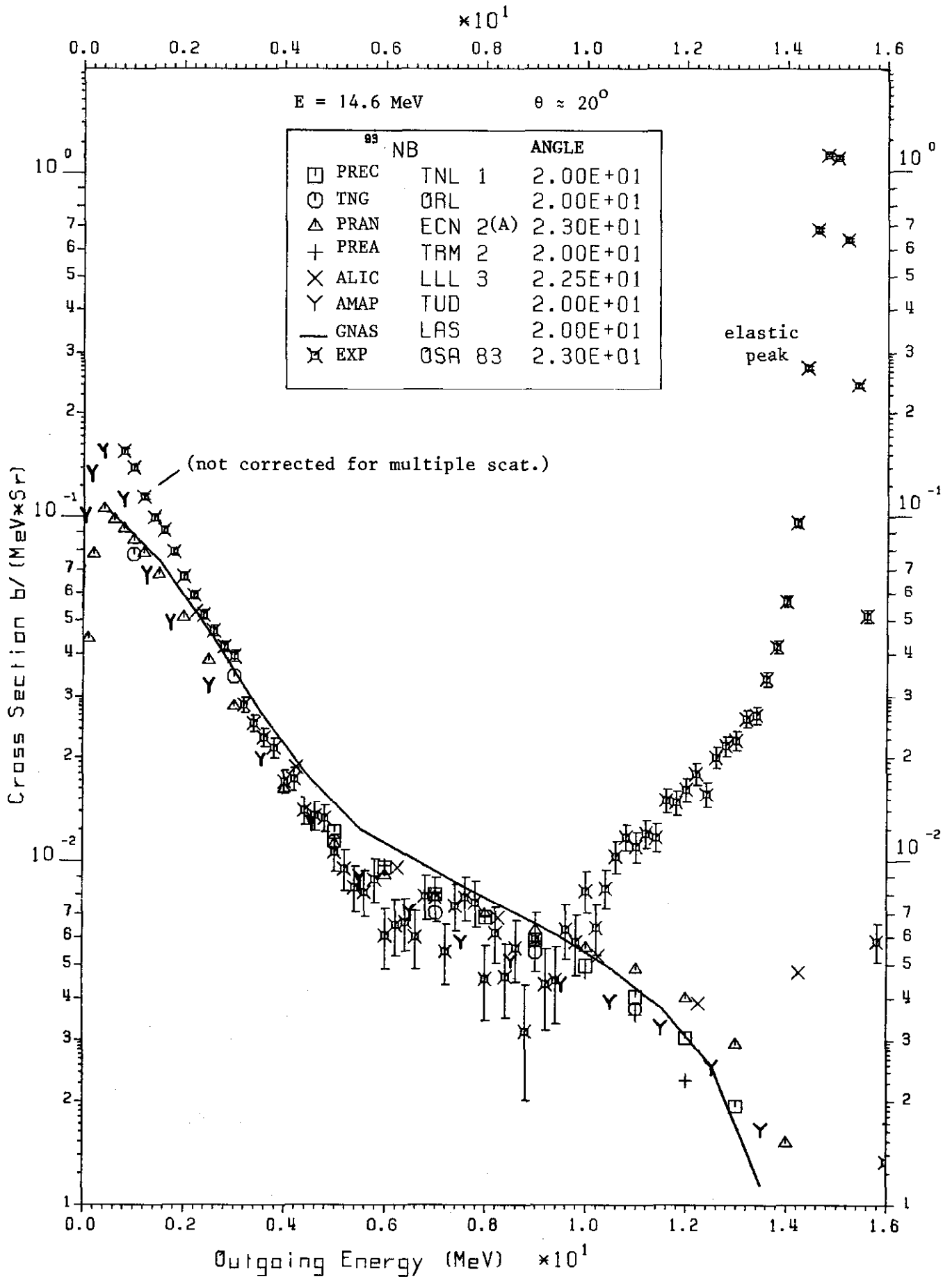


Fig. 7.

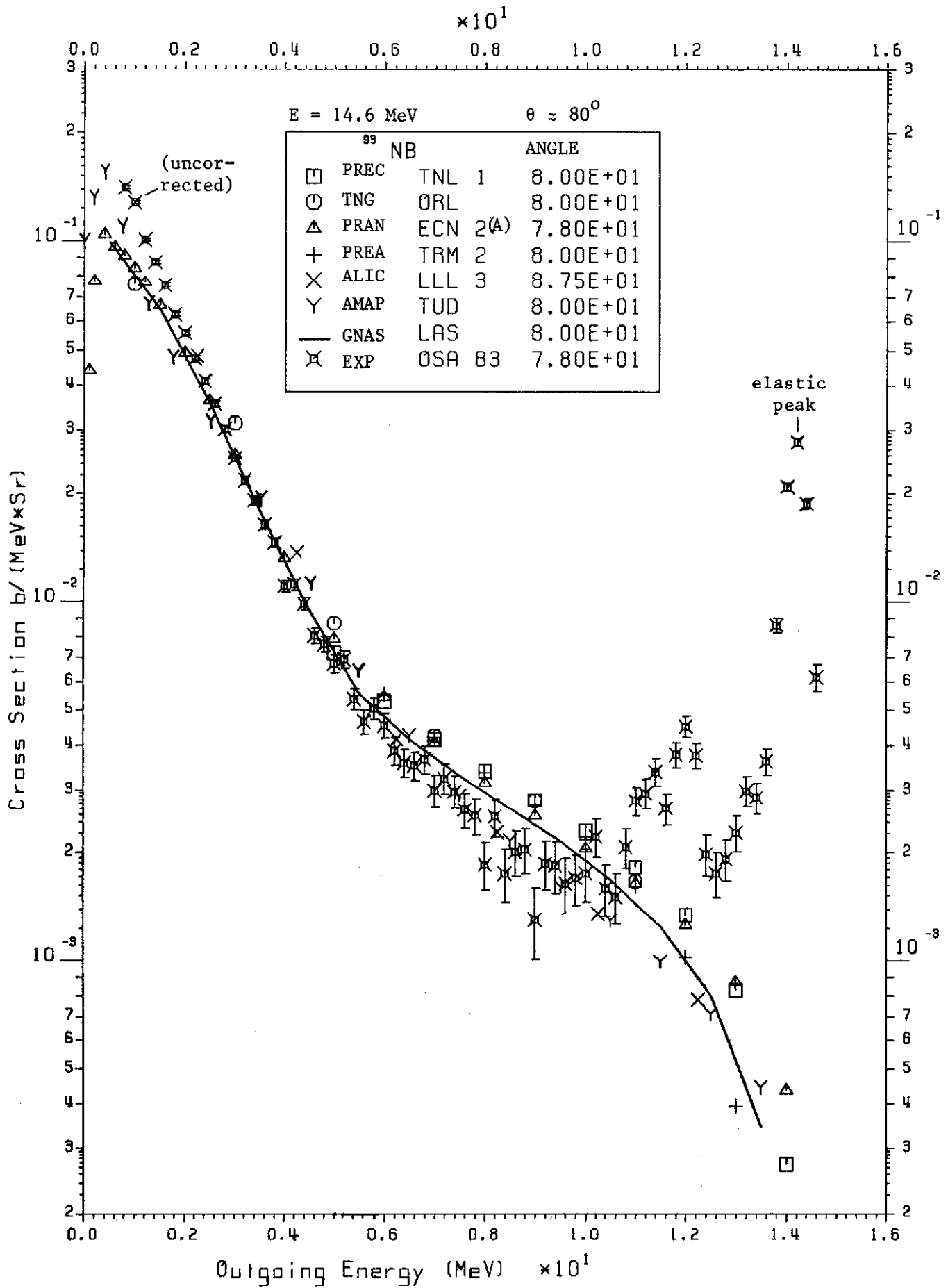


Fig. 8.

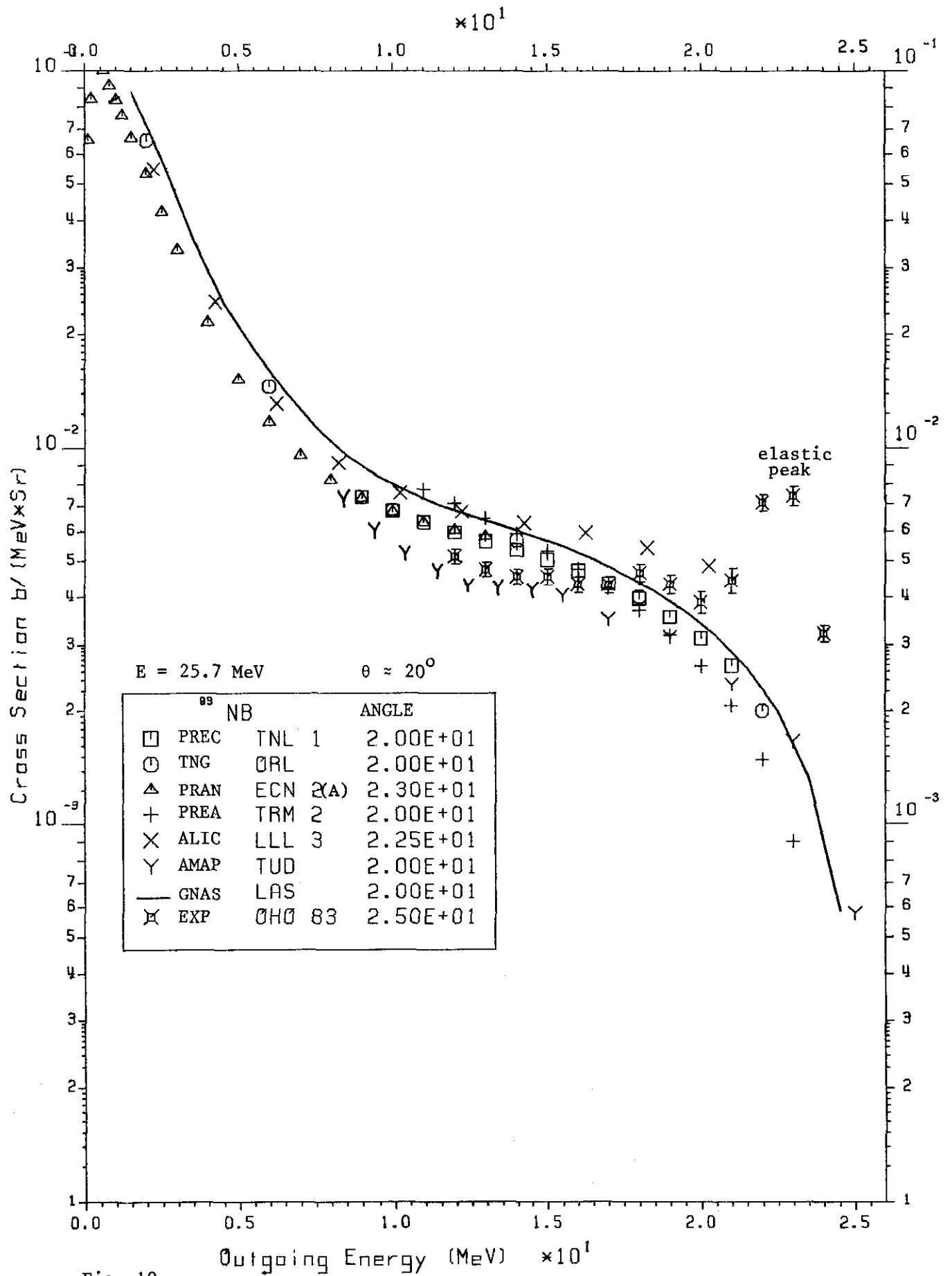


Fig. 10.

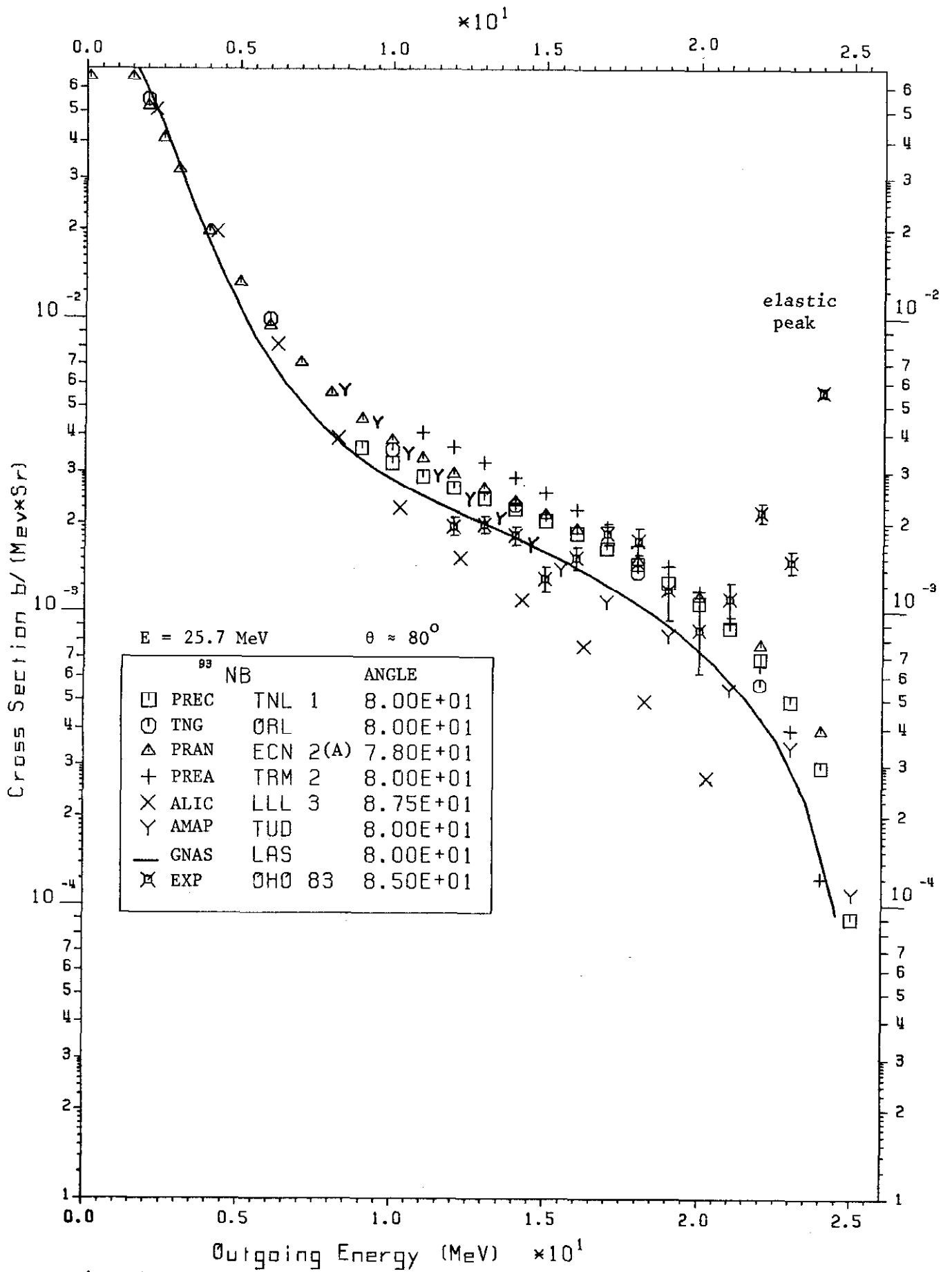


Fig. 11.

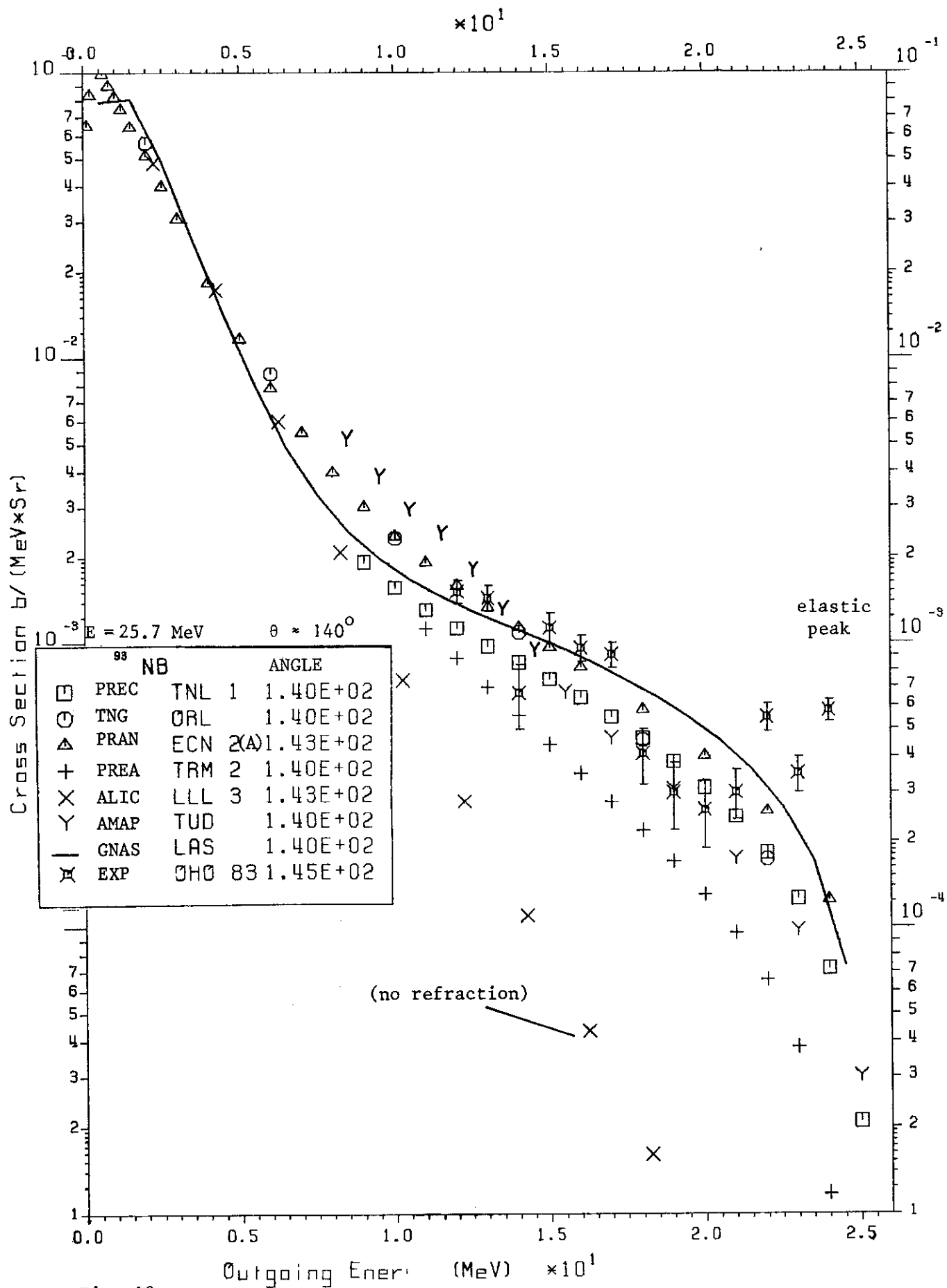


Fig. 12.

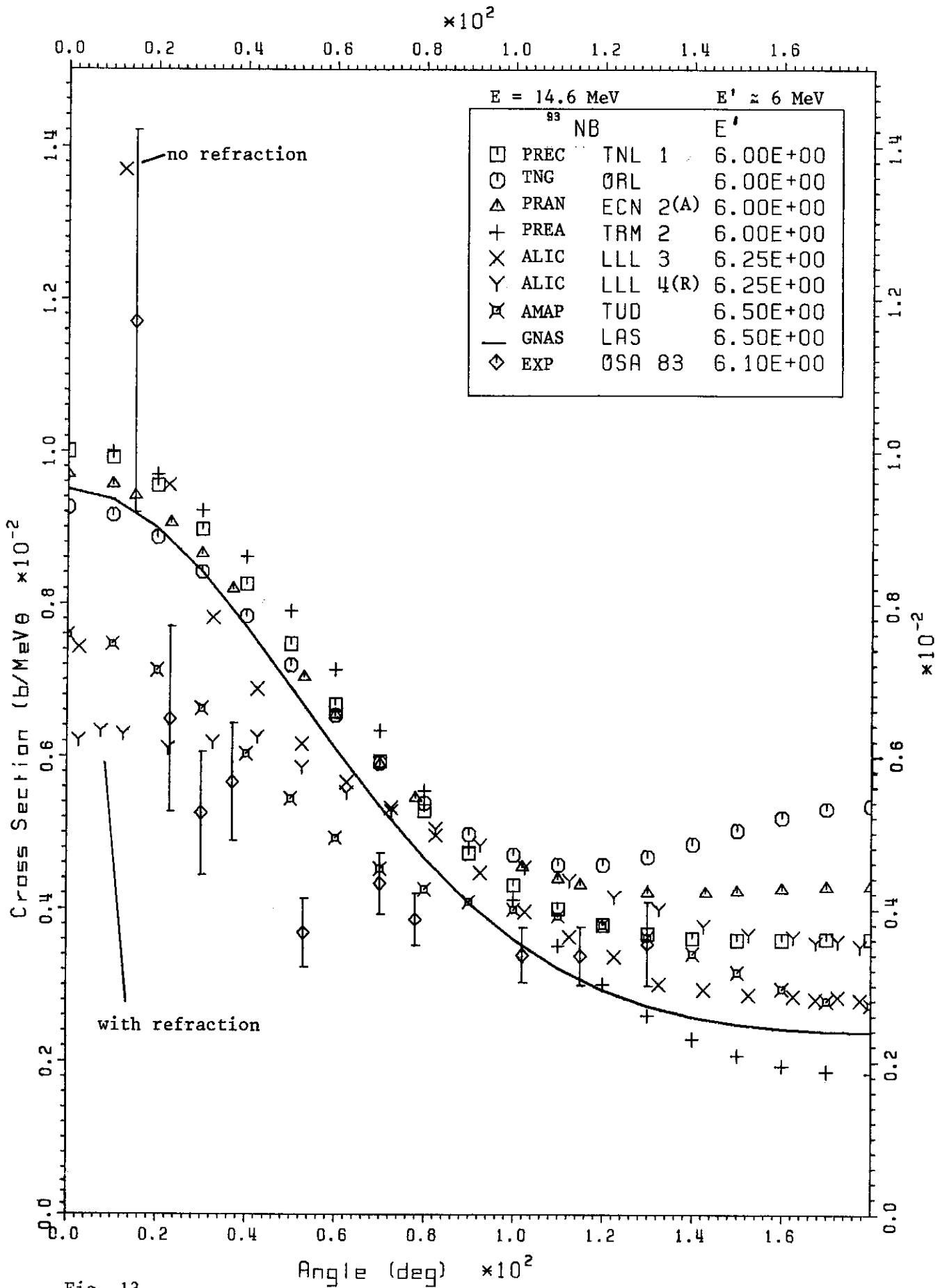


Fig. 13.

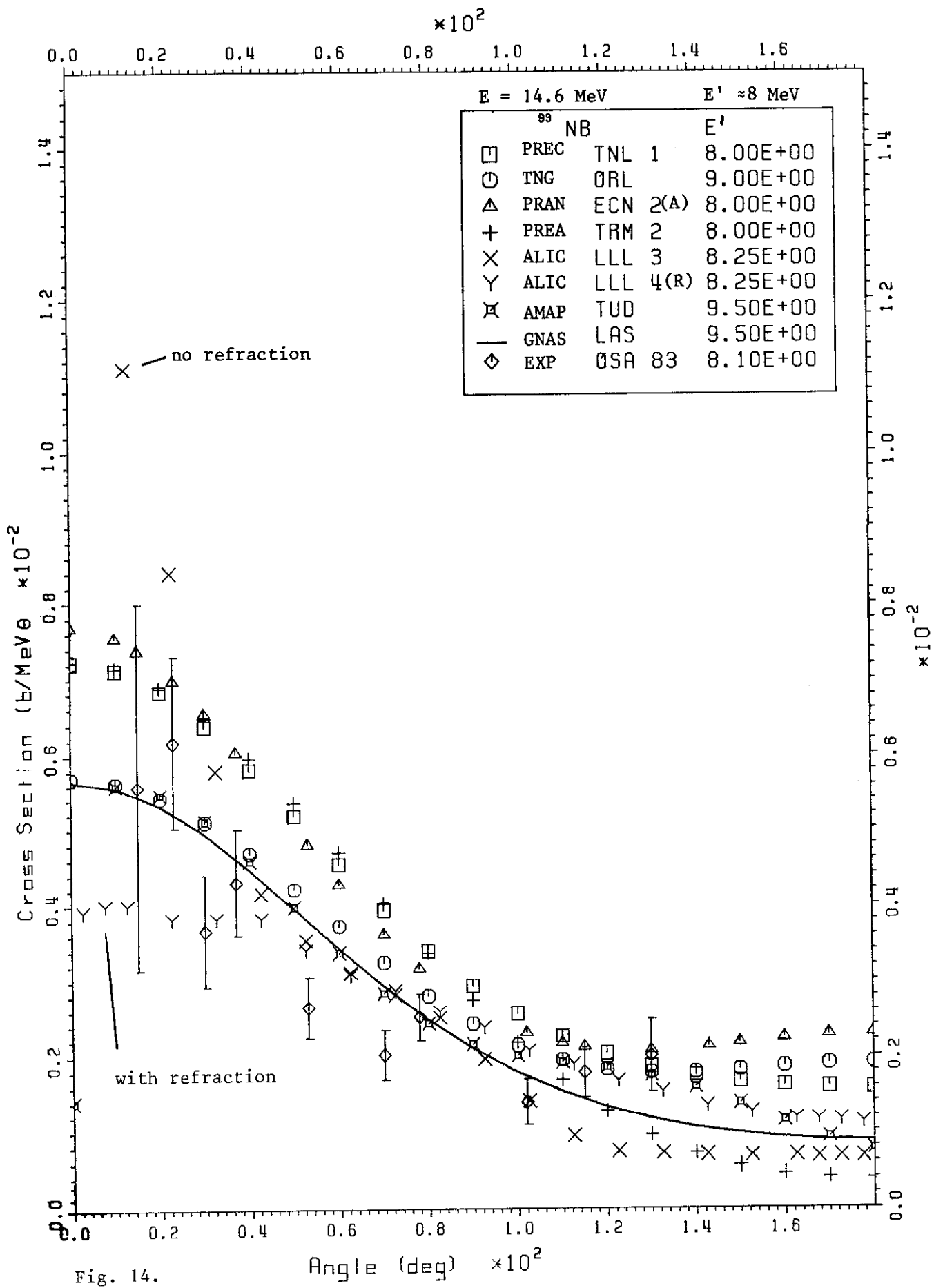


Fig. 14.

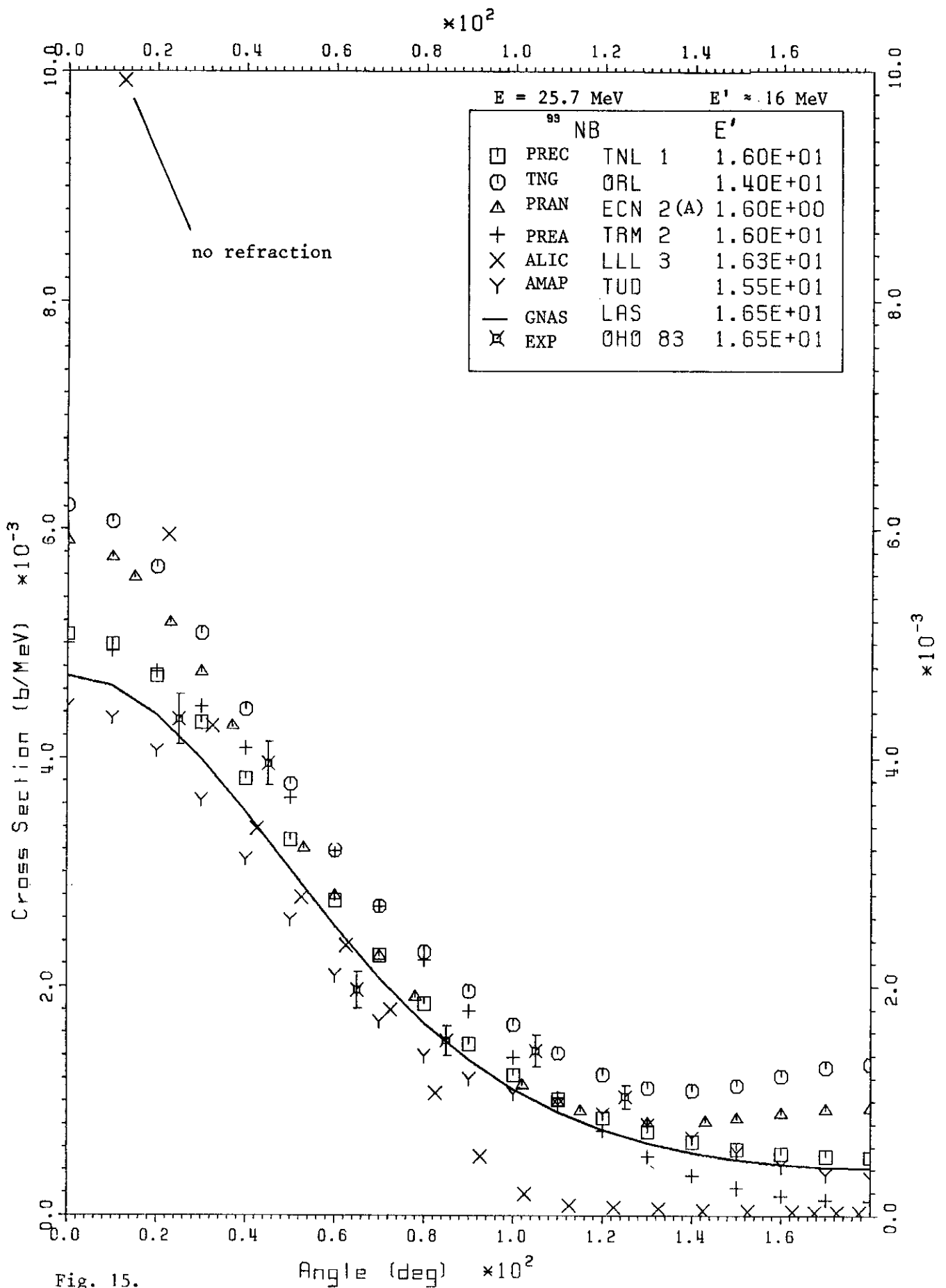


Fig. 15.

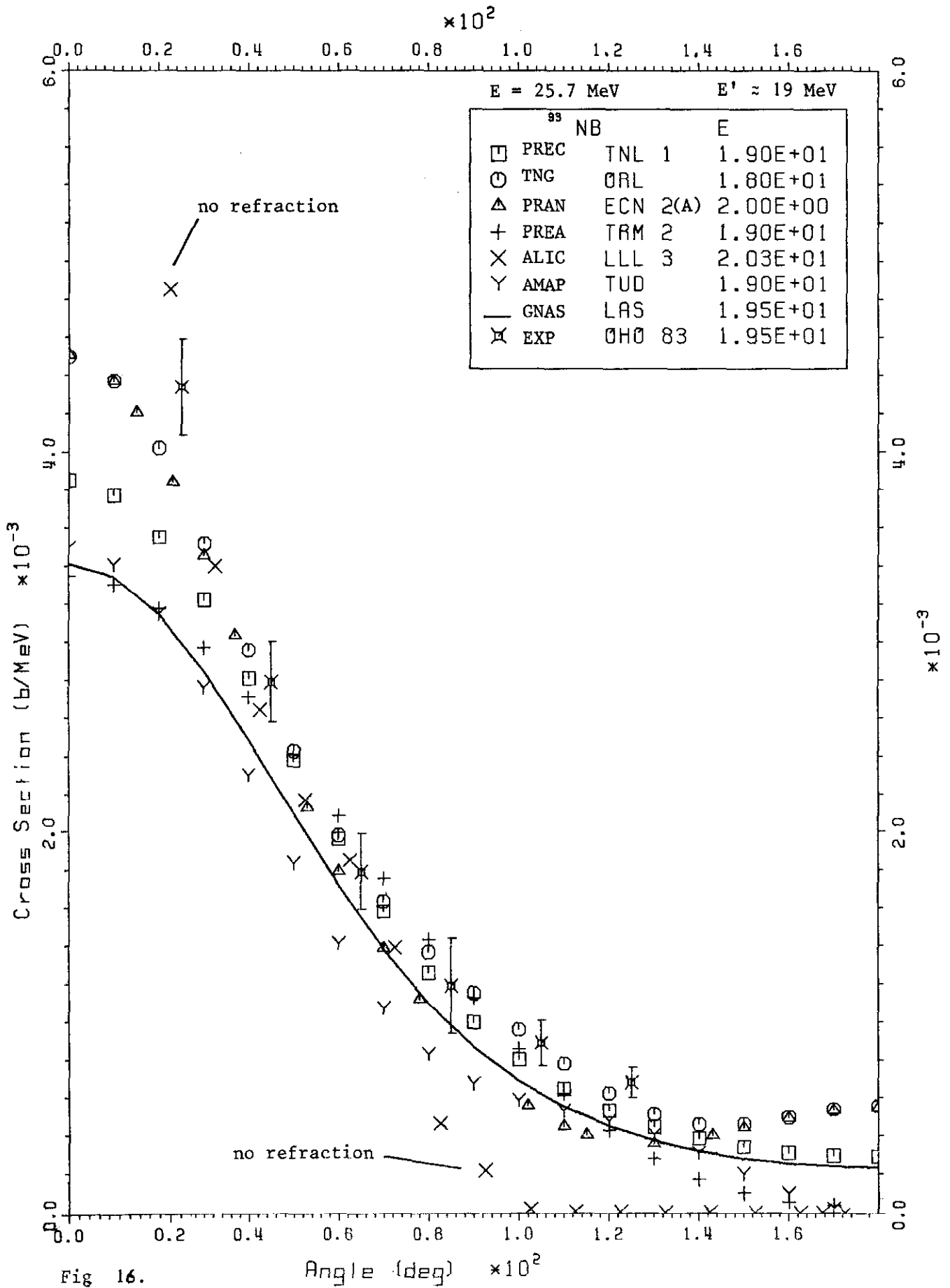
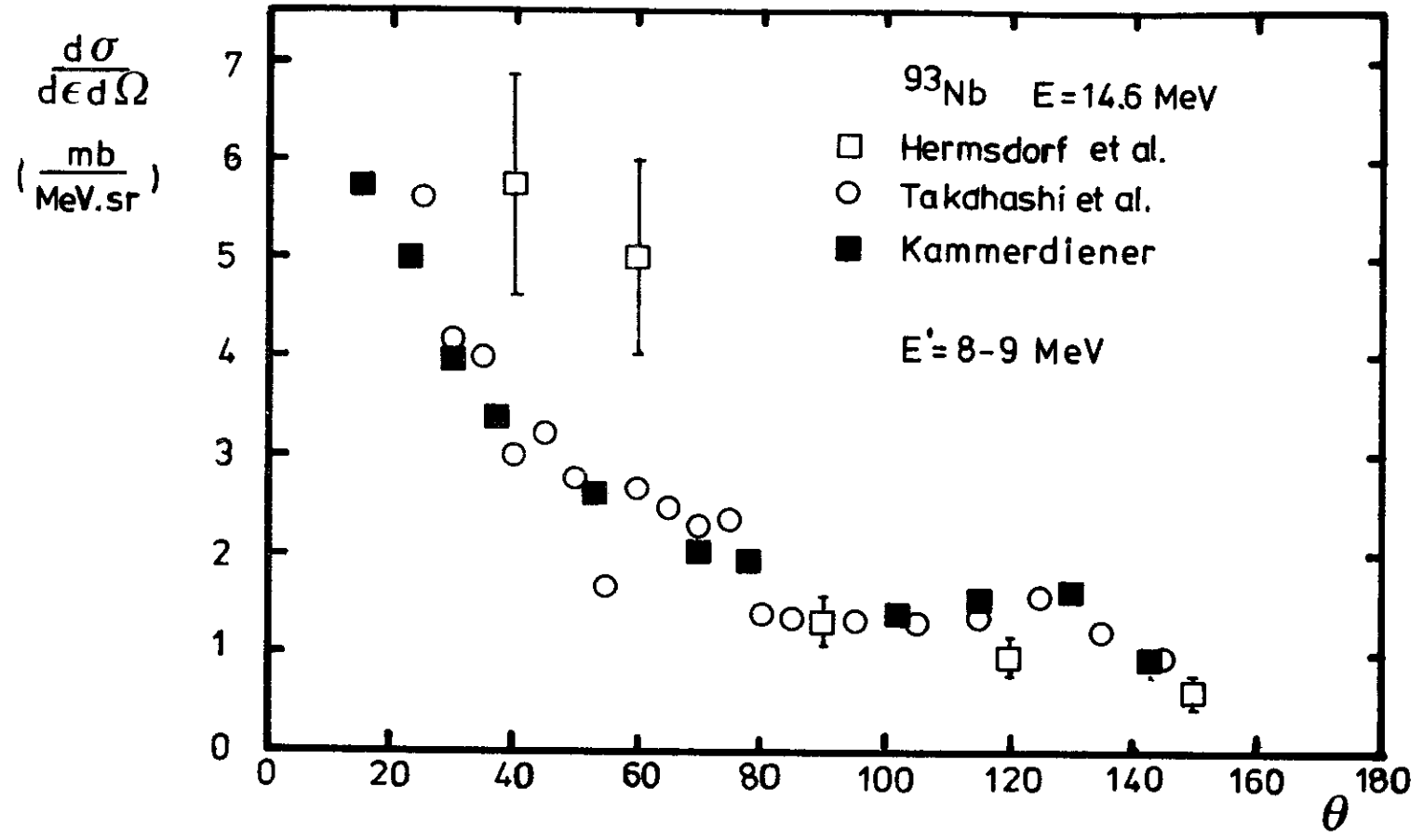
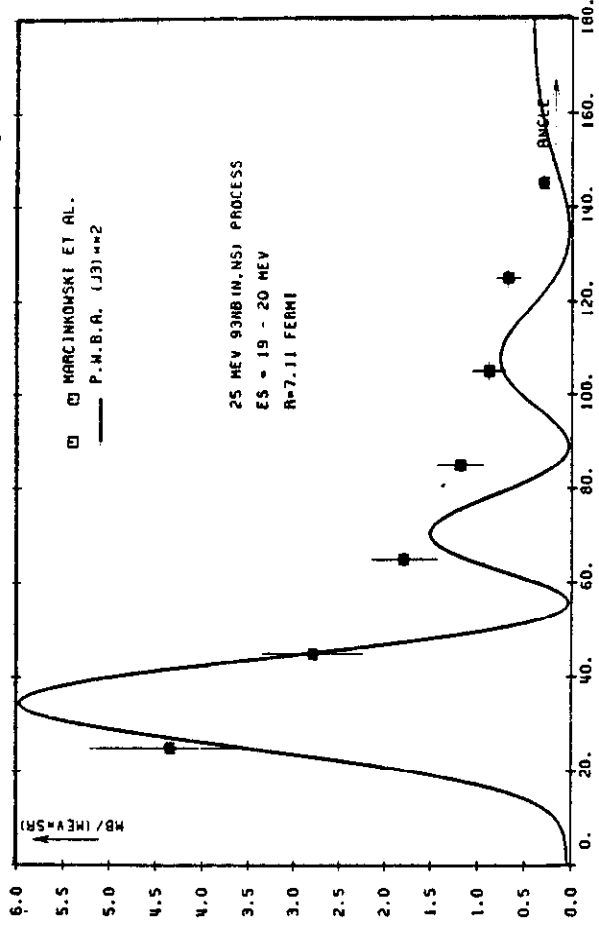
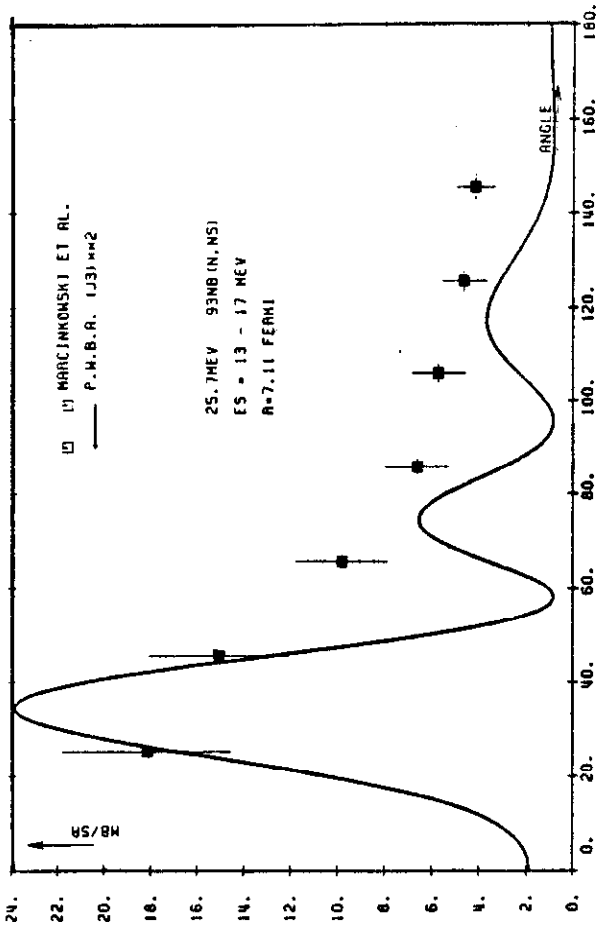
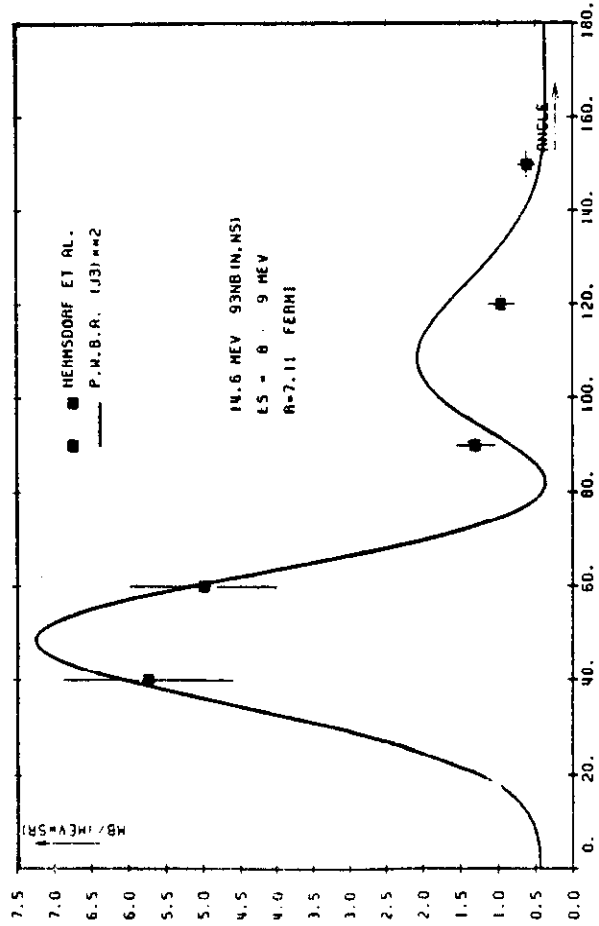
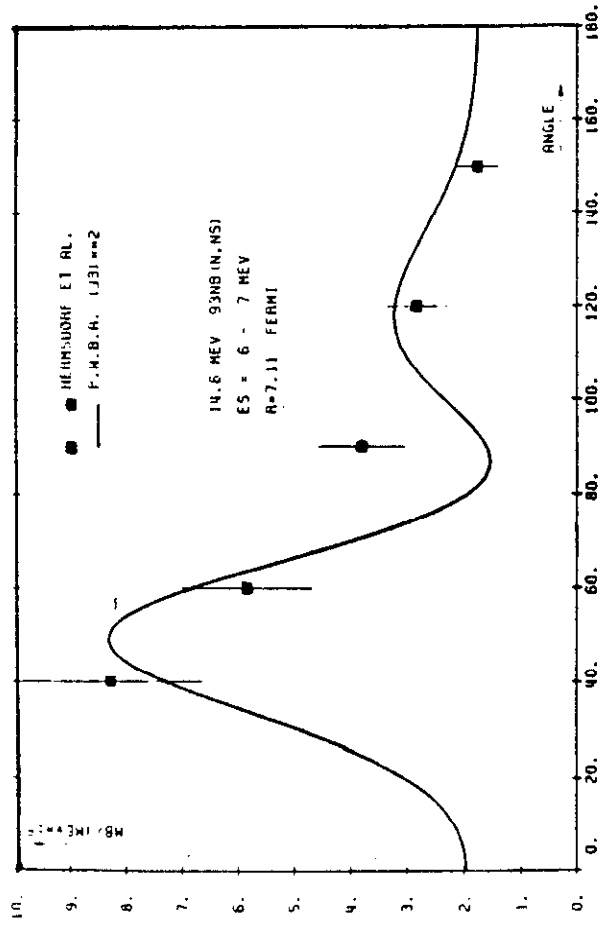


Fig 16.

Fig. 17.





ANGULAR DISTRIBUTION OF SCATTERED NEUTRONS. ERROR BARS = $\pm 20\%$

Fig. 18.

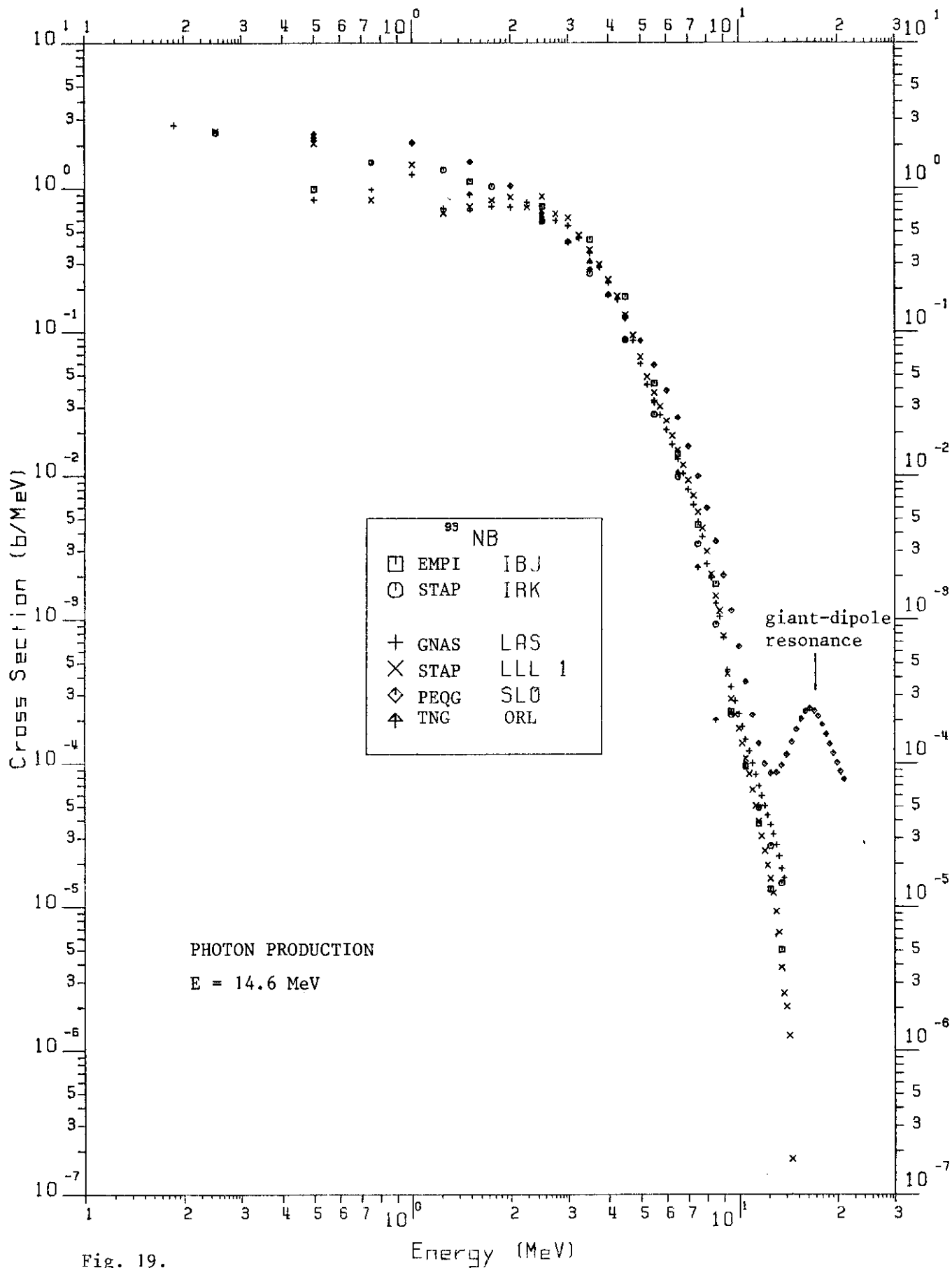


Fig. 19.

10. REFERENCES.

M. Uhl -

ACTA Phys. Austr. 31 (1970) 245.

NEA 0461/02 :

- M. Uhl and B. Strohmaier

STAPRE: A Computer Code for Particle Induced Activation Cross
Sections and Related Quantities. IRK 76/01 (1976, Upd. 1981).

11. MACHINE REQUIREMENTS.

126462 octal words CPU (without segmentation) on CYBER 73.

6 local files (tape or disk)

card reader

line printer.

12. PROGRAMMING LANGUAGE USED.

NEA 0461/02 : FORTRAN-IV

13. OPERATING SYSTEM OR MONITOR UNDER WHICH PROGRAM IS EXECUTED.

NOS/BE 1.4 (CDC version).

14. ANY OTHER PROGRAMMING OR OPERATING INFORMATION OR RESTRICTIONS.

The program description contains instructions for segmentation in
order to reduce storage requirements.

15. NAME AND ESTABLISHMENT OF AUTHOR.

M. Uhl

Institut fuer Radiumforschung und Kernphysik

Boltzmannngasse 3

A-1090 Wien

Austria

16. MATERIAL AVAILABLE -

NEA 0461/02 :

source program, test-case data, test-case output,
report IRK 76/01 (1976, Upd. 1981).

12. PROGRAMMING LANGUAGE USED.
NESCO757/01 : FORTRAN+ASSEMBLER
13. OPERATING SYSTEM UNDER WHICH PROGRAM IS EXECUTED - SCOPE.
14. OTHER PROGRAMMING OR OPERATING INFORMATION OR RESTRICTIONS - The values of NJDIM, NEEDIM, NLDIM, NLEVDIM should be left fixed at values of 40, 25, 30, and 50, respectively. The variable NKDIM can be changed, and probably is the most useful method of reducing LCM usage.
COMPASS routines, ECRD and ECWR, are included to transfer variables between SCM and LCM. These routines take the place of LASL's system routines ECRD and ECWR.
15. NAME AND ESTABLISHMENT OF AUTHORS -
P. G. Young and E. D. Arthur
Los Alamos Scientific Laboratory
P. O. Box 1663
Los Alamos, New Mexico 87545
16. MATERIAL AVAILABLE -
NESCO757/01 :
source program, test-case data, test-case output, report.

1. NAME OR DESIGNATION OF PROGRAM - HAUSER5

2. COMPUTER FOR WHICH PROGRAM IS DESIGNED AND OTHER MACHINE VERSION PACKAGES AVAILABLE -

Program-name	Package-ID	Orig. Computer	Test Computer
HAUSER-5	NESC0830/03	IBM 370/168	IBM 370/168
	NESC0830/04	UNIVAC 1110	UNIVAC 1110

3. DESCRIPTION OF PROBLEM OR FUNCTION - HAUSER5 calculates angle-integrated and, if desired, angle-differential reaction cross sections which can include capture and fission channels. Cross sections for discrete particle channels can be calculated, as well as the total for each reaction pair. Tertiary reactions can be calculated as though the reaction occurs as two sequential binary reactions. There is no restriction on the spins of the particles.

4. METHOD OF SOLUTION - HAUSER5 is based on three models of nuclear reactions - the statistical (or Hauser-Feshbach) model, the pre-equilibrium model (excitation formulation), and a statistical model for direct reactions. Transmission coefficients are interpolated from a table of previously-calculated transmission coefficients which can be supplied as input data or calculated by solving the Schroedinger equation with a spherical potential. The real spherical potential is taken to be the Woods-Saxon shape and the derivative can be Woods-Saxon or Gaussian shape. The fission transmission coefficients are based on the Hill-Wheeler equation.

5. RESTRICTIONS ON THE COMPLEXITY OF THE PROBLEM - HAUSER5 can accurately predict nuclear cross sections over most energy ranges less than about 60 MeV. Presently, the only statistical direct reaction included is the (n,ALPHA) pickup reaction. The Coulomb function may need to be replaced if heavy ions far below the Coulomb barrier are used. A maximum of six reaction pairs can be calculated. Residual nuclei can be described by 100 discrete levels and by the constant temperature level formula and/or the Fermi-gas level description. The maximum number of orbital angular momenta and energies for transmission functions and compound nuclear fractions is 32. The angular distribution expressed at equally-spaced angles from 0 to 90 degrees can be calculated for up to 20 discrete states. The program does not follow gamma ray cascades down a nucleus.

6. TYPICAL RUNNING TIME - About 30 seconds for calculating cross sections from 14.8 MeV neutrons on CU(63). The sample problem was executed by NESC in less than 2 CP minutes on an UNIVAC1100/44.

7. UNUSUAL FEATURES OF THE PROGRAM - HAUSER5 provides a single fast code covering unresolved resonance regions to beyond 50 MeV.

8. RELATED AND AUXILIARY PROGRAMS - An auxiliary program, TISO, is included in the package. TISO calculates gamma ray transmission coefficients to separate states in the final nucleus, allowing isomeric production to be calculated. HAUSER5 relies very heavily on the earlier STATIS code for the statistical model calculation and the PRECO-B code for the pre-equilibrium section. HAUSER5 was preceded by HAUSER1-HAUSER4 program and has been tested against the related HELENE, TNG, and GNASH (NECS Abstract 757) codes.

9. STATUS -

NESC0830/03	: Arrived at NEADB	August	1980
	Tested at NEADB		
NESC0830/04	: Arrived at NEADB	January	1980
	Tested at NEADB		

10. REFERENCES -

- Frederick M. Mann,
HAUSER-5, A Computer Code to Calculate Nuclear Cross Sections,
HEDL-TME 78-83, July 1979.
 - Frederick M. Mann,
HAUSER-4, A Computer Code to Calculate Nuclear Cross Sections,
HEDL-TME 76-80, September 1976.
 - R.G. Stokstad,
STATIS - Yale Internal Report #72, Wright Nuclear Structure
Laboratory, 1972.
 - C. Kalbach,
PRECO-B, program for Calculating Pre-Equilibrium Energy Spectra,
Triangle Universities Nuclear Laboratory and North California
State Chemistry Department informal report, 1977.
 - D.L. Hill and J.A. Wheeler,
Nuclear Constitution and the Interpretation of Fission Phenomena,
Physical Review, Vol. 89, No.5, pp. 1102-1145, March 1, 1953.
 - M. Blann,
Pre-Equilibrium Decay,
Annual Review of Nuclear Science, Vol. 25, pp. 123-166, 1975.
 - P.H. Cowell and A.C.D. Crommelin,
Appendix to Greenwich Observations for 1909, in J. Fox and E.T.
Goodwin, Proceedings of the Cambridge Philosophical Society, Vol.
45, No. 1, 373-383, January 1949.
 - HAUSER5, NESC No. 830, Tape Description, NESC Note 80-04, June 18,
1979.
- NESC0830/03 :
- A. Prince, G. Reffo, E. Sartori:
"Report on the International Nuclear Model Code Intercomparison,
Spherical Optical and Statistical Model Study", October 1983
NEANDC/INDC(NEA)4
- NESC0830/04 :
- A. Prince, G. Reffo, E. Sartori:
"Report on the International Nuclear Model Code Intercomparison,
Spherical Optical and Statistical Model Study", October 1983
NEANDC/INDC(NEA)4

11. MACHINE REQUIREMENTS - Input device (logical unit 5) to read card images, output devices for printed copy (units 6, 8, 10, and 11), and output devices for punched cards (units 7 and 9). HAUSER5, when overlaid, requires 58K words of memory. The auxiliary program, TISO, requires punch units 7 and 8 and 17K words of memory.
12. PROGRAMMING LANGUAGE USED.
NESC0830/03 : FORTRAN-IV
NESC0830/04 : FORTRAN-V (UNIVAC)
13. OPERATING SYSTEM UNDER WHICH PROGRAM IS EXECUTED - EXEC8.
14. OTHER PROGRAMMING OR OPERATING INFORMATION OR RESTRICTIONS -
Segments of the code are independent, allowing easy segmentation or overlay, and the storage requirements can also be reduced by eliminating underised options. The program will have to be modified to execute under the FORTRAN ASCII compiler, as the present edition of the code produces compiler errors.
15. NAME AND ESTABLISHMENT OF AUTHOR -
F.M. Mann
Hanford Engineering Development Laboratory
Westinghouse Hanford Company
P.O. Box 1970
Richland, Washington 99352
16. MATERIAL AVAILABLE -
NESC0830/03 :
report NEANDC/INDC(NEA)4, October 1983.
NESC0830/04 :
NESC Note 83-44, report NEANDC/INDC(NEA)4, October 1983.

1. NAME OR DESIGNATION OF PROGRAM - **TNG**
(a two-step Hauser-Feshbach code with precompound decays and gamma-ray cascades).
2. COMPUTER FOR WHICH PROGRAM IS DESIGNED AND OTHER MACHINE VERSION
PACKAGES AVAILABLE -

Program-name	Package-ID	Orig. Computer	Test Computer
TNG	NEA 0678/01	IBM 360 series	IBM 360 series
3. DESCRIPTION OF PROBLEM OR FUNCTION - The code is designed for calculating nuclear reaction cross sections below 20 MeV. Binary-reaction, tertiary-reaction and gamma-ray-production cross sections such as (n,gamma), (n,p), (n,2n), (n,n'gamma), (n,alpha-n-gamma) may be calculated. Energy distributions of secondary particles and gamma rays may be output in ENDF/B formats. Angular distributions of the first outgoing particles may be output in terms of Legendre coefficients.
4. METHOD OF SOLUTION - The Hauser-Feshbach formula (2) for compound binary reactions is extended to include tertiary reactions. Sequential decays without correlation between the two outgoing particles are assumed. Transmission coefficients needed for each step of the sequential decays are calculated with an in-house optical model without spin-orbit coupling. Binary-reaction part of the code, including width-fluctuation corrections, is based on the ORNL Hauser-Feshbach code HELENE (3). A precompound model (4) may be included as a correction to the energy distributions of the first outgoing particles. Gamma-ray competition with the second outgoing particles and the gamma-ray-cascades calculations are spin- and parity-dependent, thus sensitive to the angular momentum effects of the Hauser-Feshbach method. Gamma-ray branching ratios, if not available experimentally, are estimated from the tails of the electric giant dipole resonances (5). The parity selection rule of electric dipole transitions may be partially relaxed as a means of including magnetic dipole transitions.
5. RESTRICTIONS ON THE COMPLEXITY OF THE PROBLEM - Present dimensioning restricts a maximum of three types of binary particles and three types of tertiary particles.
6. TYPICAL RUNNING TIME - The running time is roughly proportional to $(E \cdot \Delta E)^2$ where E is the incident neutron energy and ΔE the continuum bin width. For E = 14 MeV, $\Delta E = 0.2$ MeV and a case that includes (n,n'x), (n,px) and (n,alpha-x) with x = gamma, n, p, or alpha and gamma-ray cascades for every residual nucleus, the running time would be roughly two minutes on IBM 360/91.
8. RELATED AND AUXILIARY PROGRAMS - Collective excitation cross sections from measurements and/or calculations may be input to TNG so that the collective effects are included in the calculated gamma-ray-production cross sections.

1. NAME OR DESIGNATION OF PROGRAM - **PREM**
2. COMPUTER FOR WHICH PROGRAM IS DESIGNED AND OTHER MACHINE VERSION
PACKAGES AVAILABLE -

Program-name	Package-ID	Orig. Computer	Test Computer
PREM	NEA 0888/01	IBM 370/168	IBM 370/168
3. DESCRIPTION OF PROBLEM OR FUNCTION - PREM computes energy spectra and cross sections of (i,xnyp) processes when an initial distribution function is given. Master equations for exciton number are solved for each generation in succession. Obtained quantities include pre-equilibrium as well as equilibrium contributions. It is also possible to obtain the equilibrium contributions only, and also the time development function for the first generation. Angular momentum conservation is not taken into account.
4. METHOD OF SOLUTION - The master equations are solved by the matrix inversion method or matrix diagonalization method.
7. UNUSUAL FEATURES OF THE PROGRAM - When the excitation energy of the compound system becomes low, the matrix in the master equations approaches a singular matrix. In such a case, the matrix inversion method switches automatically to the perturbation method, which is supposed to be correct for the limiting case. So it can compute for all energy ranges.
9. STATUS -

NEA 0888/01	: Arrived at NEADB	December 1982
	Tested at NEADB	
10. REFERENCES -
 - S. Yoshida: Z. Physik A308 (1982) 133.
 - NEA 0888/01 :
 - Gargi Keeni and Shiro Yosida:
Computer Code for Pre-Equilibrium Process With Multiple Nucleon Emission PREM. (Reprinted from The Science Reports of the Tohoku University, Series 8, Vol. 3, No. 1, June 1982)
12. PROGRAMMING LANGUAGE USED.

NEA 0888/01	: FORTRAN-IV
-------------	--------------
15. NAME AND ESTABLISHMENT OF AUTHOR -

S. Yoshida and G. Keeni
Physics Department, Faculty of Science
Tohoku University
Sendai 980, Japan.
16. MATERIAL AVAILABLE -

NEA 0888/01	:
	source program, test-case data, test-case output, report Sc.Rep.Tohoku Univ.Ser.8 Vol.3 N.1 (6/82).

11. MACHINE REQUIREMENTS - Main storage 46,675 octal words on CYBER 174.
12. PROGRAMMING LANGUAGE USED.
NEA 0809/01 : FORTRAN-IV
13. OPERATING SYSTEM UNDER WHICH PROGRAM IS EXECUTED - NOS-BE.
15. NAME AND ESTABLISHMENT OF AUTHOR -
J.M. Akkermans and H. Gruppelaar
Netherlands Energy Research Foundation
ECN, Petten, P.O. Box 1
1755 ZG PETTEN
Netherlands
16. MATERIAL AVAILABLE -
NEA 0809/01 :
CDC Control Cards, PREANG Source Program,
Sample Problem Input Data, report ECN-60 (May, 1979).

NEANDC-177U

Specifications for the

International Nuclear Model and Code Comparison

on Pre-equilibrium Effects

1 Introduction

This paper gives the specification of an intercomparison of statistical nuclear models and codes with emphasis on pre-equilibrium effects. It is partly based upon the conclusions of a meeting of an ad-hoc working group on this subject (see document NEANDC-A-137), on some criticism by Prof. M. Blann, communicated to the NEA Data Bank by Dr. M. Uhl, and on some suggestions of the present authors. We are very grateful to Drs. Betak, Blann, Fu, Gardner, Gmuca, Gupta, Herman, Mann, Ribansky, Seeliger, Garg, Uhl and Young for their comments on the draft version of this document. Most of the remarks have been included in the updated specifications given in this paper. The present proposal deviated from the previous one mainly in the choice of a somewhat heavier nucleus: ^{93}Nb instead of ^{59}Co . Using ^{93}Nb has several advantages:

1. The pre-compound part of the neutron emission spectrum is more pronounced than that of ^{59}Co .
2. This nucleus is quite well studied with respect to pre-equilibrium aspects, both experimentally and theoretically; it is often used as a "sample problem" in nuclear model calculations to illustrate pre-equilibrium effects.
3. There are experimental data for neutron emission spectra and angular distributions not only at 14.6 MeV, but also at 25.7 MeV¹. Furthermore, there are experimental data for σ_{n2n} and σ_{n3n} from 14.6 to 24 MeV². Proton-emission data including angular distributions are also available at 15 MeV^{3, 14}.

It is realised that the previous nucleus ^{59}Co is well studied in the statistical-model exercise and that it requires some additional effort by the participants to change to another nucleus. However, we think that the above-mentioned arguments are convincing, in particular point 3.

The character of this exercise differs from the equilibrium exercise in that pre-equilibrium models currently in use are quite different. Therefore it is more correct to speak about a model intercomparison rather than a code intercomparison. Since the models differ in the modelling of pre-equilibrium aspects, we cannot specify all the parameters.

Therefore we restrict these to:

1. Masses, Q-values
2. Level-scheme data (discrete levels)

APPENDIX A

3. Optical-model parameters (global spherical potential)
4. γ -ray competition parameters
5. Total level-density specification.

The parameters, specific for the precompound emission are not prescribed. Instead it is required to fit the 14.6 MeV total neutron emission spectrum $d\sigma/d\epsilon$ at $\epsilon = 6$ to 9 MeV, where precompound emission dominates. The participants should therefore specify their model and the parameters used. To facilitate this task, a questionnaire has been included (Appendix B).

The main quantity to be calculated is the total neutron emission spectrum $d\sigma/d\epsilon$ as a function of incoming energy E and outgoing energy ϵ . These angle-integrated spectra should be calculated at $E = 10, 14.6, 20$ and 25.7 MeV. Comparison with experimental data will be performed at the NEA Data Bank. If possible, also the reduced Legendre coefficients of the angular distributions should be calculated. Other important quantities to be calculated are: $\sigma_{nn'\gamma}$, σ_{n2n} , $\sigma_{np\gamma}$, $\sigma_{n\alpha\gamma}$ and their energy spectra (angle-integrated).

Finally, for the more sophisticated model codes, it is requested to calculate the total energy-integrated particle-production cross sections, the isomeric state population from the (n,n') and $(n,2n)$ reactions and the total photon production cross section (at 14.6 MeV).

It is not necessary to include width-fluctuation corrections in the calculations. There is also no need to calculate $\sigma_{n\gamma}$ in this exercise. However, γ -ray competition should be included (if possible) to calculate the multi-particle emission cross sections (and isomeric-state populations).

2 Mass, Q-values, etc.

The masses and Q-values should be taken from a recent nuclear mass table. Some values are provided in Table 3a¹⁸.

3 Level scheme data (discrete levels)

The level schemes of most of the residual nuclei are specified in Table 1. These data are usually based upon recent issues of the Nuclear Data Sheets. The first energy of the continuum calculation, E_C , is indicated in Table 3a.

Notes

1. For the codes that calculate only continuum emission, these data are not relevant.
2. For other residual nuclei, the participants should perform a continuum calculation only, assuming $E_C = 0.1$ MeV. For ^{92}Nb and ^{93}Nb γ -ray branchings are given for discrete levels.

4 Optical model

In these exercise, a spherical optical model is used, of which the definition of the parameters is given in Table 2a. The selected global optical-model parameters are given in Table 2b.

APPENDIX A

For neutrons and protons, parametrisation close to those of F.G. Perey (e.g. ³) have been selected. These parametrisations should work well at energies from 0.9 to 22 MeV. Please indicate when the channel-spin dependence of the transmission coefficients has been neglected (T_{ℓ} instead of $T_{\ell j}$).

For neutrons, we have checked that the potential is in reasonably good agreement with available experimental ⁹³Nb data for σ_t and σ_{el} from 1 to 15 MeV.

For α -particles, the potential of Igo and Huizenga⁴ has been selected.

5 Gamma-ray parameters

For the calculation of γ -ray competition the Brink-Axel giant-dipole model should be used to describe E1 transitions. For all residual nuclides, the same data are prescribed, i.e.:

$$\begin{aligned} E_r &= 16.5 \text{ MeV,} \\ \Gamma_r &= 5.0 \text{ MeV,} \\ \sigma_r &= 0.162 \text{ b.} \end{aligned}$$

Using these parameters, the following value of the total s-wave radiation width is obtained for the reaction ⁹³Nb(n, γ) ⁹⁴Nb at neutron binding energy:

$$\langle \Gamma_{\gamma}(1=0) \rangle = 165 \text{ MeV.}$$

The value $\langle \Gamma_{\gamma} / \text{Dobs} \rangle$ amounts to 0.166×10^{-4} . If necessary, a normalisation constant in the Brink-Axel formula should be used to obtain this value (the same normalisation constant should be used in each residual nucleus). The authors should specify their formalism used.

Note: If no γ -ray competition is used, the participants should clearly indicate this.

For γ -ray cascade calculations (isomeric state population), the M1 and E2 electromagnetic transitions should be allowed with the strengths of M1 and E2 set to: strength (E1/M1) = strength (M1/E2) = 10, relative to the total E₁ radiation width for s-wave resonances of the reaction ⁹³Nb(n, γ) ⁹⁴Nb at the neutron binding energy ($\Gamma_{\gamma} = 165 \text{ MeV}$) (the same normalisation constants should be used for each residual nucleus). For the energy dependences of the M1 and E2 transitions the Weisskopf formula should be used.

The branching ratios for ⁹²Nb and ⁹³Nb levels are given in Table 1. Use theory to obtain branchings for other residual nuclides (only needed for calculation of total photon production).

The participant should specify the Yrast line used in the calculation of the gamma-ray emission data.

6 Total level-density parameters

For the calculation of the equilibrium part - or in the unified codes, the combined pre-equilibrium and equilibrium parts - it is requested to fit the total level density (i.e. summed over all possible particle-hole combinations) at two energies, so that:

APPENDIX A

1. the total number of levels equals N_C at $E=E_C$;
2. the level spacing of s-wave levels equals Dobs at the neutron binding energy B.

With these conditions, the participant should preferably use the composite Gilbert-Cameron formula⁵. When this formula is not programmed, the Fermi-gas formula of Dilg et al.⁶ or another representation could be used (other formulas could be important in unified models, where it is required that the sum of all particle-hole components equals the total level density).

In Table 3a, the values of the parameters required to calculate N_C and Dobs are specified. When the Gilbert-Cameron formula is used, the pairing energies P of ref. ⁵ are also prescribed (see Table 3a). Table 3b gives the parameters a, U_x and Δ for three possible representations:

1. Gilbert-Cameron formula with improved definition of the spin cut-off parameter σ^2 :

$$\sigma^2 = 0.146 \sqrt{aU} A^{2/3}.$$

2. Gilbert-Cameron formula with original definition of the spin cut-off parameter⁵:

$$\sigma^2 = 0.0888 \sqrt{aU} A^{2/3}.$$

3. Back-shifted Fermi gas model⁶ with:

$$I_{\text{eff}} = I_{\text{rigid}}.$$

The parameter g follows from the quantity a by means of the relation:

$$a = \frac{\pi^2}{6} g.$$

Notes:

1. The participant should clearly specify the formula used. The preferred representation is formula 1.
2. At low energies the definition of σ^2 is not clear in the case of Gilbert-Cameron. It is suggested to use a linear interpolation between σ^2 at $E = E_C$ and $\sigma^2(E_x)$ at the dividing energy $E_x = U_x + P_x$. The value of σ^2_{exp} is given in Table 3a.
3. From some preliminary calculations with the Gilbert-Cameron formula and the back-shifted Fermi gas formula, it follows that the differences in the cross sections due to the use of different level density formulas cannot be neglected, particularly at energies above 10 MeV. This has to be regretted, but it is a basic uncertainty in our model calculations, as long as these simple level-density formulas are used. In some codes, different level-density formulas could be used. The participants are invited to use these options to study the effect of the different approaches. Our prefer-

ence for the Gilbert-Cameron formula is only based upon the fact that this formula is probably the most widely used.

7 Particle-hole state density

In most cases it is expected that the particle-hole state densities are based upon the expression of Williams⁸, possibly with corrections. The exact formula used should be specified, both for the initial and final state densities. When the calculations of precompound parts and compound parts parts are unified, the sum over all particle-hole level densities should satisfy the conditions given in the previous section. When the precompound calculation is used as a correction to the compound model one could use the same parameters as used in the equilibrium calculation, including energy shifts or pairing energy corrections. This would facilitate the intercomparison of the results. However, as it is noticed that another parametrisation could be more realistic for pre-equilibrium calculations, deviations are allowed, provided that they are indicated clearly. In many codes only the option $g = A/13 \text{ MeV}^{-1}$ and $P=0$ is allowed. This should be specified.

When angular momentum is conserved in the calculation, the adopted expression for the p-h spin cut-off parameter should be specified.

8 Precompound parameters

In some codes there are some "free" parameters to fit the emission spectra, such as K occurring in the expression for the average transition matrix elements, e.g.

$$\left| M^2 \right| = \frac{K}{A^3 E}$$

This, or a similar expression, should be indicated, together with the value of the parameter(s). The value(s) of the free parameter(s) should be adjusted in order to obtain agreement with the (angle-integrated) total neutron emission spectrum at $E = 14.6 \text{ MeV}$ and $\epsilon = 6$ to 9 MeV :

$$\frac{d\sigma}{d\epsilon} (6-7 \text{ MeV}) = 56.0 \pm 6 \text{ mb/MeV},$$

$$\frac{d\sigma}{d\epsilon} (7-8 \text{ MeV}) = 46.9 \pm 5 \text{ mb/MeV},$$

$$\frac{d\sigma}{d\epsilon} (8-9 \text{ MeV}) = 36.5 \pm 4 \text{ mb/MeV}.$$

These data are obtained from an analysis of the experimental data of Hermsdorf et al.⁹, performed at ECN, Petten (*). At $\epsilon = 6-9 \text{ MeV}$, most of the emission is due to pre-equilibrium: at high energies the experimental data are quite uncertain due to direct effects of uncertainties in the subtraction of the elastic scattering peak.

(*) This analysis was performed by fitting the coefficients of the function $A_0 + A_1 P_1(\cos \theta) + A_2 P_2(\cos \theta)$ through the original data of Hermsdorf et al.⁹. The results are in agreement with a similar analysis of Kammerdiener's data¹⁶ and those of Salnikov et al.¹⁷.

APPENDIX A

Other parameters, such as R or Q factors^{10,15} should also be specified. Gadioli et al.¹¹ have proposed

$$R = \frac{n \pm 1}{n},$$

where the "+" and "-" signs refer to neutron and proton emission, respectively, to account for charge conservation. For "unified" models it is desired that these parameters approach unity at equilibrium.

The treatment of the γ -channel has also to be described, e.g. according to ref ¹². When fit-parameters are used, such as form-factors, they should be specified.

Parameters for the description of angular distribution are not prescribed. The user should specify the formalism used.

9 Requested calculations

The incident energies for the calculations are $E = 10, 14.6, 20$ and 25.7 MeV. For the outgoing centre-of-mass energies ϵ , the energy mesh should be appropriate to describe the data (indicate when the spectra are stored in a histogram form). It is suggested to use at least 1 MeV bins up to 14 MeV, if possible smaller bins up to 2 MeV and 2 MeV bins above 16 MeV. The following quantities need to be calculated.

9.1 Integrated cross sections at 5 incident energies:

1. $\sigma_t, \sigma_{el}, \sigma_r$ (composite-formation cross section),
2. $\sigma_{nnx}, \sigma_{npx}, \sigma_{n\alpha x}$ (first emission of n, p, and α respectively),
3. σ_{nn} (inelastic scattering cross section), $\sigma_{n2n}, \sigma_{n3n}, \sigma_{nnp}, \sigma_{np}, \sigma_{npn}, \sigma_{n\alpha n}$ (other cross sections are relatively small),
4. total particle (and gas-) production cross sections $\sigma_{nnem}, \sigma_{npem}, \sigma_{n\alpha em}$.

Notes:

1. In cases b) to d) it is of interest to indicate the equilibrium component separately; also the full equilibrium calculation (with pre-equilibrium turned off) should be performed (specify equilibrium definition).
2. As intermediate results the transmission coefficients T_j (averaged over j) and/or the inverse reaction cross sections should be given at each incident energy and for each outgoing particle.

9.2 Angle-integrated spectra at 14.6 and 25.7 MeV

- a) $\frac{d\sigma_{nnx}}{d\epsilon}, \frac{d\sigma_{npx}}{d\epsilon}, \frac{d\sigma_{n\alpha x}}{d\epsilon}$ (first emission of n, p and α , respectively).

b) Total neutron emission spectra (excluding elastic scattering)

$$\frac{d\sigma}{d\varepsilon} \text{nnem} \text{ (summed over all outgoing neutrons).}$$

9.3 Angular distributions of (total) neutron emission spectra at 14.6 and 25.7 MeV

The preferred representation is given by reduced centre-of-mass Legendre coefficients f_ℓ ($\ell = 1, 2, 3$) where

$$\frac{d^2\sigma}{d\varepsilon d\Omega} = \frac{1}{4\pi} \frac{d\sigma}{d\varepsilon} \sum_\ell (2\ell+1) f_\ell P_\ell(\cos\theta);$$

f_ℓ should be tabulated as a function of ε (in c.o.m.).

9.4 γ -ray emission at 14.6 MeV

1. Reaction cross section for the population of the isomeric states ^{93m}Nb and ^{92m}Nb .
2. Total photon-production cross section;
3. γ -ray emission spectrum $d\sigma/d\varepsilon$.

The participants are kindly asked to send all information on their codes and to answer the questions in the questionnaire (Appendix B).

The deadline for the solutions is 1st November 1983.

APPENDIX A

9.5 References

- [1] A. Marcincowski et al., Nucl. Science and Eng., 83 (1983), p.13.
- [2] L.R. Veaser, E.D. Arthur and P.G. Young, Phys. Rev., C16 (1977), 1792.
- [3] F.G. Perey, Phys. Rev., 131 (1963), 745.
- [4] J.R. Huizenga and G. Igo, Nucl. Phys., 29 (1962), 462.
- [5] A. Gilbert and A.G.W. Cameron, Can. J. of Phys., 43 (1965), 1446.
- [6] W. Dilg et al., Nucl. Phys. A217 (1973), 269.
- [7] U.E. Facchini and E. Saetta-Menichella, Energ. Nucl., 15 (1968), 54.
- [8] F.C. Williams, Nucl. Phys., A166 (1971), 231.
- [9] D. Hermsdorf et al., ZfK-277 (1974), Zentralinstitut fuer Kernforschung, Rossendorf bei Dresden Report.
- [10] C. Kalbach, Z. fuer Physik A283 (1977), 401.
- [11] E. Gadioli, E. Gadioli-Erba and P.G. Sona, Nucl-Phys. A217 (1973), p.589.
- [12] L. Millazzo-Colli and G.M. Braga-Marcazzan, Nucl-Phys. A210 (1973), p.297.
- [13] S.M. Grimes et al., Phys. Rev. C17 (1978) 508.
- [14] H.K. Vonach, private communication (1983).
- [15] S.K. Gupta, Z. Phys. A303 (1981) 329.
- [16] J.L. Kammerdiener, UCRL-51232 (1972).
- [17] O.A. Salnikov et al., Yad. Konstanty 7 (1971) 134.
- [18] A.H. Wapstra and K. Bos, Atomic data and Nuclear Data tables, 19 (1977) 177.

TABLE 1 Level scheme data

LEVELS FOR 86RB

1	0.0	-2.0
2	0.4881	+1.0
3	0.5560	-6.0
4	0.5569	-3.0
5	0.7795	-7.0
6	0.8732	-3.0
7	0.9785	-4.0
8	1.0271	+1.0
9	1.0327	-3.0
10	1.0925	-4.0
11	1.1059	+2.0
12	1.1220	+1.0
13	1.1560	+0.0
14	1.1962	-3.0
15	1.2472	-4.0
16	1.3050	+3.0

LEVELS FOR 89SR

1	0.0	+2.5
2	1.0320	+0.5
3	1.4734	+3.5
4	1.9402	+2.5
5	2.0076	+1.5
6	2.0574	-1.5
7	2.0613	+4.5
8	2.0790	-5.5
9	2.2801	+0.5
10	2.4516	+1.5
11	2.5701	-1.5
12	2.6710	+3.5

LEVELS FOR 93ZR

1	0.0	+2.5
2	0.2669	+1.5
3	0.9471	+0.5
4	1.018	+0.5
5	1.151	+0.5
6	1.222	+0.5
7	1.4255	+1.5
8	1.4356	+0.5
9	1.4504	+1.5
10	1.4702	+2.5
11	1.477	+3.5
12	1.597	+2.5
13	1.648	+1.5

LEVELS FOR 90Y

1	0.0	-2.0
2	0.2025	-3.0
3	0.6820	+7.0
4	0.7768	+2.0
5	0.9537	+3.0
6	1.0474	+5.0
7	1.1895	+4.0
8	1.2147	-0.0
9	1.2982	+6.0
10	1.3710	-1.0

LEVELS FOR 92Y

1	0.0	-2.0
2	0.2415	+0.0
3	0.3100	-2.0
4	0.4306	+1.0
5	0.4403	-3.0
6	0.7801	-0.0
7	0.8924	+1.0
8	0.9534	-4.0

LEVELS FOR 92ZR

1	0.0	+0.0
2	0.9345	+2.0
3	1.3828	+0.0
4	1.4954	+4.0
5	1.8473	+2.0
6	2.0667	+2.0
7	2.1500	+4.0
8	2.3397	-3.0
9	2.3983	+4.0

LEVELS FOR 89Y

1	0.0	-0.5
2	0.9092	+4.5
3	1.5074	-1.5

APPENDIX A

LEVELS FOR 91NB

1	0.0	+4.5
2	0.1045	-0.5
3	1.1868	-2.5
4	1.3126	-1.5
5	1.5810	+3.5
6	1.6125	-1.5
7	1.6370	+4.5
8	1.7904	-4.5
9	1.8448	-2.5
10	1.8850	+0.5
11	1.9631	+2.5
12	1.9844	-6.5
13	2.0345	-8.5

LEVELS FOR 94NB

1	0.0	+6.0
2	0.0410	+3.0
3	0.0587	+4.0
4	0.0787	+7.0
5	0.1184	+5.0
6	0.1404	-2.0
7	0.3119	+5.0
8	0.3342	+2.0

LEVELS FOR 92NB

1	0.0	+7.0
2	0.1355	+2.0
3	0.2259	-2.0
4	0.2856	+3.0
5	0.3574	+5.0
6	0.3898	-3.0
7	0.4802	+4.0

γ -RAY BRANCHINGS

GAMMA:	TO LEVEL 2	(1.0)
	2	(1.0)
	1	(1.0)
	2	(0.03)
	3	(0.96)
	4	(0.01)
	4	(0.76)
	5	(0.24)

LEVELS FOR 93NB
(UPDATED)

1	0.0	+4.5
2	0.0304	-0.5
3	0.686	-1.5
4	0.7440	+3.5
5	0.8087	+2.5
6	0.8101	-1.5
7	0.9499	+6.5
8	0.9791	+5.5
9	1.0826	+4.5
10	1.127	+2.5
11	1.29	-1.5
12	1.2974	+4.5
13	1.3156	-1.5
14	1.3351	+8.5

γ -RAY BRANCHINGS

GAMMA:	TO LEVEL 2	(1.0)
	1	(1.0)
	1	(0.9877)
	4	(0.0123)
	2	(1.0)
	2	(1.0)
	1	(1.0)
	1	(0.265)
	4	(0.663)
	8	(0.072)
	5	(1.0)
	3	(1.0) ?
	1	(0.53)
	4	(0.3)
	8	(0.17)
	4	(1.0)
	7	(1.0)

APPENDIX A

TABLE 2a

Definition of Optical Potential

according to Becchetti and Greenlees, Phys. Rev. 182, 1190 (1969)

<u>expression</u>	<u>explanation</u>
$U_{opt}(r) = -V_R f_R$	central real
$+ \left[\frac{h/2\pi}{m c} \right]^2 \frac{v_{SO}}{r} \left(\frac{d}{dr} f_{SO} \right)$	$\rightarrow \rightarrow$ 1. σ spin orbit
$\left \begin{array}{l} + \frac{Zze^2}{2R_c} \left[3 - \left(\frac{r}{R_c} \right)^2 \right] \\ + \frac{Zze^2}{r} \end{array} \right.$	for $r \leq R_c$ for $r \geq R_c$ Coulomb
$- iW_V f_I$	imaginary volume
$+ i4a_I W_{SF} \left(\frac{d}{dr} f_I \right)$	imaginary surface
where $f_x = f(r, R_x, a_x) = [1 + \exp(r - R_x)/a_x]^{-1}$	
$R_x = r_x A^{1/3}$	
$R_x = r_x' A^{1/3} + r''$ for heavier projectiles (such as alphas)	
$r_c =$ Coulomb Radius	

Note: Whenever a parameter is omitted, it is assumed that the corresponding potential is not considered.

TABLE 2b**Optical Model Parameters****Neutron Parameters**

$$V_R = 48.0 - 0.293E \text{ (E in MeV-Lab)}$$

$$r_R = 1.27 \text{ fm}, \quad a_R = 0.66 \text{ fm}$$

$$W_{SF} = 9.6 \text{ MeV}$$

$$r_I = 1.27 \text{ fm}, \quad a_I = 0.47 \text{ fm}$$

$$V_{SO} = 7.2 \text{ MeV}$$

$$r_{SO} = 1.27 \text{ fm}, \quad a_{SO} = 0.66 \text{ fm}$$

Proton Parameters (ref. 3)

$$V_R = 53.3 - 0.55E + 0.4 Z/A^{1/3} + 27.0 (N-Z)/A \text{ (E in MeV-Lab)}$$

$$r_R = 1.25 \text{ fm}, \quad a_R = 0.65 \text{ fm}$$

$$W_{SF} = 13.5 \text{ MeV}$$

$$r_I = 1.25 \text{ fm}, \quad a_I = 0.47 \text{ fm}$$

$$V_{SO} = 7.50 \text{ MeV}$$

$$r_{SO} = 1.25 \text{ fm}, \quad a_{SO} = 0.65 \text{ fm}$$

$$r_C \text{ (coulomb radius)} = 1.25 \text{ fm}$$

Alpha Parameters (ref. 4)

$$V_R = 50.0 \text{ MeV}$$

$$r_R' = 1.17 \text{ fm}, \quad a_R = 0.576 \text{ fm}, \quad r_R'' = 1.77 \text{ fm}$$

$$W_V = 13.74 \text{ MeV}$$

$$r_I' = 1.17 \text{ fm}, \quad a_I = 0.576 \text{ fm}, \quad r_I'' = 1.77 \text{ fm}$$

$$r_C = 1.17 \text{ fm}$$

Note: If the code does not allow for the second form of the radius expression in Table 2a, an effective radius parameter has to be calculated for each mass number (i.e. $r_x = 1.56$ for $A = 93$).

TABLE 3aCalculation of level-density parameters^{a)}

Nucleus (Composite nucleus)	Mass (amu)	B (MeV)	J^π (target)	b) σ^2 exp	c) P (MeV)	E_c ^{d)} (MeV)	e) N c	Dobs (eV)
86Rb	85.911	8.650	5/2-	7.24	0	1.309	15.5	201.4
89Sr	88.907	6.364	0+	5.31	1.24	2.707	11.5	37438
89Y	88.906	11.469	4-	6.42	0.93	1.745	2.5	140.0
90Y	88.907	6.857	1/2-	9.49	0	1.417	9.5	4414
92Y	91.909	6.544	1/2-	3.12	0	1.030	7.5	869.5
92Zr	91.905	8.635	5/2+	6.12	1.92	2.486	8.5	336.6
93Zr	92.907	6.732	0+	2.46	1.20	1.735	12.5	3678
91Nb	90.907	12.055	8+	9.36	0.93	2.065	12.5	51.2
92Nb	91.907	7.883	9/2+	11.6	0	0.501	6.5	267.3
93Nb	92.906	8.832	7+	6.70	0.72	1.364	13.5	41.5
94Nb	93.907	7.230	9/2+	12.0	0	0.396	7.5	99.6

a) The level density is characterised by the total number of levels N_c at energy E_c and the s-wave level spacing Dobs at the neutron binding energy B.

b) Spin cut-off parameter σ^2 , derived from experimental spin distribution of levels up to $E=E_c$.

c) Pairing energy correction for Gilbert-Cameron formula, from [5].

d) E_c = first energy of continuum calculation.

e) "Average" number of levels at energy E_c .

TABLE 3b
Level-density parameters^{a)}

Nucleus	Gilbert-Cameron 1 ^{b)}		Gilbert-Cameron 2 ^{c)}		Dilg et al. ^{d)}	
	a (MeV ⁻¹)	U _x (MeV)	a (MeV ⁻¹)	U _x (MeV)	a (MeV ⁻¹)	Δ(MeV)
86Rb	10.01	4.998	9.278	5.060	9.214	-1.069
89Sr	9.501	3.477	8.375	3.883	8.924	0.4802
89Y	8.600	2.213	8.112	1.537	8.460	0.3116
90Y	9.318	3.792	8.390	4.066	8.914	-0.7409
92Y	12.10	2.628	11.02	2.705	11.30	-0.5117
92Zr	11.83	4.047	10.92	3.995	10.43	0.7695
93Zr	12.69	4.607	11.46	4.774	10.63	-0.1563
91Nb	9.400	5.132	9.415	4.407	8.725	-0.2954
92Nb	10.30	6.400	9.762	6.259	8.923	-1.747
93Nb	12.58	4.678	12.39	4.270	11.24	-0.4636
94Nb	12.51	5.707	11.86	5.603	10.65	-1.553

a) Level-density parameters calculated from the data given in Table 3a.

b) Improved Gilbert-Cameron formula, with $\sigma^2 = 0.146 \sqrt{aU} A^{2/3}$ [5].

c) Original Gilbert-Cameron formula, with $\sigma^2 = 0.0888 \sqrt{aU} A^{2/3}$ [7].

d) Back-shifted Fermi gas formula of Dilg et al. [6].

Questionnaire on Pre-equilibrium/Equilibrium Model Codes

1 Participant

2 Code name and references, availability (give date):

3 Equilibrium-model part

3.1 Weisskopf-Ewing type (no conservation of angular momentum; no discrete levels)

3.2 Hauser-Feshbach (H.F.) type

3.3 Else, or comment:

APPENDIX B

4 Pre-equilibrium model part

- 4.1 Full master equation approach ($n_0 = 3$) with or without quantum mechanical conservation of angular momentum (and parity).
- 4.2 Never-come back assumption (only λ^+ -transitions starting from $n_0 = 3$)
- 4.3 (Geometry-dependent) hybrid model, indicate $n_0 =$
- 4.4 Two-component model (protons and neutrons are explicitly distinguished as in Ref.¹¹).
- 4.5 Else, or comment:

5 Relation of equilibrium to pre-equilibrium parts

- 5.1 Unified model of pre-equilibrium and equilibrium emission with conservation of angular momentum and with or without treatment of discrete levels.
- 5.2 Pre-equilibrium is treated as a correction to the statistical model (indicate relation below)
- 5.3 Else, or comment (give definition of equilibrium and/or pre-equilibrium, if this is useful):

6 Options

- 6.1 Cross sections (angle and energy integrated).
- 6.2 Particle spectra (angle-integrated).
- 6.3 Angular distributions.
- 6.4 Multi-particle emission up to outgoing particles with or without multiple precompound decay treatment.
- 6.5 Else, or comment.

7 Total level density in equilibrium part

- 7.1 Gilbert-Cameron¹
 $(\sigma^2 = 0.0888 \sqrt{aU} A^{2/3} \text{ })$.
 $(\sigma^2 = 0.146 \sqrt{aU} A^{2/3} \text{ })$.
- 7.2 Back-shifted Fermi-gas model of Dilg et al.².
- 7.3 Modifications or comments (e.g. σ^2 at low E):

APPENDIX B

8 Particle-hole level density

- 8.1 Williams state density³ with or without an energy shift or pairing energy correction (if there is an n-dependent energy shift, indicate expression below).
- 8.2 $g = A/13 \text{ MeV}^{-1}$ and no pairing energy correction.
- 8.3 Williams' level density with n-dependent spin distribution, indicate σ_n^2 below.
- 8.4 Else, or comment:

9 Discrete levels

- 9.1 Included in equilibrium calculation only.
- 9.2 Not considered, $E_c = 0.1 \text{ MeV}$.
- 9.3 Else, or comment (e.g. when direct models are used or included in the model:

10 Internal transition rates

10.1 Average transition probability
 $\lambda^{\pm} = \frac{2\pi}{\hbar/2\pi} \langle M^2 \rangle \omega_f^{\pm}$ with ω_f^{\pm}
 according to:

- Williams³
- Oblozinsky et al.⁴
- Else, or modifications

and $\langle M^2 \rangle$ according to

- $\langle M^2 \rangle = cA^{-3}E^{-1}$ with $c =$
- Kalbach0, indicate fit parameters below.
- Else, or comment

10.2 Else, or comment:

APPENDIX B

11 Emission rates

11.1 Use of R- and Q-factors:

- Cline (without renormalisation to 1 at both values of n').
- Kalbach's Q-factor, normalised to 1 at high values of n'
- Gadioli, et al.⁸.
- Else, or comment:

11.2 Treatment of α -emission

- α -particle emission rate according to ref.¹⁰.
- Form factor used $\gamma_{\alpha} =$
- Else, or comment (give reference):

11.3 Transmission coefficients

- Inverse reaction cross sections used in precompound part.
- Transmission coefficients used in compound and precompound part, with or without j-dependence.
- Else, or comment:

12 Spectrum calculations

12.1 Complexity

- Only first-emitted particles calculated.
- Total particle production spectra calculated.
- Emission spectra are calculated for every reaction, and every outgoing particle (e.g. two spectra for $n,2n$).
- γ -ray cascade calculation possible.
- Else, or comment:

12.2 Representation

- Spectrum is represented in energy bins of equal or variable width.
- Spectrum is given by point data at equidistant or non-equidistant energies.
- Else, or comment:

APPENDIX B

13 Angular distribution calculation

- 13.1 Only in H.F.-part, for (in)elastic neutron scattering to discrete levels.
- 13.2 Systematics of kelbach and mannfor angular distributions in pre-compound part.
- 13.3 Model of Mantzouranis et al.¹⁰, specify version below.
- 13.4 DWBA-type of calculation for emission from $n=n_0$ only.
- 13.5 Other model, specify below, give reference.

14 Gamma-Ray emission

- 14.1 No gamma-ray competition included.
- 14.2 No gamma-ray spectrum calculation or isomeric-state population calculation.
- 14.3 Specify Brink-Axel formula below. E1-normalisation constant used for all nuclei =
- 14.4 Specify Weisskopf formula for M1 and E2 below.
M1 - normalisation constant used for all nuclei =
E2 - normalisation constant used for all nuclei =
- 14.5 Specify expression for Yrast line below, e.g,

$$\left(\frac{\hbar}{2\pi}\right)^2 J_{\max}^2 = 2 I (E-\delta) \geq \left(\frac{\hbar}{2\pi}\right)^2 J_{\min}^2 \quad (12)$$

or the Augustyniak et al.¹¹ prescription.

15 Additional comments:

16 References to Appendix B

- [1] A. Gilbert and A.G.W. Cameron, Can. J. of Phys. 43 (1965), 1446.
- [2] W. Dilg et al., Nucl. Phys. A217 (1973), 269.
- [3] F.C. Williams, Nucl. Phys. A166 (1971), 231
- [4] P. Oblozinsky, I. Ribansky and E. Betak, Nucl. Phys. A226 (1974), 347.
- [5] C. Kalbach, Z. Fuer Physik A283 (1978), 319.
- [6] C.K. Cline, Nucl. Phys. A193 (1972), 417.
- [7] C. Kalbach, Z. fuer Physik A283 (1977), 401.
- [8] E. Gadioli, E. Gadioli-Erba and P.G. Sona, Nucl. Phys. A217 (1973), p.589.
- [9] L. Millazzo-Colli and G.M. Braga-Marcazzan, Nucl. Phys. A210 (1973), p.297.
- [10] G. Mantzouranis et al., Phys. Lett., 57B (1975), 220.
- [11] S.K. Gupta, Z. Phys. A303 (1981) 329.
- [12] D.G. Gardner, Proc. of NEANDC/NEACRP Specialists' meeting on fast neutron capture cross sections, Argonne, 1982: NEANDC(US)-214/L; ANL-83-4 (1983) p.57; UCRL-87438 (1982).
- [13] W. Augustyniak and A. Marcinkowski, Acta Physica Polonica 4 (1979) 357.

- 68946 -